B PHYSICS

HARRY NEWTON

Philosophiae Doctor

University of Edinburgh

MCMXCIX

In Memoriam

DERRICK NEWTON

26 VII 1918 – 6 XI 1997

Abstract

I introduce and define Quantum Chromodynamics. I describe various well-known non-perturbative techniques for calculating quantities from the theory and discuss their merits and deficiencies. I then motivate and define a non-relativistic formulation (NRQCD) of the theory. I discuss the mechanics of the extraction of numbers from numerical simulations, and present general arguments as to the expected form of these data. I present results and details of their extraction from simulations of heavy-heavy and heavy-light mesons using NRQCD. I compare these results with those from other calculations and with experimental data, where they exist. I make suggestions for further work. An appendix contains details of the code used in the simulation together with the input parameters of the simulation.

Contents

Declaration

This thesis was composed and written wholly by me. It is a report of work I carried out alone at the University of Edinburgh. The code to generate the NRQCD Green's functions, and to correlate them was written and designed by me. All the correlators were generated by me. The data were analysed by me.
Some of the results are reported in

H. Shanahan, P. Boyle, C.T.H. Davies, and H. Newton
A Non-Perturbative Calculation of the mass of the B_c
hep-lat/9902025 — Physics Letters B **453** 289-294

The scaling of the heavy-light spectrum will appear in:

J. Hein and H. Newton
Scaling of the B and D meson spectrum in lattice QCD
In Preparation

The data will also be used in a future calculation of heavy-light matrix elements: at the time of writing, work is in progress to generate the improvement terms for this calculation.

Acknowledgments

I thank my mother for her support and love over the course of my stay in Edinburgh.
Thanks are also due to all members of the Edinburgh NRQCD group.
The work reported in this thesis was funded by several government agencies.

ET IGNOTAS ANIMUM DIMITTIT IN ARTES
NATURAMQUE NOVAT.

OVID, METAMORPHOSES, VIII, 188

Preface

Although the bulk long-lived matter of the world around us is made up of down and up quarks, the physics of particles containing beauty quarks is becoming increasingly important in the process of proving QCD. These particles, which occur only briefly in particle accelerators, are the heaviest bound states of quarks — the top quark being unable to form bound states (Quigg, 1997). Specifically, B decays and mixing will lead to complete determination of the elements of the CKM matrix. These elements describe the *weak* decay of one quark flavour into another, and are not directly measurable. To extract them from the experimentally measured decay rates, the theoretical estimates of the appropriate hadron matrix elements are required. Of course, one can't expect to get the matrix elements right until the spectrum has been calculated correctly.

1

Introduction

1.1 Introduction

Every since Democritus humanity has believed that the fundamental entities of nature are discrete in characteristic. In contemporary physics, this view is enshrined in the quantum theory.

This thesis is concerned with calculations in a particular part of quantum theory, Quantum Chromodynamics, QCD. QCD is the most widely accepted theory of quark interaction; however its status as the theory is not yet fully established. Perturbative calculations have been successful at short distances/high energies where the quark-gluon running coupling is small. However, to study low and intermediate energy regimes, the coupling rises and prohibits perturbative techniques. It is here that non-perturbative methods must be used.

1.2 What is QCD ?

1.2.1 Philosophical Aside

As mentioned before quantum field theories are concerned with discrete entities. The classical idea of discrete particles of matter affected by continuous of fields of force is replaced by the paradigm of two types of particle, continually interacting with each other. One type clump together to form bulk matter (the fermions) whilst the other type do not, and mediate what was once thought of as the force. Both types are described by operator fields which create-annihilate the particles states. These operator fields are identified with particles species - quarks, gluons etc rather than individual particles. This is reflected in the idea of indistinguishability of particles that was recognised early on in the gestation of quantum theory; such a lack of individuality does not occur in classical mechanics. These operator fields then are the basic objects which occur in the theory. However they are not the objects that are available to experiment; there are two reasons for this. In general, for quantum field theories, it is not possible to separate the particle from the interactions that it feels: the fields and parameters of the theory must be adjusted (the process is called Renormalisation) to correspond with those that are seen in the real world - *i.e.* at the scales in which we live. Secondly, as is the case in QCD, the fundamental objects - quarks - are never observed alone, but only together in bound states. These bound states are what are seen in the real world.

1.2.2 Defining QCD

The starting point is the Lagrangian density:

$$\mathcal{L} = \sum_{f=1}^{N_{\text{flavours}}} \overline{\psi}_f(x)\left(\mathrm{i}\not{D} - m_f\right)\psi_f(x) - \frac{1}{4}\sum_b F^b_{\mu\nu}(x)F_b^{\mu\nu}(x)$$

in which the gauge fields live in the adjoint representation of SU(3), whilst the fermion fields live in the fundamental representation. The fields carry colour, spin, and Lorentz indices which have been suppressed: $\psi^j_{f\alpha}(x)$, $F_{\mu\nu}(x) = \left(F^a_{\mu\nu}\right)^{ij}$ — in which the colour indices i, j can vary over $\{1,2,3\}$, the Lorentz indices μ, ν can vary over $\{0,1,2,3\}$, the Dirac (or spin) index α can vary over $\{0,1,2,3\}$, and the gluon index a can vary between $\{1,2,3,4,5,6,7,8\}$.

$$\not{D} \stackrel{=}{\text{def}} \gamma^\mu D_\mu$$

and the coupling between the quark fields and the gluon fields is specified by the definition of the covariant derivative:

$$D^{ij}_\mu = \delta^{ij}\partial_\mu + \mathrm{i}gA^{ij}_\mu(x)$$

$$A_\mu(x) = T^a A^a_\mu(x)$$

The colour field tensor is defined:

$$[D_\mu, D_\nu] = +\mathrm{i}gF_{\mu\nu}$$

so that:

$$F^a_{\mu\nu}(x) = \partial_\mu A^a_\nu - \partial_\nu A^a_\mu - gf^{abc}A^b_\mu(x)A^c_\nu(x)$$

$$F_{\mu\nu}(x) = \sum_{a=1}^{8} T^a F^a_{\mu\nu}(x)$$

and the eight 3×3 matrices, T^{ij}_a are the generators † of the fundamental representation of the SU(3) group, and obey the Lie algebra:

$$[T_a, T_b] = \mathrm{i}f_{abc}T_c$$

and are normalised:

$$\mathrm{Tr}\,(T_aT_b) = \frac{1}{2}\delta_{ab}$$

Putting

$$\Lambda^{ij}(x) = \mathrm{e}^{-\mathrm{i}g\lambda_b(x)T_b^{ij}}$$

the Lagrangian is invariant under the gauge transformation:

$$\psi^i(x) \longrightarrow \Lambda^{ij}(x)\psi^j(x)$$

$$A^{il}_\mu(x) \longrightarrow \Lambda(x)^{ij}\left(A^{jk}_\mu(x) - \mathrm{i}\frac{1}{g}\partial_\mu\delta^{jk}\right)\left(\Lambda^{-1}(x)\right)^{kl}$$

† Usually one works in terms of the Gell-Mann matrices $\lambda_a = 2T_a$

1.2.3 Path Integrals

The path integral relates vacuum expectation values of time-ordered products of field operators to weighted averages of fields:

$$\langle\Omega|\top\mathcal{O}\left(\psi(x_1),\ldots,\ \psi(x_n),\overline{\psi}(y_1),\ldots,\overline{\psi}(y_n)\right)\perp|\Omega\rangle$$
$$= \frac{1}{\mathcal{Z}}\int\mathfrak{D}\overline{\psi}\mathfrak{D}\psi\mathfrak{D}A\ \mathcal{O}\left(\psi(x_1),\ldots,\psi(x_n),\overline{\psi}(y_1),\ldots,\overline{\psi}(y_n)\right)\mathrm{e}^{\mathrm{i}S[\psi,\overline{\psi},A]}$$

in which I have shown the time-ordering of the fields by placing them in between the symbols $\top$ and $\perp$. The normalisation factor is given by:

$$\mathcal{Z} = \int\mathfrak{D}\overline{\psi}\mathfrak{D}\psi\mathfrak{D}A\ \mathrm{e}^{\mathrm{i}S[\psi,\overline{\psi},A]}$$

The fields appearing under the integral are not operators but ordinary variables (c-number or Grassmann number valued). There are some hidden difficulties in this expression. As they disappear in numerical lattice calculations, I only mention them briefly here. The path integral as it stands is infinite because it over counts the gauge field contributions by including all gauge fields that are related by gauge transformations. This happens because the theory as formulated includes unphysical gauge degrees of freedom. If one wishes to analytically calculate from this path integral, one must fix the gauge to define the gauge field propagator, and include a Faddeev-Popov determinant to prevent the over counting. I shall show that neither of these is necessary for numerical lattice calculations.

The vacuum expectation values are Green's functions of the theory, and hold all the physical content of the theory. They are related to the transition amplitudes between the external n-particle states that are measured experimentally by the reduction formula of Lehmann, Symanzik, and Zimmermann (1955). As will be shown later, physical information is typically extracted from the Green's functions in a more direct manner in lattice studies.

I shall find it useful to introduce source terms into the action:

$$\mathcal{Z}\left[\sigma,\overline{\sigma},J_\mu\right] = \int\mathfrak{D}\overline{\psi}\mathfrak{D}\psi\mathfrak{D}A\ \mathrm{e}^{\mathrm{i}\int\mathrm{d}^4x\mathcal{L}\left[\psi,\overline{\psi},A_\mu\right]+\overline{\sigma}(x)\psi(x)+\overline{\psi}(x)\sigma(x)+A_\mu(x)J_\mu(x)}$$

One can then obtain the Green's functions directly from the generating functional:

$$\langle\Omega|\top\psi(x_1)\ldots\psi(x_n)\overline{\psi}(y_1)\ldots\overline{\psi}(y_n)\perp|\Omega\rangle = G\left(x_1,\ldots,x_n;y_1,\ldots,y_n\right)$$

by way of:

$$\mathrm{i}^{2n}\ G\left(x_1,\ldots,x_n;y_1,\ldots,y_n\right) = \frac{\delta^{2n}}{\delta\overline{\sigma}(x_1)\cdots\delta\overline{\sigma}(x_n)\delta\sigma(y_1)\cdots\delta\sigma(y_n)}\quad\mathcal{Z}\left[\sigma,\overline{\sigma},J_\mu\right]\Big|_{\overline{\sigma}=\sigma=J_\mu=0}$$

1.2.4 Euclidean Field Theory

The complex phase in the path integral causes the integrand to fluctuate excessively; this can cause cancellations between widely separated areas of the configuration space of the field variables making Monte Carlo integration infeasible. In addition, a probability interpretation is not possible.

The problem is overcome by manipulating the time variable in the path integral so that it becomes wholly imaginary:

$$x_0 = \mathrm{i}x_4 \qquad \text{with } x_4 \in R$$

The action so formed is called the Euclidean action. The Green's functions of the Euclidean action are the analytic continuations § in the time variable of the Minkowski space Green's functions to the imaginary axis. These continuations are valid provided no singularities are crossed in rotating the contour. This is usually the case at each order in perturbation theory, but not necessarily so non-perturbatively. To get round this problem, the theory is defined in Euclidean space and the Green's functions calculated there. These can be then continued back to Minkowski space: however, quantities such as energies are invariant under the continuation and so may be calculated directly from the Euclidean space Green's functions.

One can determine the Euclidean action by defining Euclidean versions of vectors in terms of their counterparts in Minkowski space:

$$A_{\mathrm{E}} = \left(\boldsymbol{A}^{\mathrm{E}}, A_4\right) = \left(\boldsymbol{A}^{\mathrm{M}}, -\mathrm{i}A_0\right)$$

and Euclidean versions of the Dirac matrices:

$$\gamma^{\mathrm{E}} = \mathrm{i}\gamma^{\mathrm{M}} \qquad\qquad \gamma_4 = \gamma_0$$

and then writing the Minkowski expressions in terms of the Euclidean quantities. Specifically one sees that Minkowski scalar products are replaced by Euclidean ones (and hence the name):

$$A^{\mu}B_{\nu} \longrightarrow -A^{\mathrm{E}} \cdot B^{\mathrm{E}} = -\sum_{j=1}^{4} A_j^{\mathrm{E}} B_j^{\mathrm{E}}$$

and the gamma matrices satisfy:

$$\{\gamma_{\mu}^{\mathrm{E}}, \gamma_{\nu}^{\mathrm{E}}\} = 2\delta_{\mu\nu}$$

$$\gamma_5^{\mathrm{E}} = \gamma_1^{\mathrm{E}}\gamma_2^{\mathrm{E}}\gamma_3^{\mathrm{E}}\gamma_4^{\mathrm{E}}$$

In Euclidean space, $\not{D}$ becomes

$$\mathrm{i}\gamma^{\mathrm{E}} \cdot D^{\mathrm{E}} = \mathrm{i}\sum_{j=1}^{4} \gamma_j^{\mathrm{E}} D_j^{\mathrm{E}} \equiv \not{D}^{\mathrm{E}}$$

The criteria for the Euclidean theory to be well-defined, *i.e.* for the continuation to Minkowski space to be possible were studied by Osterwalder and Schrader (1975). The main one is Reflection Positivity, which requires that there exists an anti-linear ¶ mapping Θ of an arbitrary function F of the fields at positive times to a function of the fields at negative times, such that:

$$\langle (\Theta F)\, F \rangle \geq 0$$

The importance of this criterion is that it allows one to define a Hilbert space with positive norm, and a positive transfer matrix in the space. Put another way, the SO(4) invariant Euclidean theory acquires a special direction to act as a time co-ordinate.

---

§ usually known as Wick rotations

¶ An anti-linear mapping Θ is one for which $\Theta(\lambda F) = \overline{\lambda}\Theta F \qquad \forall \lambda \in \mathbb{C}$

1.3 Euclidean Lattice Action

Following the prescription above one can write down the Euclidean action. From now on everything will be in Euclidean space, and so the explicit labels are dropped.

$$S = \int \mathrm{d}^4x \; \overline{\psi}(\not{D} + m)\psi + \frac{1}{4} F_{\mu\nu} F^{\mu\nu}$$

First of all one wants a finite difference version of this expression, preserving its symmetries. Replacing the derivatives of quark fields with finite differences ¶

$$\partial_\mu \psi(x) \longrightarrow \frac{1}{2a} \left[\psi(x + a\widehat{\mu}) - \psi(x - a\widehat{\mu}) \right]$$

is not sufficient because the quantities are not gauge covariant. The continuum expression:

$$\overline{\psi}(x) \left(\exp \mathrm{i}g \int_x^y \mathrm{d}z^\mu \; A_\mu(z) \right) \psi(y)$$

is though. Approximating the integral by its mid-point value:

$$\mathrm{i}g(y - x) A_\mu \left(x + \left(\frac{y - x}{2} \right) \right)$$

and then setting $y = x + a\widehat{\mu}$, where $\widehat{\mu}$ is a unit vector pointing from x to y leads to:

$$\exp \mathrm{i}ga A_\mu \left(x + \frac{1}{2} a\widehat{\mu} \right)$$

This expression is usually denoted $U_\mu(x)$ and is called the link variable. It is the most basic gauge quantity on the lattice: all expressions involving gauge fields are formulated in terms of the link variables. They belong to the fundamental representation of SU(3), *i.e.* in moving from the continuum to the lattice, the gauge degrees of freedom are described by the Lie group rather than the Lie algebra su(3). It is the fact that one can describe the gauge degrees of freedom by the compact group, SU(3), that makes the path integral finite and allows one to put them on the lattice — see the next section.

Here are the gauge covariant finite differences:

$$\Delta_\mu^{\mathrm{F}} \stackrel{=}{\mathrm{def}} \frac{1}{a} \left[U_\mu(x) \psi(x + a\widehat{\mu}) - \psi(x) \right]$$

$$\Delta_\mu^{\mathrm{B}} \stackrel{=}{\mathrm{def}} \frac{1}{a} \left[\psi(x) - U_\mu^\dagger(x - a\widehat{\mu}) \psi(x - a\widehat{\mu}) \right]$$

$$\Delta_\mu^{\mathrm{C}} \stackrel{=}{\mathrm{def}} \frac{1}{2a} \left[U_\mu(x) \psi(x + a\widehat{\mu}) - U_\mu^\dagger(x - a\widehat{\mu}) \psi(x - a\widehat{\mu}) \right]$$

in which the F, B, and C superscripts stand for Forward Euler, Backwards Euler, and Central Difference.

The continuum gauge transformations become on the lattice:

$$U_\mu(x) \longrightarrow \Lambda(x) U_\mu(x) \Lambda^\dagger(x + a\widehat{\mu})$$

¶ This is the Central Difference which has errors at $\mathcal{O}(a^2)$ rather than at $\mathcal{O}(a)$ for the Euler differences.

with $\Lambda(x) \in \mathrm{SU}(3)$, in the same representation as the U_μ 's.

1.4 Gauge Action

The simplest gauge invariant quantity that can be formed is the trace of a product of four link variables forming a closed path:

$$\mathrm{Tr}U^{\square}_{\mu\nu}$$

in which:

$$U^{\square}_{\mu\nu}(x) \stackrel{=}{\mathrm{def}} U_\mu(x)U_\nu(x+a\widehat{\mu})U^\dagger_\mu(x+a\widehat{\nu})U^\dagger_\nu(x)$$

Such a quantity is known as a plaquette, and its trace is related to the field strength tensor as:

$$\begin{aligned}\Re\mathrm{e}\mathrm{Tr}U^{\square}_{\mu\nu} &= N_{\mathrm{colour}} - \frac{g^2}{2}a^4\mathrm{Tr}\left(F^2_{\mu\nu}(x)\right) + \mathcal{O}(a^6) \\ &= N_{\mathrm{colour}} - \frac{g^2}{4}a^4\sum_{b=1}^{8}\left(F^b_{\mu\nu}(x)\right)^2 + \mathcal{O}(a^6)\end{aligned}$$

From this one may write down a discrete version of the gauge action:

$$\sum_x\sum_{\mu<\nu}\frac{2}{g^2}\left[N_{\mathrm{colour}} - \Re\mathrm{e}\mathrm{Tr}\left(U^{\square}_{\mu\nu}(x)\right)\right] + \mathcal{O}(a^2)$$

The constant term is not relevant in calculating expectation values and will be ignored. Finally

$$S_{\mathrm{Gauge}} = \frac{-\beta}{N_{\mathrm{colour}}}\sum_{\substack{x\\ \mu<\nu}}\Re\mathrm{e}\mathrm{Tr}U^{\square}_{\mu\nu}$$

is known as the Wilson Pure Gauge action (Wilson, 1974); I have followed convention by putting $\beta = 2N_{\mathrm{colour}}/g^2$. The continuum path integral $\int \mathfrak{D}A_\mu$ is replaced by:

$$\int\mathfrak{D}U = \prod_{x,\mu}\int \mathrm{d}U_\mu(x)$$

A well-defined measure, the Haar measure can be constructed for the SU(3) group. It is gauge invariant.

On a finite lattice the number of variables is finite. As the domain of integration is compact, the functional integral is well defined.

If one wishes to numerically calculate gauge invariant quantities nothing else is needed. If one wishes to calculate non-gauge invariant quantities then one calculates the configurations and fixes the gauge on each configuration. To perform analytic lattice calculations one must gauge fix and incorporate a Faddeev-Popov determinant as in the continuum.

1.5 Fermion Action

This is a little more complicated. I work with a single flavour of quark for the time being. The straightforward prescription of replacing the covariant derivatives with their difference

counterparts yields a theory with a continuum limit containing 2^4 species of fermion of equal mass, *i.e.* two fermions per dimension.

This phenomena, known as fermion doubling, is a characteristic of bilinear, translationally invariant, Hermitian lattice actions with chiral symmetry (Nielsen and Ninomiya, 1981). One can overcome this by adding an irrelevant term to the action:

$$-a^4 \sum_x \sum_\mu \frac{ar}{2} \overline{\psi}(x) \Delta_\mu^{(2)} \psi(x)$$

with

$$\Delta_\mu^{(2)}(x) \stackrel{=}{\text{def}} \frac{1}{a^2} \left[U_\mu(x)\psi(x + a\widehat{\mu}) + U^\dagger(x - a\widehat{\mu})\psi(x - a\widehat{\mu}) - 2\psi(x) \right]$$

which is the lowest order finite difference approximation to $\partial_\mu \partial_\mu$. The variable r is arbitrary, and usually set to 1, which makes the action reflection positive. The term varies at $r\mathcal{O}(a)$ and so vanishes as $a \to 0$. With this term 15 of the 16 doublers decouple from the theory in the continuum limit by acquiring masses of $\mathcal{O}(\frac{r}{a})$. However, the action is no longer chiral invariant. The action is usually written

$$S_{\text{Wilson}} = \sum_{x,y} \overline{\psi}(x) M^{\text{Wilson}}(x,y) \psi(y)$$

$$M^{\text{Wilson}} = \left(\mathbb{1} - \kappa \not{D}^{\text{Wilson}} \right)$$

where

$$\not{D}^{\text{Wilson}} = \sum_{\mu=1}^{4} (r - \gamma^\mu) U_\mu(x) \delta(x + a\widehat{\mu}, y) + (r + \gamma^\mu) U^\dagger(x - a\widehat{\mu}) \delta(x - a\widehat{\mu}, y)$$

by scaling the fields:

$$\psi \to \sqrt{2\kappa}\psi$$

The quantity κ is known as the hopping parameter, and is related to the bare quark mass by;

$$am = \frac{1}{2} \left(\frac{1}{\kappa} - \frac{1}{\kappa_{\text{critical}}} \right)$$

κ_{critical} is the value of the hopping parameter corresponding to zero quark mass, and for the free theory is $1/8r$. In the interacting theory the lack of chiral symmetry means that the fermion can (and usually will) acquire dynamical mass and so alter the value of κ_{critical}. So the zero mass limit cannot be established *a priori* and must either be measured in a simulation or calculated in perturbation theory.

This action differs from the continuum action at $\mathcal{O}(a)$.

1.6 Improvement

1.6.1 Symanzik's Programme

The basis (Symanzik, 1983) is that the lattice action, $S^\#$, can be expanded:

$$S^{\#} = S_0 + ac_1S_1 + a^2c_2S_2 + \cdots$$
$$= \int \mathrm{d}^4x\ \mathcal{L}_0(x) + ac_1\mathcal{L}_1(x) + a^2c_2\mathcal{L}_2(x) + \cdots$$

where S_0 is the continuum action and the remaining terms are local and constructed from the continuum fields. The $\{c_j | j = 1, 2, \cdots\}$ are coefficients. Possible operators used in the construction of these higher order terms must have the right dimension and symmetries (*e.g.* parity, charge conjugation). The idea of the programme is to reduce the difference between the lattice action and that of the continuum by adding higher order terms. As I have shown

$$S^{\#}_{\text{Wilson}} = \overline{\psi}\left(\not{D} + m\right)\psi + \overline{\psi}\frac{ar}{2}D^2\psi + \mathcal{O}(a^2)$$

and

$$S^{\#}_{\text{Gauge}} = \int \mathrm{d}^4x\ \frac{1}{4}F^b_{\mu\nu}F^{\mu\nu}_b + \mathcal{O}(a^2)$$

So it is sensible to improve the Wilson action so that the errors appear at $\mathcal{O}(a^2)$. The complete set of dimension five operators is

$$\mathcal{O}_1(x) = \overline{\psi}(x)\mathrm{i}\sigma_{\mu\nu}F^{\mu\nu}(x)\psi(x)$$
$$\mathcal{O}_2(x) = \overline{\psi}(x)\left(\overrightarrow{D}_\mu\overrightarrow{D}_\nu + \overleftarrow{D}_\mu\overleftarrow{D}_\nu\right)\psi(x)$$
$$\mathcal{O}_3(x) = m\mathrm{Tr}\left(F_{\mu\nu}(x)F^{\mu\nu}(x)\right)$$
$$\mathcal{O}_4(x) = m\left(\overline{\psi}\not{D}\psi - \overline{\psi}\overleftarrow{\not{D}}\psi\right)$$
$$\mathcal{O}_5(x) = m^2\overline{\psi}(x)\psi(x)$$

I have used the definition $\sigma_{\mu\nu} = \frac{1}{2}\left[\gamma_\mu, \gamma_\nu\right]$, writing the factor of i explicitly. Of these, $\mathcal{O}_2$ and $\mathcal{O}_4$ can be eliminated by using the equations of motion, for on-shell quantities only. $\mathcal{O}_3$ and $\mathcal{O}_5$ are simply redefinitions of the coupling constant, g, and mass respectively. One obtains the action of Sheikholeslami and Wohlert (1985):

$$S_{\text{SW}} = S_{\text{Wilson}} - \frac{\mathrm{i}rc_{\text{SW}}}{4}a^5\sum_x \overline{\psi}(x)\sigma_{\mu\nu}F^{\mu\nu}(x)\psi(x)$$

in which, $F^{\mu\nu}$ is a lattice version of the colour field tensor, and is typically given by the clover-leaf expression:

$$gF_{\mu\nu}(x) = \frac{1}{4a^2}\sum_{\text{plaquettes}}\frac{1}{2\mathrm{i}}\left(U^{\square}_{\mu\nu}(x) - \left(U^{\square}_{\mu\nu}\right)^\dagger(x)\right)$$

which is usually employed because it is a nearest neighbour quantity. At tree level, the value of the coefficient c_{SW} is 1 (Sheikholeslami *op.cit.*) however, non perturbative measurements have shown it to be substantially different (Lüscher, 1996). The bare coupling dependence from these calculations is empirically:

$$c_{\text{SW}} = \frac{1 - 0.656g_0^2 - 0.152g_0^4 - 0.054g_0^6}{1 - 0.922g_0^2}$$

which yields a value of 1.61387 for β6.2.

1.7 Mean Field Improvement

Lepage and Mackenzie (1993) noticed that the relation between the lattice and continuum gauge fields:

$$U_\mu(x) \equiv \mathrm{e}^{\mathrm{i}agA_\mu(x)}$$

is spoiled by tadpole diagrams arising from quantum corrections to higher order terms of this expansion. Specifically, the relation when expanded doesn't converge to the continuum analogue with vanishing lattice spacing:

$$U_\mu(x) \not\to \ 1 + \mathrm{i}gaA_\mu(x)$$

Lepage and Mackenzie argue that if the first form is used, large renormalizations between the bare lattice coupling and the continuum coupling will occur. This leads to large coefficients for perturbative expansions in the lattice couplings, *i.e.* they converge poorly. The actual relation is:

$$U_\mu(x) = u_0\left(1 + \mathrm{i}gaA_\mu(x)\right)$$

They suggest that much better behaviour of loop corrections is obtained if $U_\mu(x)/u_0$ is used as the lattice approximation of the continuum field.

The mean field improvement programme is to divide the gauge links by the mean value of the links, u_0. Gauge invariance is preserved if u_0 is a constant. A common definition is:

$$u_0^4 = \left\langle \frac{1}{3}\mathrm{Tr}U^{\square}_{\mu\nu} \right\rangle$$

This can be achieved by dividing the links by u_0 or by rescaling κ and c:

$$\kappa \to \tilde{\kappa} = \kappa u_0$$
$$c \to \tilde{c} = c/u_0^3$$

1.8 Quenching

One doesn't simulate the anti-commuting Grassmann variables directly. Techniques have recently been discovered that allow one to do this (Creutz, 1998), but in general these are far too difficult to be practicable. The variables can however, be integrated out analytically if the action is bilinear in them, by making use of the properties:

$$\int \mathrm{d}\psi_i = 0$$

$$\int \mathrm{d}\psi_i \ \psi_i = 1 \qquad \text{No summation over } i$$

$$\{\psi_i, \psi_j\} = \{\mathrm{d}\psi_i, \psi_j\} = \{\mathrm{d}\psi_i, \mathrm{d}\psi_j\} = 0 \qquad \forall i, j$$

The generating functional:

$$\mathcal{Z}\left[\sigma, \overline{\sigma}, J_\mu\right] = \int \mathfrak{D}\psi\mathfrak{D}\overline{\psi}\mathfrak{D}U_\mu \ \exp\left\{-\int \mathrm{d}^4x \ \left[\mathcal{L}(\overline{\psi}, \psi) + \overline{\sigma}(x)\psi(x) + \overline{\psi}(x)\sigma(x)\right] + U_\mu(x)J_\mu(x)\right\}$$

becomes:

$$\mathcal{Z}\left[\sigma, \overline{\sigma}, J_\mu\right] = \int \mathfrak{D}U_\mu \ (\mathrm{Det}M) \exp\left\{-\sum_{xy} \overline{\sigma}(x)M^{-1}(x,y)\sigma(y) + \sum_x \ U_\mu(x)J_\mu(x) + S_{\text{Gauge}}\right\}$$

in which $M(x,y)$ is the kernel of the particular fermion action one is using. It is known usually as the fermion matrix. It is a functional of the link variables only. One can view the procedure as giving rise to a modification of the gluon action:

$$S_{\text{Gluon}} \longrightarrow S_{\text{Gluon}}[U] - \ln \text{Det} M[U] = S_{\text{Gluon}} - \text{Tr} \ln M[U] \stackrel{=}{\text{def}} S_{\text{Effective}}$$

One sees that any quantity one now can calculate is a function of the link variables only.

Typically one wishes to calculate combinations of pairs of quark fields. Each pair will introduce a factor of $G = M^{-1}$ into the gauge integration.

$$\langle \Omega \,|\, \top \psi(y_1)\overline{\psi}(x_2) \ldots \psi(y_n)\overline{\psi}(y_n) \perp |\, \Omega \rangle = \int \mathfrak{D}U \; \mathrm{e}^{-S[U]} \; \left[\varepsilon^{z_1 \cdots z_n}_{y_1 \cdots y_n} G(z_1, x_1) \ldots G(z_n, x_n)\right]$$

where the ε symbol is 1 if the upper indices are an even permutation of the lower ones, -1 if the permutation is odd, and zero otherwise. The path integral over link variables is often notated

$$\left\langle \varepsilon^{z_1 \cdots z_n}_{y_1 \cdots y_n} G(z_1, x_1) \ldots G(z_n, x_n) \right\rangle_{S_{\text{Effective}}}$$

to emphasis that it is a weighted average over one variable and to show the action used in the weighting. For the Quenched approximation, the effective action becomes the pure gauge action, S_{Gluon}.

One calculates the integral by Monte Carlo methods. If one has a way of generating configurations of the gauge fields with probability:

$$P[U_j] = \frac{1}{Z} \exp \; -S^{\text{Eff}}[U_j]$$

where each configuration is labelled as U_j, then one can estimate the integral by the sample mean:

$$\overline{\mathcal{O}} = \frac{1}{N_{\text{Configuration}}} \sum_j \mathcal{O}[U_j]$$

The technical details of generating configurations with this distribution are outwith the scope of this thesis. One can see that the calculation of the fermion determinant, which will typically have to be done many times before an acceptable configuration is found, is of considerable cost because it is very non-local. One approach is to set the determinant equal to a constant. This is called the Quenched approximation and corresponds to neglecting the effects of virtual quark loops. One does not know the effect this has on the accuracy of one's simulations. One does know that the different calculated quantities give different values for the lattice spacing. This is believed to be because the strong coupling runs differently in the real world than it does in the quenched theory. It is only recently that computer resources have become sufficiently powerful to allow for partial unquenching. All calculation in this work were made in the quenched approximation.

1.9 The Continuum Limit

So far I have constructed a discrete version of the QCD action, and have observed that the action reduces to the continuum version in the limit of vanishing lattice spacing.

However there are an infinite number of discrete actions which have the same naive continuum limit. Indeed I shall make use of this ambiguity in the improvement programmes, and have already done so in constructing the Wilson action. But there is no reason, *a priori,* why

the discrete theory should possess a continuum limit corresponding to QCD. Let η be some observable with dimension d_η, and let $\eta^\#$ be the corresponding dimensionless lattice quantity, which depends on the bare parameters of the theory. If the theory possesses a continuum limit, then:

$$\eta\left(g_0, a\right) = \left(a^{-1}\right)^{d_\eta} \eta^\#\left(g_0\right)$$

approaches a finite limit as $a \to 0$ if g_0 is tuned with a in an appropriate way, with $g_0(a)$ approaching the critical coupling g_0^*

$$\eta\left(g_0(a), a\right) \stackrel{a\to 0}{\longrightarrow} \eta_{\text{physical}}$$

Therefore, if the functional dependence of $\eta^\#$ on g_0 is known, one can determine $g_0(a)$ from the first equation for sufficiently small a by fixing the left hand side at its physical value. This determines g_0 as a function of $a\left(\eta_{\text{physical}}\right)^{1/d_\eta}$. For finite lattice spacing the functional dependence of $g_0(a)$ will differ for differing observables. For sufficiently small a however, a universal function should exist. This is scaling and is guaranteed to occur near critical points.

Suppose the existence of the continuum limit has been established. One wants to know whether it is QCD or not. In the case of QCD one can actually determine the functional dependence of g_0 on a for sufficiently small a. Then, the dependence of any lattice observable on the bare coupling near criticality will be known and can be used as a signal for the approach of the continuum. In actual numerical calculations on a finite lattice there will in general only be a narrow region in coupling constant space where scaling exists — the scaling Window. If g_0 and therefore a becomes too small the physics one wishes to simulate won't fit on the lattice — finite size effects. Conversely, if g becomes too big to account for small scale fluctuations one leaves the scaling region.

1.10 Practicable lattices

Assuming one is in the continuum region, current lattices have inverse lattice spacings in the range of 1.5 to 3.5 GeV (0.13 fm to 0.056 fm), and volumes between 12^3 and 24^3 *i.e.* $(1.5\text{ fm})^3$ and $(1.8\text{ fm})^3$. The Compton wavelength of the lightest meson, the pion, is 1.5 fm, and so one can see that current lattices are roughly the same size as the pion. One would expect considerable finite size effects from the pion wrapping around the lattice and interfering with itself. The direct solution, lattices much larger than the Compton wavelength of the lightest state is not feasible with to-day's computers. Instead, the indirect solution of simulating heavier quarks than are required and then extrapolating to the physical regime is employed. This has the additional advantage of making the fermion matrix inversion quicker. The hopping parameter values that are typically employed are around those that correspond to the strange quark. The bare quark mass is defined as:

$$am_0 = \frac{1}{2}\left(\frac{1}{\kappa} - \frac{1}{\kappa_{\text{critical}}}\right)$$

in which κ_{critical} is the value of the hopping parameter corresponding to quark mass of zero. In the free theory this is 1/8. Although κ_{critical} can be calculated perturbatively, it is usually measured on the lattice by determining the pseudo-scalar mass at various κ 's. The Partially

Conserved Axial-vector Current relation relates the mass of the light degenerate pseudo-scalar to the mass of its constituent quarks:

$$m_{\mathrm{PS}}^2(m_{\mathrm{q}}) \propto m_{\mathrm{q}}$$

or on the lattice:

$$m_{\mathrm{PS}}^2(\kappa_{\mathrm{q}}) = a_{\mathrm{PS}} \left(\frac{1}{\kappa} - \frac{1}{\kappa_{\mathrm{critical}}} \right)$$

the value of $\kappa_{\mathrm{critical}}$ being the intercept of m_{PS}^2 against $1/\kappa$

There is also a problem at the other extreme. If one tries to simulate particles that are too heavy then their Compton wavelength is comparable with the lattice spacing and then the lattice is not fine enough to describe their structure: they are so heavy they fall through the lattice. For example, $\mathrm{B_s}$= 5369 MeV, with a Compton size of roughly 0.36 fm; $\Upsilon \approx$ 9460 MeV, 0.21 fm.

There are various ways round the problem. For Heavy-Light systems one can use the static approximation, or the Heavy Clover formulation (El-Khadra 1997), or extrapolate the Wilson-SW data to the B. The work reported in this thesis makes use of a non-relativistic approximation of the Dirac equation.

1.11 Rationale for a Non Relativistic approach

If the typical momentum scale of quarks inside hadrons is $\mathcal{O}(\Lambda_{\mathrm{QCD}})$ † then the b and c quarks inside the Υ and η_{c} systems have $v^2 \ll c^2$ and so can be described by a non-relativistic formulation with leading relativistic corrections included.

1.12 Building NRQCD

I first estimate the sizes of the fields involved in terms of m and v. Note that one can have the electric and magnetic fields appearing separately because the formulation is not Lorentz invariant. This treatment follows Lepage *et al.* (1992).

1.12.1 Sizes of Fields

The number operator for heavy quarks:

$$\int \mathrm{d}^3x \; \psi^\dagger(x)\psi(x)$$

has an expectation value near 1 for a quarkonium meson. The quark in such a meson is localized within a region of size $\Delta x \sim 1/p$, and so one estimates:

$$\int \mathrm{d}^3x \sim \frac{1}{p^3}$$

and therefore

$$\psi^\dagger(x)\psi(x) \sim p^3 \qquad \psi \sim p^{3/2}$$

† $\Lambda_{\mathrm{QCD}} \sim 150$ MeV

The Kinetic Energy operator

$$\int \mathrm{d}^3x\ \psi^\dagger(x)\frac{\boldsymbol{D}^2}{2m}\psi(x)$$

has expectation K and so one estimates:

$$\boldsymbol{D} \sim \sqrt{2mK} \sim p$$

Using the field equation:

$$\left(\mathrm{i}D_t + \frac{\boldsymbol{D}^2}{2m}\right)\psi = 0$$

and so:

$$D_t \sim \frac{\boldsymbol{D}^2}{2m} \sim K$$

From the definitions of the Chromo-electric and Chromo-magnetic fields:

$$[D_t, \boldsymbol{D}]\,\psi = \mathrm{i}g\boldsymbol{E}\psi$$

one estimates

$$Kp \sim g\boldsymbol{E} \quad i.e.\ g\boldsymbol{E} \sim m^2v^3$$

and from

$$[D_i, D_j]\,\psi = -\mathrm{i}g\epsilon_{ijk}B^k\psi$$

one estimates

$$g\boldsymbol{B} \sim m^2v^4$$

1.12.2 Building the Action

One uses the lattice as a regulator to exclude relativistic momenta. One can then describe the quark dynamics by the Schrödinger equation. The leading terms are:

$$S_0 = \int \mathrm{d}^4x\ \psi^\dagger(x)\left[\mathrm{i}D_t + \frac{\boldsymbol{D}^2}{2m}\right]\psi(x)$$

One now add corrections that respect the symmetries of the original theory: gauge invariance, parity, rotational symmetry, unitarity, &c.. The corrections should also be local. The bilinear terms are:

$$\begin{aligned}\delta\mathcal{L} = {} & c_1\frac{1}{m^3}\psi^\dagger\boldsymbol{D}^4\psi \\ & + c_2\frac{g}{m^2}\psi^\dagger\left(\boldsymbol{D}\cdot\boldsymbol{E} - \boldsymbol{E}\cdot\boldsymbol{D}\right)\psi \\ & + c_3\frac{\mathrm{i}g}{m^2}\psi^\dagger\boldsymbol{\sigma}\cdot\left(\boldsymbol{D}\wedge\boldsymbol{E} - \boldsymbol{E}\wedge\boldsymbol{D}\right)\psi \\ & + c_4\frac{g}{m}\psi^\dagger\left(\boldsymbol{\sigma}\cdot\boldsymbol{B}\right)\psi\end{aligned}$$

to $\mathcal{O}(v^4)$. No terms involving time derivatives of the quark field are included. Such terms complicate the evaluation of the Green's functions. They can be eliminated by redefining the quark fields, so that factors of $\mathrm{i}D_t$ are replaced by factors of $-\boldsymbol{D}^2/2m$ as follows from the lowest order field equation. Such transformations do not affect physical quantities such as masses &c..

Four fermion contact interactions involving quark and antiquark are also possible:

$$\begin{aligned}\delta\mathcal{L}_{\text{contact}} &= d_1 \frac{1}{m^2}\psi^\dagger\chi\cdot\chi^\dagger\psi \\ &= d_2 \frac{1}{m^2}\psi^\dagger\boldsymbol{\sigma}\chi\cdot\chi^\dagger\boldsymbol{\sigma}\psi\end{aligned}$$

Although these appear to be suppressed only by a single power of v, similar interactions do not appear in the relativistic theory and therefore such terms can only appear at one loop order. Thus the coefficients:

$$d_j \sim \mathcal{O}(\alpha_S^2(\pi/a))$$

making these interactions considerably less important than the bilinears.

Four fermion operators can also couple to coloured states. Colour singlet mesons are affected by such interactions as the meson can become coloured by emitting a virtual gluon. However, as gluon emission is suppressed by v^2, these terms are not as important as the bilinears.

The values of the coupling coefficients are determined by matching with full QCD. One gets

$$\begin{aligned}c_1 &= \frac{1}{8} \\ c_2 &= \frac{1}{8} \\ c_3 &= \frac{1}{8} \\ c_4 &= \frac{1}{2}\end{aligned}$$

to tree level. c_1 comes from looking at the non-relativistic dispersion relation. c_2 and c_3 come from looking at the $\mathcal{O}(g)$ amplitude for scattering a quark off a static electric field, and c_4 comes from considering the amplitude for scattering a quark off a static vector potential.

1.12.2.1 Continuum limit.

The couplings c_j all depend on the ultraviolet cut off Λ. One can't take the cut off to infinity because the couplings contain divergences of the form:

$$\alpha_{\text{strong}}(a)\frac{\Lambda}{m}$$

These make perturbation theory useless if Λ is made too large; practicably one is limited to $\Lambda \sim 1/m$. This is nothing to worry about — NRQCD is an effective theory, valid for only a certain regime. The cut-off dependence of the couplings is just a reflection of the fact that one can't use it to simulate all physics. One doesn't need to take the coupling to infinity (or equivalently, the lattice spacing to zero) if one can demonstrate flat scaling of the results over a reasonable range of lattice spacings. If this happens, one has corrected for the finite lattice spacing and one has essentially continuum results.

1.12.2.2 Removal of mass term.

One eliminates the mass term $m\psi^\dagger\psi$ from the Lagrangian to allow one's mesons to fit on the lattices one has available. One can do this because in a non-relativistic theory such a term only fixes the zero-point energy: it has no effect on mass splittings, wave functions &c..

1.13 Discrete version of the NRQCD action

Here is the continuum NRQCD action in Euclidean space:

$$\mathcal{L}_{\text{Euclidean}} = \psi^{\dagger}(x)\left(D_t - \frac{1}{2m}\boldsymbol{D}^2\right)\psi(x) + \mathcal{L}_{\text{Corrections}}$$

To contruct a discrete version, I follow Lepage *et al.* (1992). Considering at first just the leading term, the kernel of the action is

$$\left(D_t - \frac{1}{2m}D^2\right)$$

One knows that the Green's function is the inverse of the kernel:

$$KG = \mathbb{1}^{(4)}$$

and so one has:

$$\left(\Delta_t - \frac{1}{2m}\Delta^{(2)}\right)G = \mathbb{1}^{(4)}$$

If one chooses the Forward Euler difference for the time difference above, one can write:

$$U_4(\boldsymbol{x},t)G(\boldsymbol{x},t+a\widehat{4}) - G(\boldsymbol{x},t) - \frac{1}{2m}\Delta^{(2)}G(\boldsymbol{x},t) = \mathbb{1}^{(4)}$$

Rearranging this and labelling the 4 dimensional delta function as *source*

$$G(\boldsymbol{x},t+a\widehat{t}) = U_4^{\dagger}(x)\left(\mathbb{1} - aH_0\right)G(\boldsymbol{x},t) + \textit{source}$$

in which

$$H_0 = -\sum_j \frac{1}{2m}\Delta_j^{(2)}$$

is the kinetic energy operator. The Green's function is zero before and on the timeslice on which the source lives. However, there is a problem with this as it stands. Let $G^{\#}(\boldsymbol{x},t)$ be the solution of the finite difference equation above, and $\widetilde{G}(\boldsymbol{x},t)$ be the solution of the continuum analogue. One can write the lattice evolution as

$$\boldsymbol{G}^{\#}_{t+1} = \mathbf{A}_t\boldsymbol{G}^{\#}_t$$

in which $\mathbf{A}_t$ is the evolution matrix, taking the Green's function at timeslice t to timeslice $t+1$, and I have assembled the Green's functions into vectors indexed by site. The error vector:

$$\mathcal{E}_t = \boldsymbol{G}^{\#}_t - \widetilde{\boldsymbol{G}}_t$$

also obeys the lattice evolution equation:

$$\mathcal{E}_{t+1} = \mathbf{A}_t\mathcal{E}_t$$

Smooth evolution, in which the errors remain bounded, is ensured if the eigenvalues of the evolution matrix have absolute magnitude less than or equal to 1, (for example, see Richtmyer, 1967). One can calculate the eigenvalues of $\mathbf{A}_t$ for the free theory:

$$\lambda_j = 1 - \frac{4}{2m}\sin^2\frac{j\pi}{2N_{\text{sites}}}$$

i.e. , one has stability if

$$\left|1 - \left(\frac{2}{m}\right)\sin^2\frac{j\pi}{2N_{\text{sites}}}\right| \leq 1$$

that is, $1 < m$. In three dimensions, $3 < m$. The interaction would make little difference to this conclusion. The origin of this instability is the non-unitarity of one's lattice evolution operator: the norm of the solution grows monotonically with time and is increasingly dominated by high-momentum modes. One can't solve the problem by using higher order derivatives, though I shall employ them for other reasons. Nor can one use implicit methods † as they entail matrix inversions which are prohibitively expensive. Alternating Direction methods are not of use because of the non-abelian nature of the theory. The formal solution of the equation:

$$G(\boldsymbol{x}, t) = \exp(-tH) \times \textit{source}$$

is not of use because the sparse Hamiltonian doesn't remain sparse under exponentiation. The solution I adopt is to raise the evolution matrix to a power ¶ thus:

$$G(\boldsymbol{x}, t + a\hat{4}) = U_4^\dagger(x) \left[\mathbb{1} - \frac{1}{n} H_0\right]^n G(\boldsymbol{x}, t)$$

This form of the evolution equation has better stability properties, *i.e.* the stability criterion is less restrictive. The procedure corresponds to a change in the Lagrangian to:

$$\psi^\dagger \left(\Delta_t + H_0 - \frac{1}{4} H_0^2\right) \psi$$

for the case $n = 2$. Actually all I am doing here is including more terms from the formal solution:

$$\begin{aligned} G(\boldsymbol{x}, t) &= \exp(-tH) \times \textit{source} \\ &= U_4^\dagger(x) \left[\mathbb{1} - tH_0 + \frac{1}{2!} t^2 H_0^2 + \cdots\right] \times \textit{source} \end{aligned}$$

I'm not making the evolution equation completely unitary, just more so than before. The importance of the stability criterion is given by a theorem due to Lax:

> Given a properly posed initial boundary value problem, and a finite difference approximation to it that satisfies the consistency condition, the stability is the necessary and sufficient condition for convergence.

1.14 Improvement

The last four terms in the NRQCD action have size $\mathcal{O}(mv^4)$. Any discretization error bigger than this must be eliminated so that the evolution be properly accurate to $\mathcal{O}(mv^4)$.

There is no point improving the clover-leaf approximation to the colour field tensor, as it only appears in the highest order terms of the Lagrangian. Similarly the central difference operator only appears in the $\mathcal{O}(mv^4)$ terms and so doesn't require improvement. To see if the discretization errors of the Laplacian and the forward Euler differences indicate improvement, I write out the first few terms of the modified evolution equation:

---

† those in which the integral equations are simulated

¶ actually just the Hamiltonian part as the link variable $U_4^\dagger$ doesn't contribute to the numerical instability

$$G^{t+1} = \left[\mathbb{1} + \frac{\Delta^{(2)}}{2m} + \frac{\left(\Delta^{(2)}\right)^2}{4m^2} \cdot \frac{1}{2!} \cdot \frac{n!}{n^2(n-2)!} + \cdots\right] G^t$$
$$= \left[\mathbb{1} + \frac{\Delta^{(2)}}{2m} + \frac{\left(\Delta^{(2)}\right)^2}{2!4m^2} - \frac{\left(\Delta^{(2)}\right)^2}{2!n4m^2} + \cdots\right] G^t$$

Comparing this with the exact two-level difference formula:

$$G^{t+1} = \exp \frac{2}{a} \sum_{j=1}^{3} \left(\sinh^{-1} \frac{1}{2} \sqrt{\Delta_j^{(2)}}\right)^2 \times G^t$$

where the argument of the exponential is an exact expression for the Laplacian. This will allow me to see which terms require improvement. Expanding this:

$$G^{t+1} = \Bigg\{ \mathbb{1}$$
$$+ \frac{1}{2m} \left[\sum_j \Delta_j^{(2)} - \frac{1}{12} \sum_j \left(\Delta_j^{(2)}\right)^2 + \frac{1}{90} \sum_j \left(\Delta_j^{(2)}\right)^3 - \cdots\right]$$
$$+ \frac{1}{4m^2} \frac{1}{2!} \left[\left(\sum_j \Delta_j^{(2)}\right)^2 + \cdots\right] \Bigg\} \times G^t$$

which I write as:

$$G^{t+1} = \Bigg\{ \mathbb{1}$$
$$+ \frac{1}{2m} \left[\Delta^{(2)} - \frac{1}{12} \Delta^{(4)} - \cdots\right]$$
$$+ \frac{1}{4m^2} \frac{1}{2!} \left[\left(\Delta^{(2)}\right)^2 + \cdots\right] \Bigg\} \times G^t$$

I have set:

$$\Delta^{(4)} = \sum_j \left(\Delta^{(2)}\right)^2$$

The additional terms in the first square bracket are the improvements to the Laplacian operator. The terms appearing in the the second square brackets correspond to improvements in the time derivative. The Laplacian improvement term:

$$\frac{1}{12} \frac{\Delta^{(4)}}{2m} \sim \frac{a^2 \left(mv^2\right)^2}{m} \sim mv^4$$

and so requires improvement. One sees that the time derivative improvement term is already present in the evolution equation, but is accompanied by a term of the same size that is a relic of the introduction of the n parameter. Its size is

$$\frac{a \left(\Delta^{(2)}\right)^2}{2!n4m^2} \sim mv^4$$

1.15 Final choice of Evolution Equation

I choose the evolution equation to be:

$$G(\boldsymbol{x},t+a)=\left(1-a\frac{\delta H}{2}\right)\left(1-a\frac{H_0}{2n}\right)^n U_4^\dagger(x)\left(1-a\frac{H_0}{2n}\right)^n\left(1-a\frac{\delta H}{2}\right)G(\boldsymbol{x},t)+source$$

where

$$H_0=-\frac{1}{2m}\sum_{j=1}^{3}\Delta_j^{\mathrm{F}}\Delta_j^{\mathrm{B}}$$

$$\begin{aligned}\delta H=&-\frac{1}{8m^3}\left(\Delta^{(2)}\right)^2\\&+\frac{ig}{8m^2}\left(\boldsymbol{\Delta}\cdot\boldsymbol{E}-\boldsymbol{E}\cdot\boldsymbol{\Delta}\right)\\&-\frac{g}{8m^2}\boldsymbol{\sigma}\cdot\left(\boldsymbol{\Delta}\wedge\boldsymbol{E}-\boldsymbol{E}\wedge\boldsymbol{\Delta}\right)\\&-\frac{g}{2m}\boldsymbol{\sigma}\cdot\boldsymbol{B}\\&+\frac{a^2}{24m}\Delta^{(4)}\\&-\frac{a}{16nm^2}\left(\Delta^{(2)}\right)^2\end{aligned}$$

The difference operators act on all fields to their right. The $(\boldsymbol{\Delta}\cdot\boldsymbol{E}-\boldsymbol{E}\cdot\boldsymbol{\Delta})$ term may be simplified as its net effect is to differentiate the $\boldsymbol{E}$ field alone. However, this requires a new definition of finite difference when acting on the $\boldsymbol{E}$ field alone, in order to preserve gauge covariance.

$$\boldsymbol{\Delta}\cdot\boldsymbol{E}\stackrel{=}{\mathrm{def}}\frac{1}{2a}\sum_j U_j(x)E^j(x+a\hat{j})U_j^\dagger(x)-U_j^\dagger(x-a\hat{j})E^j(x-a\hat{j})U_j(x-a\hat{j})$$

I calculate the electric and magnetic fields from a slightly different definition of the colour field tensor from that employed in the Sheikholeslami-Wohlert action:

$$gF_{\mu\nu}(x)=\frac{1}{4a^2}\sum_{\text{plaquettes}}\mathbb{X}\left(U^{\square}_{\mu\nu}(x)\right)$$

in which the operator $\mathbb{X}$ forces the tensor to be traceless and Hermitian. It is defined:

$$\mathbb{X}\left[m\right]\stackrel{=}{\mathrm{def}}\frac{m-m^\dagger}{2\mathrm{i}}-\frac{1}{3}\Im\mathfrak{m}\left[\mathrm{Tr}\ m\right]$$

The Chromo-electric and Chromo-magnetic fields are in terms of the field tensor:

$$\begin{aligned}E^j(x)&=F_{j4}(x)=-F_{4j}(x)\\B^j(x)&=-\frac{1}{2}\varepsilon_{jkl}F_{kl}\end{aligned}$$

The evolution equation so defined is symmetric with respect to time reversal.

1.16 Heavy-Light Physics

I have motivated NRQCD in terms of the physics of heavy-heavy systems. I now ask if it is applicable to heavy-light systems. Again assuming the typical momentum scale is of the order of Λ_{QCD}:

$$p_Q \sim p_q \sim \Lambda_{QCD}$$

and thence:

$$\frac{v_Q}{c} \sim \frac{\Lambda_{QCD}}{m_Q}$$

and one sees that $v_Q \sim 0.1c$ for the b in B systems, *i.e.* it is actually less relativistic than the b in Υ systems.

One can perform a power counting analysis for heavy-light systems as well:

$$D_t \sim \boldsymbol{D}^2 \sim \Lambda_{QCD}$$

and so:

$$\frac{\boldsymbol{D}^2}{2m_Q} \sim \frac{\Lambda_{QCD}^2}{m_Q}$$

and

$$\boldsymbol{E} \sim \boldsymbol{B} \sim \Lambda_{QCD}^2$$

so that

$$\frac{\boldsymbol{\sigma} \cdot \boldsymbol{B}}{m_Q} \sim \frac{\Lambda_{QCD}^2}{m_Q}$$

and

$$\frac{\boldsymbol{\sigma} \cdot \boldsymbol{D} \wedge \boldsymbol{E}}{m_Q^2} \sim \frac{\Lambda_{QCD}^2}{m_Q^2}$$

and one sees that for heavy-light systems, the NRQCD Lagrangian is a $1/m_Q$ expansion, in contradistinction to the heavy-heavy case, in which terms at different order in $1/m_Q$ appeared at the same order in v_Q^2. The leading term is D_t. The $\mathcal{O}(1/m_Q)$ terms are the kinetic operator and $\boldsymbol{\sigma} \cdot \boldsymbol{B}$ spin coupling. These are the first terms to know about heavy flavour and its spin. Any splitting that requires this knowledge will therefore appear first to order $1/m_Q$.

1.17 Simulating Mesons

In Quantum Chromo-Dynamics, the theory is formulated in terms of quark fields. However, as the theory exhibits confinement, quarks do not appear in isolation, only in colourless combinations of two, forming mesons, and three, forming baryons.

The particle states of Nature are characterized by their transformation properties. In seeking to describe them on the lattice one must select operators with the same transformation properties. In fact, there is no one-to-one correspondence between the operators and physical states. In particular, the absence of a good radial quantum number ¶ means that a state created on the lattice will be sum of radial excitations sharing the same quantum numbers. The simplest operator is the point operator:

$$\mathcal{O}(x) = \overline{\chi}^i_\alpha(x)\Gamma_{\alpha\beta}\delta^{ij}\psi^j_\beta(x)$$

where the two quark flavours have fields χ and ψ, and Γ is a Dirac matrix determining the spin structure. Such operators create mesons in the S wave. To construct operators for states in the

¶ *i.e.* one that corresponds to a symmetry

Table 1.1 Meson Operators

$^{2S+1}L_J$	J^{PC}	Operator
$^1S_0$	0^{-+}	$\bar{l}h$
$^3S_1$	1^{--}	$\bar{l}\sigma h$
$^1P_1$	1^{+-}	$\bar{l}\Delta h$
$^3P_0$	0^{++}	$\bar{l}\sigma \cdot \Delta h$
$^3P_1$	1^{++}	$\bar{l}\sigma \wedge \Delta h$
$^3P_2(T)$	2^{++}	$\bar{l}(\sigma_i\Delta_j + \sigma_j\Delta_i)h$
$^3P_2(E)$	2^{++}	$\bar{l}(\sigma_i\Delta_i - \sigma_j\Delta_j)h$

P wave, one needs to ensure they have the opposite parity transformation properties. This can only be achieved by point split operators, and to ensure gauge invariance, this means that the quark fields must be joined by gauge links. The operators I shall be using are shown above. (Thacker and Lepage, 1991):

One labels the states with the J^{PC} quantum numbers. This is only appropriate for degenerate mesons. For heavy-light states, which are charged, the charge conjugation number is not defined. However, one can use the same operators. This means that the states created by the $^3P_1$ and $^1P_1$ operators will be a mixture of the energy eigenstates with quantum numbers $J^P = 1^-$. I shall discuss the extraction of the numbers later. There are two operators with the correct quantum numbers for the $^3P_2$ state: these come from the T and E representations of the lattice cubic group. I shall refer to them as $^3P_2(T)$ and $^3P_2(E)$.

1.18 Smearing

A local meson operator as described above will couple to the ground state and radial excitations with the appropriate quantum numbers. Current lattice calculations do not have sufficient statistics to allow satisfactory determination of these. In particular, the signal may have descended into noise by the time the excited state contributions have died out. The object of smearing is to increase the overlap of the operator with the ground state. It amounts to a spatial extension of the meson operator, with the necessary symmetry properties. The function that is chosen to achieve this extension is the spatial propagator of a colour singlet particle.

$$J(\boldsymbol{x},\boldsymbol{y}) = \left\langle \chi_i(\boldsymbol{x})\chi_i^\dagger(\boldsymbol{y}) \right\rangle$$

One finds this by inverting the three-dimensional scalar action:

$$\left\langle \chi_i(\boldsymbol{x})\chi_i^\dagger(\boldsymbol{y}) \right\rangle = \left\langle K^{-1}(\boldsymbol{x},\boldsymbol{y}) \right\rangle$$

where the kernel is:

$$K(\boldsymbol{x},\boldsymbol{y}) = \delta(\boldsymbol{x},\boldsymbol{y}) - \kappa\Delta^2(\boldsymbol{x},\boldsymbol{y})$$

Rather than calculate this exactly, the iterative Jacobi algorithm is used in its critical regime. The point is that one retains the required symmetries of the solution, but can make it physically large quickly. One can smear the Green's function either at the source or the sink. Source smearing is achieved by using the smearing function as input to the solver, and sink smearing by right operating on the Green's functions with the Jacobi operator:

$$G^{\mathrm{SL}}(\boldsymbol{x},\boldsymbol{y}) = J^{(N)}(\boldsymbol{x},\boldsymbol{y})G^{\mathrm{LL}}(\boldsymbol{y},\mathbf{o})$$

where :

$$J^{(N)}(\boldsymbol{x},\boldsymbol{y}) = \delta(\boldsymbol{x},\boldsymbol{y}) + \sum_{n=1}^{N} \left(\kappa D^2(\boldsymbol{x},\boldsymbol{z})\right)^n J^{(0)}(\boldsymbol{z},\boldsymbol{y})$$

invariably $J^{(0)}(\boldsymbol{x},\boldsymbol{y}) = \delta(\boldsymbol{x},\boldsymbol{y})$ so that:

$$J^{(N)}(\boldsymbol{x},\boldsymbol{y})G^{\mathrm{LL}}(\boldsymbol{y},\mathbf{o}) = G^{\mathrm{LL}}(\boldsymbol{x},\mathbf{o}) + \sum_{n=1}^{N} \left(\kappa D^2(\boldsymbol{x},\boldsymbol{z})\right)^n G^{LL}(\boldsymbol{z},\mathbf{o})$$

This is usually implemented as an iterative scheme:

$$J^{(N)}(\boldsymbol{x},\boldsymbol{y}) = \delta(\boldsymbol{x},\boldsymbol{y}) + \kappa D^2(\boldsymbol{x},\boldsymbol{z})J^{(N-1)}(\boldsymbol{z},\boldsymbol{y})$$

so that :

$$J^{(N)}(\boldsymbol{x},\boldsymbol{y})G^{\mathrm{LL}}(\boldsymbol{y},\mathbf{o}) = G^{\mathrm{LL}}(\boldsymbol{x},\mathbf{o}) + \kappa D^2(\boldsymbol{x},\boldsymbol{z})J^{(N-1)}(\boldsymbol{z},\boldsymbol{y})G^{\mathrm{LL}}(\boldsymbol{y},\mathbf{o})$$

To avoid numerical overflow caused by the norm of the Jacobi function growing, one should normalise the smearing function as $\mathrm{e}^{-4N(\kappa-\kappa_{\mathrm{Jacobi}})}$ afterwards, or per-iteration $\mathrm{e}^{-N(\kappa-\kappa_{\mathrm{Jacobi}})}$. The value is empirically determined (Baxter, 1993) as $\kappa_{\mathrm{Jacobi}} \approx 0.185$

1.19 Fuzzing

Lacock and Michael (1995) suggest a different procedure.

They first make *fat links* from the normal gauge fields by the following iterative formula:

$$U'_j(x) = cU_j(x) + \sum_{i\neq j}\left[U_i^{\mathrm{Staple}}(x, x+\widehat{j}) + U_{-i}^{\mathrm{Staple}}(x, x+\widehat{j})\right]$$

$$U_j(x) = \mathbf{P}U'_j(x)$$

in which $\mathbf{P}$ projects its argument back onto SU(3). These fat links are then used to create a *fuzzed* source by parallel transporting the quark fields a number of links N_{fuzz} along each axis using the fat links. Typically, N_{fuzz} is 5. The advantage of this procedure over smearing is that it separates two distinct processes. The quark independent part, the creation of the fat links, can be done once per configuration. As this is the computationally intensive part, it represents a considerable saving in computer time over the course of a large calculation. The quark dependent part, the parallel transport of the quark fields is relatively inexpensive. In Jacobi smearing, these two processes are in effect combined, and one is repeating the expensive iterative part for each quark propagator.

1.20 Hybrid method

This simply involves feeding fat links into the Jacobi algorithm. The idea is that this will allow one to achieve suitably sized smearing functions with far fewer iterations than would be

needed with a normal Jacobi method. It differs from the fuzzing method in that it creates a solid function rather than a hollow one. This was the method that was used in the calculations in this work.

1.21 Meson Correlators

Having decided upon the meson operators, one must now use them to create objects from which one can extract the numbers one wants to calculate. Consider:

$$c(\boldsymbol{p},t) = \sum_{\boldsymbol{x}} \langle \Omega | \mathcal{O}(\boldsymbol{x},t)\mathcal{O}^{\dagger}(\mathbf{o},0)|\Omega\rangle \, \mathrm{e}^{\mathrm{i}\boldsymbol{p}\cdot\boldsymbol{x}}$$

The periodic boundary conditions limit the allowed momenta to

$$\boldsymbol{p} = \frac{2\pi}{N}(n_x, n_y, n_z)$$

where N is the number of lattice sites per direction, and the n_j 's are integers, $0 \leq n_j < N$

Using the lattice completeness relation:

$$\mathbb{1} = \frac{1}{N^3}\sum_{S,k} \frac{1}{2E_S^{\#}(k)} |S(k)\rangle \langle S(k)| + \cdots$$

in which the sum is over all single meson states, the omitted terms being multiple particle states. Then:

$$\mathcal{O}(x) = \mathrm{e}^{aHt + \mathrm{i}\boldsymbol{p}\cdot\boldsymbol{x}}\mathcal{O}(0)\mathrm{e}^{-aHt - \mathrm{i}\boldsymbol{p}\cdot\boldsymbol{x}}$$

and the discrete lattice Dirac function:

$$\delta(q) = \frac{1}{N^3}\sum_{\boldsymbol{x}} \mathrm{e}^{\mathrm{i}\boldsymbol{q}\cdot\boldsymbol{x}}$$

One arrives at the expression:

$$c_{\mathcal{O}_1\mathcal{O}_2}(t;\boldsymbol{p}) = \sum_{S} \frac{\mathrm{e}^{-aE_s(\boldsymbol{p})t}}{2aE_s(\boldsymbol{p})} \langle \Omega|\mathcal{O}_1(0)|S(\boldsymbol{p})\rangle\langle S(\boldsymbol{p})|\mathcal{O}_2^{\dagger}(0)|\Omega\rangle$$

1.22 Analysis

One extract estimates of the mass of a particle by fitting the timesliced correlator to a decaying exponential $A\mathrm{e}^{-Et}$

1.22.1 Fitting

One performs the fit by choosing the parameters of the functional form $\{\Lambda_j\}$ to minimise the χ^2 statistic:

$$\chi^2 = \sum_{i,j=1}^{i,j=N} (y_j - y(x_j;\lambda)) \times \mathbf{Cov}^{-1}(x_j, x_i) \times (y_i - y(x_i;\lambda))$$

For reasons of numerical stability, the Correlation matrix :

$$\mathbf{Corr}(x_j, x_i) = \frac{\mathbf{Cov}(x_j, x_i)}{\sqrt{\mathbf{Cov}(x_j, x_j)\mathbf{Cov}(x_i, x_i)}}$$

is inverted, and then the inverse Covariance matrix is reconstructed. For uncorrelated data, the Covariance matrix reduces to the identity matrix, and the correlated χ^2 degenerates to the uncorrelated χ^2. (Or rather, for data that are believed to be uncorrelated, the off-diagonal entries of the covariance matrix are set to zero.) The covariance matrix has diagonal entries which are the uncertainties on the quantity, and skew-diagonal entries of the covariance between pairs of timeslices. The Covariance matrix is estimated by a Jack-knife method - see next section.

For highly correlated data, the covariance matrix may become singular. It will also become singular as its dimension approaches the size of the data set, N. The minimisation of the merit function is achieved through a Marquardt Levenberg algorithm. I invert the correlation matrix using an SVD algorithm.

1.22.2 Fit assessment

The Incomplete Gamma Function † is defined as:

$$Q(a, x) = \frac{1}{\Gamma(a)} \int_x^\infty \mathrm{d}t \; \mathrm{e}^{-t} t^{a-1} \tag{1.1}$$

Then $Q(\nu/2, \chi^2/2)$ is the probability that the χ^2 statistic should exceed the particular value appearing in the argument by chance, where ν is the number of degrees of freedom. If Q is very small for some particular data set, then the apparent discrepancies are probably due to the model being wrong, or the measurement errors are much larger than assumed.

The χ^2/N_{dof} statistic has expectation of 1 and standard deviation of $\sqrt{2/\nu}$.

1.22.3 Error Estimation

I use two methods to estimate the errors in the calculation. I require errors for the raw correlator data to enable me to do the minimisation, and errors on the fitted parameters.

1.22.4 The Bootstrap

The Bootstrap estimation of the uncertainty δq^{B} on a quantity q calculated from data

$$\mathcal{D} = \{d_1, d_2, \ldots, d_N\}$$

by means of some procedure

$$q \leftarrow \mathcal{D}$$

is given by

$$\delta q^{\mathrm{B}}_{\pm} = \frac{1}{2}(\delta^+ - \delta^-)$$

† Several quantities are known as the Incomplete Gamma Function, differing from one another by the coefficient: the one shown here is relevant for the purpose of fit quality assessment.

The upper and lower bounds, $\delta^{\pm}$, are given by:

$$\left|\{q_j^{\mathrm{B}} \in \mathcal{Q}^{\mathrm{B}} || q_j^{\mathrm{B}} < \delta^{\pm}\}\right| = \frac{N}{2}(1 \pm \text{confidence level})$$

where the confidence level is typically 68%. And where

$$\mathcal{Q}^{\mathrm{B}} = \{q_1^{\mathrm{B}}, q_2^{\mathrm{B}}, \ldots, q_{N_{\mathrm{B}}}^{\mathrm{B}}\}$$

and each element of this set is calculated in the normal manner from bootstrap datasets, $\mathcal{D}_j^{\mathrm{B}}$

$$q_j^{\mathrm{B}} \leftarrow \mathcal{D}_j^{\mathrm{B}}$$

These bootstrap datasets are assembled from the original dataset by drawing N data at random and with replacement from the original dataset.

Typically I use four times as many boot samples as original configurations.

1.22.5 The Jack-knife

The Jack-knife is a cognate to the bootstrap. The Jack-knife data sets are made by dropping each element of the original data set in turn; one ends up then with N such data sets. The quantity of interest is then calculated from each of the jack-knife data sets in each turn:

$$q_j^{\mathrm{J}} \leftarrow \{\mathcal{D}_j^{\mathrm{J}}\}$$

and the Jack-knife estimate of uncertainty in q is given by

$$\delta q^{\mathrm{J}} = \sqrt{\frac{N-1}{N}\sum_{j=1}^{N}(q_j^{\mathrm{J}} - \overline{q^{\mathrm{J}}})^2}$$

where the average over Jack-knife samples is given by:

$$\overline{q^{\mathrm{J}}} = \frac{1}{N}\sum_{i=1}^{N} q_j^{\mathrm{J}}$$

The coefficient is chosen so as to make the Jack-knife give the right answer when the data function is a sum - i.e. to be identical to the Sample Standard Deviation of the Mean. The Jack-knife estimate of the Covariance matrix is :

$$\mathbf{Cov}^{\mathrm{J}}(t_j, t_i) = \frac{(N-1)}{N}\sum_{k=1}^{N}[D_k^{\mathrm{J}}(t_j) - \overline{D^{\mathrm{J}}(t_j)}] \times [D_k^{\mathrm{J}}(t_i) - \overline{D^{\mathrm{J}}(t_i)}]$$

where $D_k^{\mathrm{J}}(t)$ is the data function calculated from the Jack-knife set labelled k, and $\overline{D^{\mathrm{J}}(t)}$ is the average over Jack-knife samples:

$$\overline{D^{\mathrm{J}}(t)} = \frac{1}{N}\sum_{i=1}^{N} D_i^{\mathrm{J}}(t)$$

1.22.6 Miscellaneous

The Jack-knife is used to calculate the covariance matrix for the data. The data to be fitted are averaged over configurations

$$A(t) \approx \langle A(t) \rangle$$

These data are the primary quantities in the analysis. They are typically meson correlators.

Estimates of secondary quantities are obtained as functions of these averages:

$$\mathcal{F}\left(\langle A(t) \rangle, \langle B(t) \rangle, \cdots\right)$$

rather than the other way round:

$$\left\langle \mathcal{F}(A(t), B(t), \cdots) \right\rangle$$

1.22.7 Concertina Analysis

The time dependence of the timesliced correlator data is given by a sum of decaying exponentials. I could only fit single exponentials to single correlators. In this case, the correct isolation of the ground state is of vital importance. I employed a concertina analysis to achieve this. This involves making a series of fits, systematically varying the initial timeslice whilst keeping the final timeslice fixed. I then search for stability in the fitted energies and also look for reasonable values of χ^2/N_{dof} . The rationale is the stable region or plateau in the fitted energy is that region where there is little or no contamination by excited states.

1.22.8 Ratio Fits

To determine some of the mass splittings I employ ratio fits, in which I fit a single exponential to the ratio of two correlators. The parameter controlling the exponential fall off in the leading term is the difference between the ground state energies of the two correlators.

The point of a ratio fit is that it *can* offer a way of reducing the effects of higher state contamination. The idea is that the terms involving higher state energies are more suppressed relative to the ground state in the ratio than in the individual correlators. Typically the errors are smaller as well. However, one needs to be very careful to ensure that one has isolated the lowest energy state, and concertina analysis is even more important.

1.22.9 Matrix of Correlators

Given a set of operators $\mathcal{O}_j$ $(j = 1, 2, \ldots, m)$, all with the same quantum numbers, one can create a set of m^2 timesliced correlators, $c_{ij}(t)$ using all possible combinations of the operators to create and destroy the particles:

$$c_{ij}(t) = \sum_{\boldsymbol{x}} \left\langle \Omega | \mathcal{O}_i(\boldsymbol{x}, t) \mathcal{O}_j^\dagger(\mathbf{o}, 0) | \Omega \right\rangle \mathrm{e}^{\mathrm{i}\boldsymbol{p}\cdot\boldsymbol{x}}$$

If these are assembled into a matrix:

$$\begin{bmatrix} c_{11}(t) & \cdots & c_{1j}(t) \\ \vdots & \ddots & \vdots \\ c_{j1}(t) & \cdots & c_{jj}(t) \end{bmatrix}$$

and this matrix diagonalized then, in the case of a 2×2 matrix, one eigenvalue is dominated by the ground state energy and the other by the first excited state energy (Lüscher and Wolff, 1990). This method will be used in connection with the $^3P_1$ and $^1P_1$ operators for heavy-light mesons.

1.23 Simulation Energies

In NRQCD the quantity controlling the exponential fall-off of the meson correlators is not the meson energy because the quark mass term was removed from the action. Instead the correlator fall-off is determined by the so-called simulation energy:

$$\begin{aligned} E^{\text{simulation}} &= M_{\text{meson}} - \Delta \\ &= M_{\text{meson}} - (Z_{\text{m}} m_0 - E_0) \end{aligned}$$

in which Z_{m} is the mass renormalization constant relating the bare quark mass to the pole mass, and E_0 is the shift in the energy of the quark. These two quantities can be calculated in perturbation theory. The shift Δ may be measured non-perturbatively in the simulation. For a heavy-heavy meson, the correlator of which falls-off with simulation energy $E_{\text{simulation}}$

$$M_{\text{Q}\overline{\text{Q}}}^{\text{kinetic}} = 2\Delta + E_{\text{simulation}}$$

The kinetic mass is measured from the dispersion relation.

1.24 Dispersion Relation

The relativistic dispersion relation for a meson with momentum $\boldsymbol{p}$;

$$E = \sqrt{\boldsymbol{p}^2 + M^2}$$

can be expanded:

$$E = M + \frac{\boldsymbol{p}^2}{2M} - \frac{\boldsymbol{p}^4}{8M^3} + \cdots$$

If one measures the dispersion from the simulation one doesn't expect this form to be followed exactly. Distinguishing each of the masses:

$$E(\boldsymbol{p}) = M_0 + \frac{\boldsymbol{p}^2}{2M_1} - \frac{\boldsymbol{p}^4}{8M_2^3} + \cdots$$

where $M_0 \neq M_1$ because the rest mass has been removed from the theory; $M_1 \neq M_2$ because the relativistic corrections away from the $\boldsymbol{p}^4$ term have not been included. I shall use the dynamical mass, M_1 as my definition of the ground state mass of the meson I'm looking at.

1.25 Heavy Quark Symmetry

In the limit $m_{\text{Q}} \to \infty$, QCD has an SU($2N_{\text{Flavour}}$) symmetry, where N_{Flavour} is the number of flavours of heavy quark. A very comprehensive survey of the field is contained in Neubert (1994). This can be seen for the NRQCD Lagrangian, $\mathcal{L} \to \psi^\dagger D_t \psi$ as $m \to \infty$, so heavy quarks become spinless and any distinction between flavours disappears, modulo the zero energy set by

the missing mass terms. The physical picture is of a static heavy quark surrounded by a cloud of the light degrees of freedom — the so called 'brown muck'. Interactions at momentum scales appropriate to the brown muck can't see the detail of the heavy quark. Radial and orbital excitations, *i.e.* those that change the light degrees of freedom, should be roughly independent of the heavy quark flavour. One expects changes in the heavy quark (flavour or spin) to lead to smaller splittings with strong m_Q dependence between states of different $\boldsymbol{S}_Q$.

1.25.1 Structure of the Heavy Light Spectrum

Heavy quark spin, $\boldsymbol{S}_Q$, is a good quantum number in the heavy quark limit, so one can classify states according to $\boldsymbol{j}_{\rm light} = \boldsymbol{J} - \boldsymbol{S}_Q$. Each $\boldsymbol{j}_{\rm light}$ state becomes upon addition of the heavy quark, a doublet with $J = j_{\rm Light} \pm 1/2$. The lightest states are $L = 0, j_{\rm Light} = 1/2$, that is the pseudo-scalar and vector doublet.

For the P wave, the light quark spin $\boldsymbol{S}_q$ is coupled to the orbital angular momentum, to make states:

$$j_{\rm Light} = \frac{1}{2} \qquad \text{2 polarizations}$$

$$j_{\rm Light} = \frac{3}{2} \qquad \text{4 polarizations}$$

With the addition of the heavy quark spin,

$$j_{\rm Light} = \frac{3}{2} + S_Q \rightarrow J = 2 \qquad B_2^*$$

$$J = 1 \qquad B_1'$$

giving 8 states altogether, and

$$j_{\rm Light} = \frac{1}{2} + S_Q \rightarrow J = 2 \qquad B_0$$

$$J = 1 \qquad B_1$$

giving 4 states altogether. Therefore in the $j - j$ coupled basis, one reproduces the same 12 states as the LS coupled $^1P_1\,^3P_0\,^3P_1\,^3P_2$ multiplet. However, the spin 1 states are a mixture of the $^1P_1$ and $^3P_1$ because there is no charge conjugation. In the $m_Q \rightarrow \infty$ limit, only splittings due to light degrees of freedom remain. The $j - j$ basis becomes the correct one and all the $j_{\rm Light} = 3/2$ states become degenerate , but split from all the $j_{\rm Light} = 1/2$ states.

The difference between the $j_{\rm Light} = 1/2$ and the $j_{\rm Light} = 3/2$ members of a doublet is due to a spin flip of the heavy quark. The leading term that can do this is the $\boldsymbol{\sigma} \cdot \boldsymbol{B}$ term, and therefore this splitting is proportional to $1/m_Q$ at leading order.

One also expects some splittings to be controlled by the light degrees of freedom:

— heavy-strange and heavy-chiral splitting

— radially excited S and ground state S splitting

— orbital splittings between P and S states

For these last splittings, one should calculate the splitting between spin-average states to remove the spin dependent $1/m_Q$ effects and to show more clearly the m_Q independent light quark effects.

The $j_{\rm Light} = 1/2$ and $j_{\rm Light} = 3/2$ splitting is approximately independent of m_Q.

2

Heavy Heavy Spectrum

Here are the results and details of the analyses of meson correlators constructed purely from NRQCD Green's functions. I consider the S wave and P wave data separately, and look at the mass splittings after having discussed the simulation energies. I then look at the dispersion of the S wave correlators, and finally discuss the estimation of the scale for the heavy heavy systems.

2.1 S wave

I calculated correlators with all four smearing combinations, LL, LS, SL, and SS, at momenta $|\boldsymbol{p}|^2 = 0, 1, 2, 3, 4$.

2.1.1 Simulation Energies

Here are the concertina plots for the pseudo-scalar from (LL,1.2) at zero momentum, the final timeslice in the fit being 47:

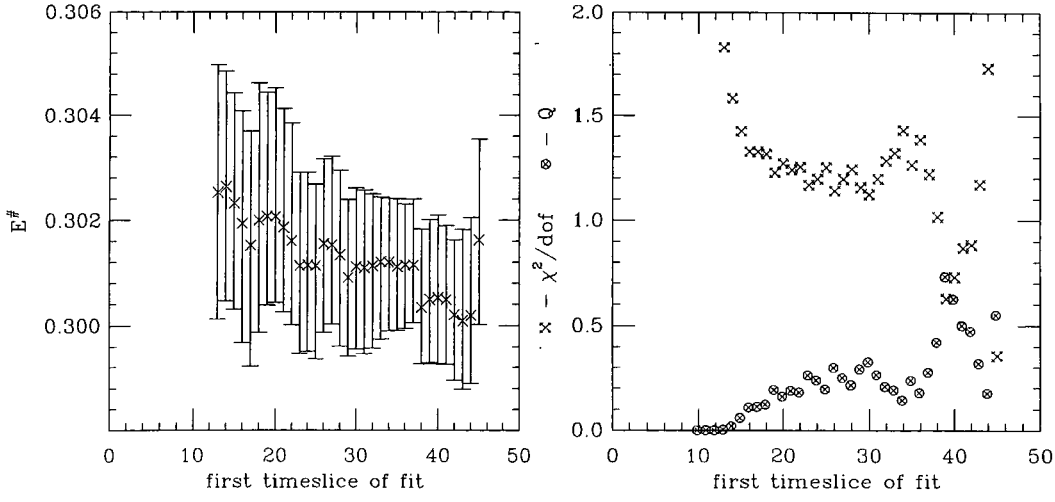

Figure 2.1 Concertina plots for Pseudo-scalar from (LL, 1.2)

The final plateau occurs on fits beginning on or after timeslice 38; the lowest χ^2/N_{dof} occurs for the fit beginning on timeslice 39 §. The simulation energy obtained from the fit over [39,47] is consistent at the $\sigma/2$ level with that obtained from the fit over [29,47].

§ apart from the fit beginning on timeslice 45 — this fit has one degree of freedom and is fitting to little more than noise, so I shall not consider it.

The fits to the SS data by contrast:

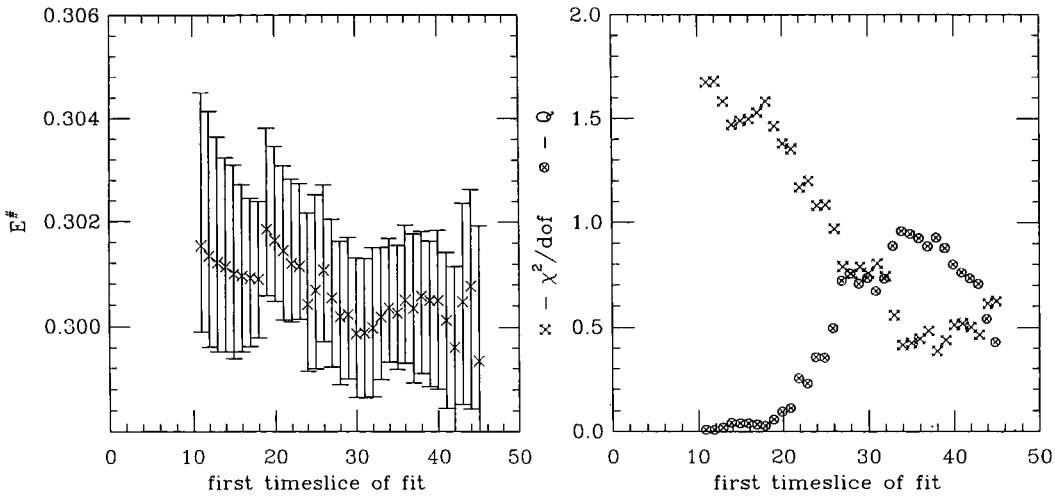

Figure 2.2 Concertina plots for Pseudo-scalar from (SS, 1.2)

show stability from timeslice 28 onwards. The fits beginning on timeslice 34 show lower $\chi^2/N_{\rm dof}$ and give very similar fitted energies. I chose the [34,47] fit for my estimate of the simulation energy.

The vector channel is by and large very similar. Here are data:

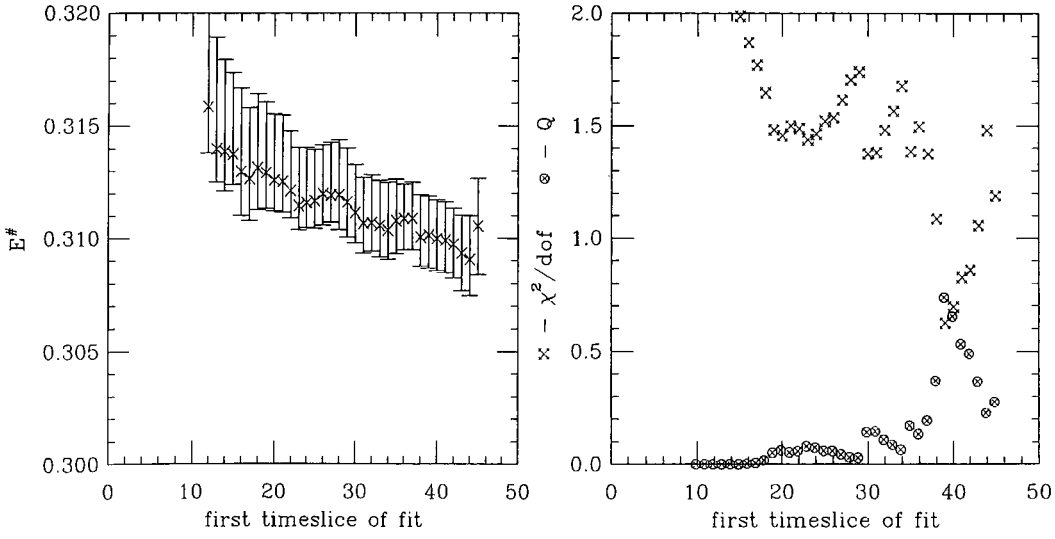

Figure 2.3 Concertina plots for Vector from (LL, 1.2)

I took the fit over [40,47] as the best estimate of the simulation energy.

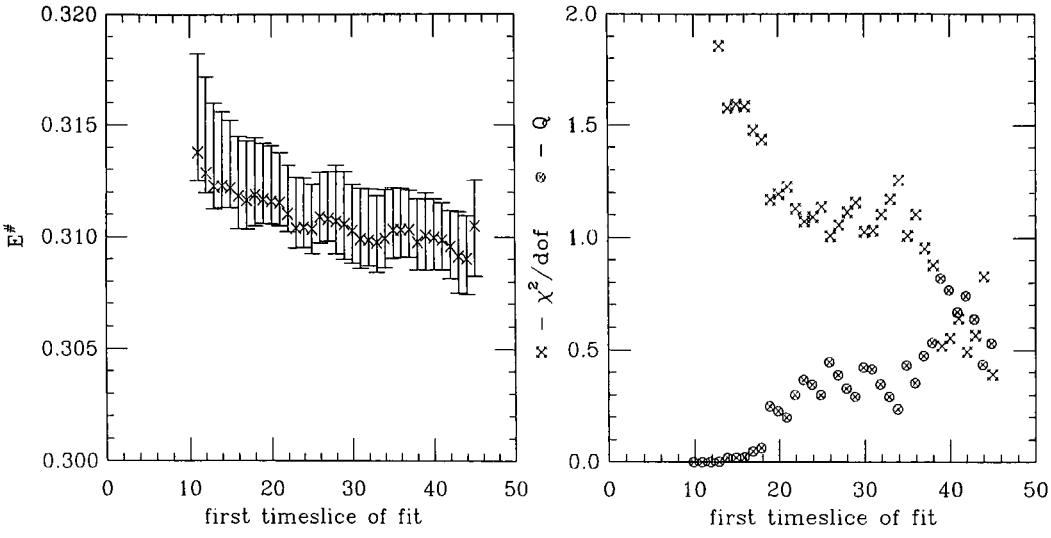

Figure 2.4 Concertina plots for Vector from (SL, 1.2)

For the SL data shown above, the fit over [23,47] was used. This is a liberal choice, but is justified on the grounds of acceptability of $\chi^2/N_{\rm dof}$; it is consistent within errors with a more conservative choice of, for example, [32,47].

For the SS data:

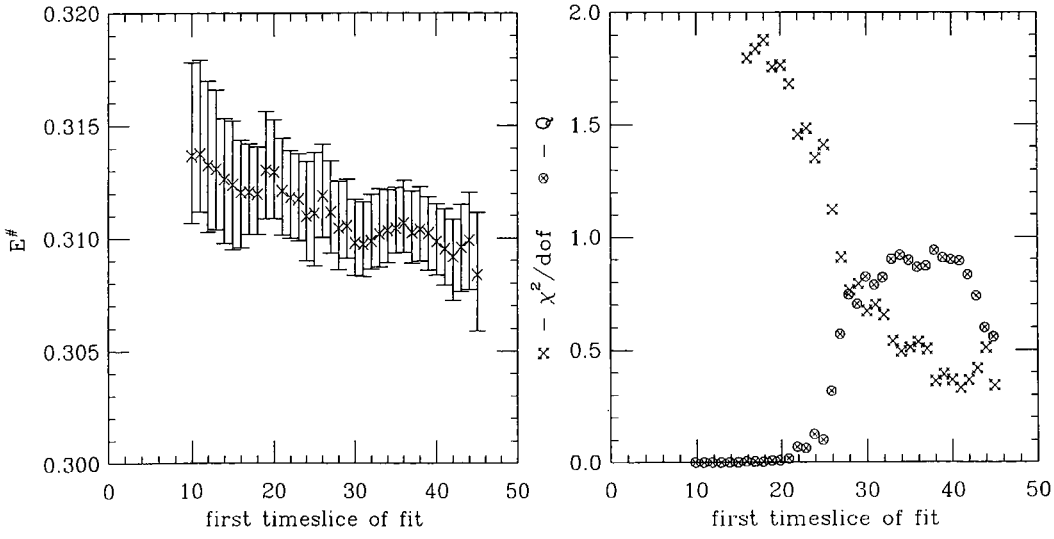

Figure 2.5 Concertina plots for Vector from (SS, 1.2)

I took the best fit to be over timeslices [28,47].

The above graphs are typical of the data from the lightest masses. To illustrate the quality of the data from the heavier masses, here are the concertina graphs for (SL,4.0):

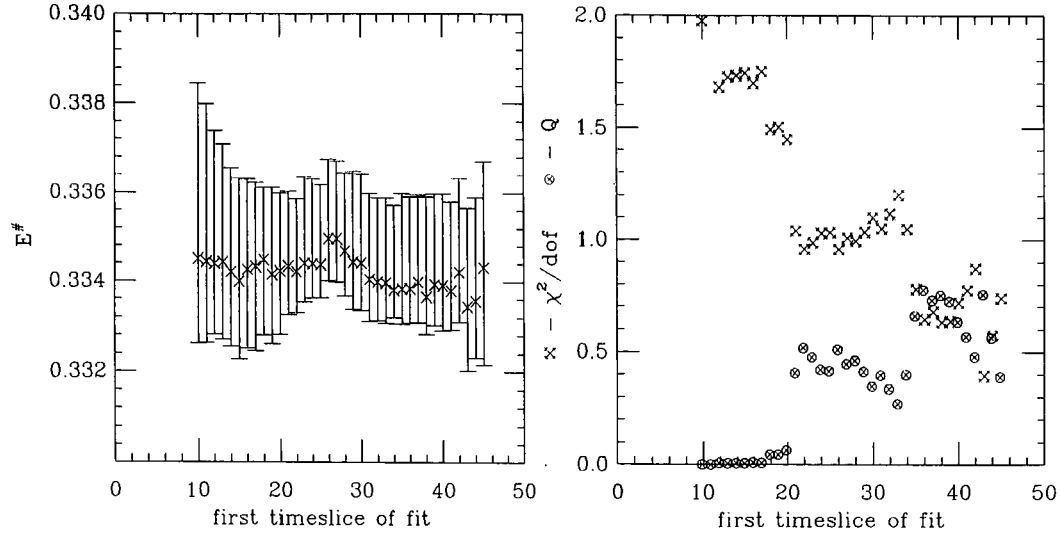

Figure 2.6 Concertina plots for Pseudo-scalar from (SL, 4.0)

I used similar methods for the other channels. The fit ranges obtained for the LL and LS channels were small, typically being over [40,47]. This is related to the difficulty in identifying the final plateaux of these smearings, and although the energies obtained from them are consistent with those from the SL and SS channels, I do not consider them further. Here are the final numbers:

Table 2.1 Fitted simulation energies for Pseudo-scalar

	SL		*SS*	
Mass	$E^{\#}$	$\chi^2/N_{\rm dof}$	$E^{\#}$	$\chi^2/N_{\rm dof}$
1.1	0.2778^{+16}_{-12}	0.81	0.2776^{+12}_{-11}	0.46
1.2	0.3008^{+13}_{-11}	0.88	0.3004^{+13}_{-10}	0.41
1.3	0.3142^{+14}_{-12}	1.04	0.3138^{+13}_{-11}	0.40
2.0	0.3529^{+17}_{-9}	0.51	0.3534^{+14}_{-11}	0.36
4.0	0.3338^{+21}_{-8}	0.65	0.3341^{+21}_{-16}	1.40
6.0	0.2931^{+16}_{-10}	1.22	0.2943^{+21}_{-19}	1.65

Table 2.2 Fitted simulation energies for Vector

	SL		*SS*	
Mass	$E^{\#}$	$\chi^2/N_{\rm dof}$	$E^{\#}$	$\chi^2/N_{\rm dof}$
1.1	0.2886^{+19}_{-9}	1.02	0.2889^{+21}_{-16}	0.84
1.2	0.3104^{+23}_{-9}	1.07	0.3105^{+21}_{-18}	0.76
1.3	0.3228^{+22}_{-12}	1.12	0.3232^{+18}_{-14}	0.45
2.0	0.3593^{+19}_{-12}	0.94	0.3595^{+21}_{-15}	0.63
4.0	0.3375^{+23}_{-8}	0.81	0.3388^{+28}_{-16}	1.45
6.0	0.2962^{+20}_{-12}	1.46	0.2974^{+27}_{-21}	1.54

The consistency between the SL and SS is very good.

2.1.2 Hyperfine Splitting

I extract the Hyperfine splitting from the ratio of the vector and the pseudo-scalar correlators. Here are two typical sets of concertina plots:

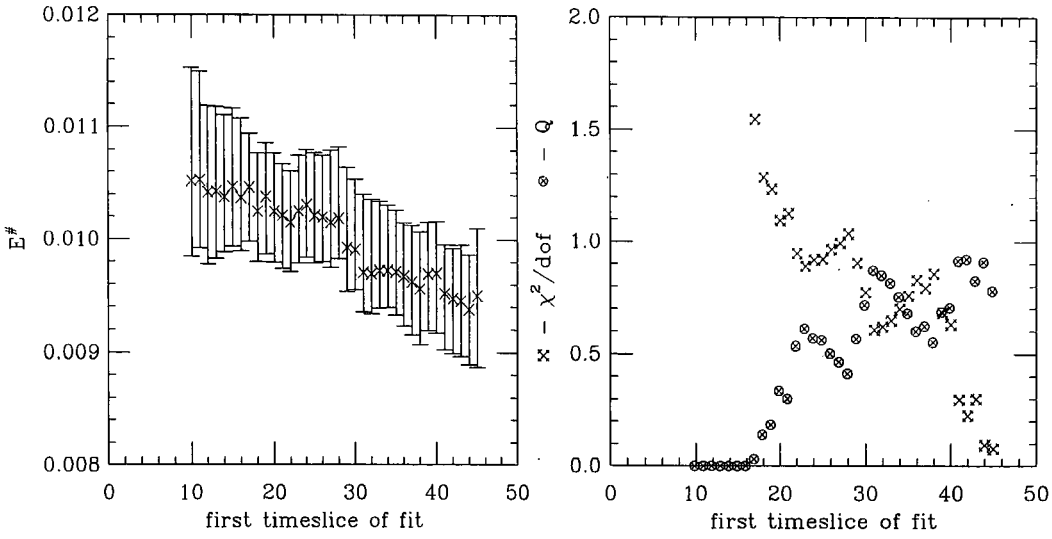

Figure 2.7 Concertina plots for Hyperfine from (SL, 1.2)

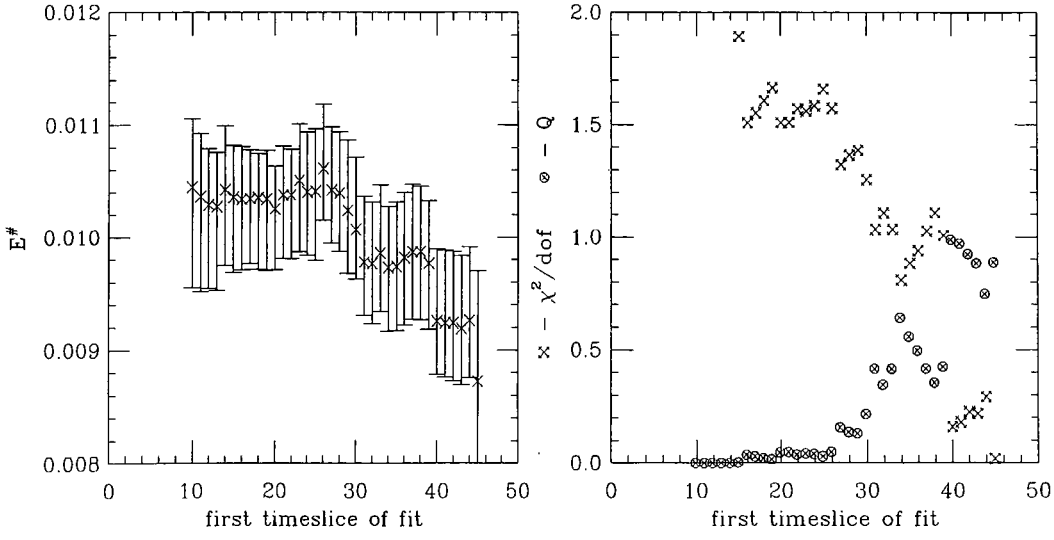

Figure 2.8 Concertina plots for Hyperfine from (SS, 1.2)

I interpret the three part behaviour as follows. The final plateau (after timeslice 40) is formed from fits with few degrees of freedom and over the noisiest part of the raw data. It is more difficult to ascribe a physical meaning to the other two plateaux. The energies as determined from points in the two plateaux are consistent within σ, and fall either side of the difference between the previously determined vector and pseudo-scalar energies, the error in

the difference encompassing all the regions in the ratio results. I've no way of telling if the first region is anything other than a statistical effect from the minimization routine. I therefore determine the hyperfine splitting from the largest fit in the second region. The fits in the second region also have far better values of $\chi^2/N_{\rm dof}$ than those in the first. For example, for the (1.2,SS) data illustrated, I pick the fit over [32,47].

The final numbers are:

Table 2.3 Fitted Hyperfine splitting

	SL		*SS*	
Mass	$\delta E^{\#}$	$\chi^2/N_{\rm dof}$	$\delta E^{\#}$	$\chi^2/N_{\rm dof}$
1.1	$0.01080\,^{+62}_{-68}$	1.24	$0.01060\,^{+75}_{-40}$	0.54
1.2	$0.00976\,^{+55}_{-53}$	1.11	$0.00970\,^{+66}_{-36}$	0.62
1.3	$0.00898\,^{+56}_{-43}$	1.04	$0.00900\,^{+61}_{-30}$	0.77
2.0	$0.00598\,^{+41}_{-31}$	1.72	$0.00627\,^{+49}_{-29}$	1.76
4.0	$0.00381\,^{+24}_{-22}$	0.96	$0.00384\,^{+25}_{-14}$	2.11
6.0	$0.00288\,^{+21}_{-20}$	0.68	$0.00298\,^{+13}_{-11}$	0.82

The agreement between the two smearings is excellent. The values of the $\chi^2/N_{\rm dof}$ statistic are relatively high for the $m_{\rm Q} = 2.0$ data: I don't think there is any particular reason for this. The only other high value is for the SS $m_{\rm Q} = 4.0$ data, and the number obtained is completely consistent with the SL data which has a much lower $\chi^2/N_{\rm dof}$.

2.2 P wave

I found the P wave operators to produce more equivocal data. I shall therefore go through the details of the analysis at greater length.

The P wave operators all required smearing: either SL or SS. The LL and LS seemed to be heavily contaminated with excited states. I didn't use them to extract any numbers.

2.2.1 Simulation Energies

The P wave correlators were computed out to timeslice 28. By this time the signal has broken up completely into noise. The concertina fits to determine the simulation energies all had their final timeslice fixed to slightly earlier than this, at timeslice 24. All the operators produced a plateau lasting for about half a dozen timeslices from roughly timeslice 8. After these timesteps the signal showed another plateau at a lower energy than the first, lasting until timeslice 20 or so. This plateau were noisier and less clear-cut.

The first plateaux were at different energies for different operators, but were consistent between operators at the level of σ. The final plateaux were far more consistent, to well within $\sigma/2$. The agreement between the two types of plateaux was within σ for each operator.

All these features can be seen in the $^1P_1$:

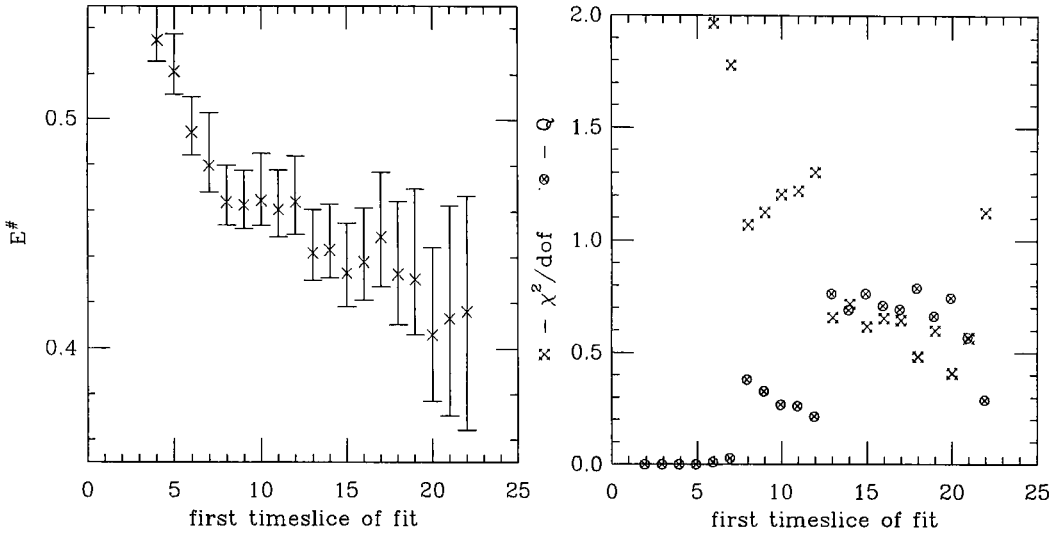

Figure 2.9 Concertina plots for $^1P_1$ (SL, 1.1)

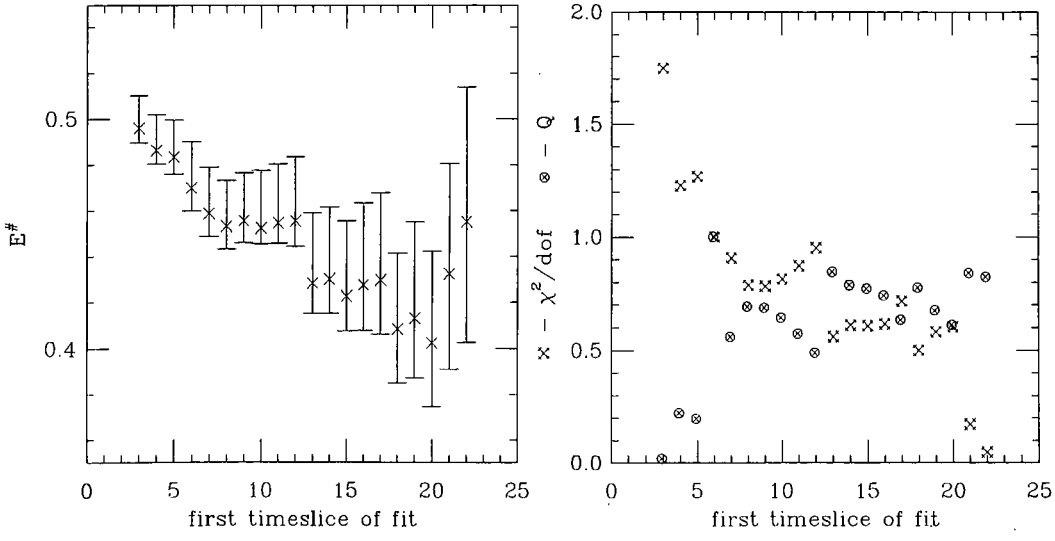

Figure 2.10 Concertina plots for $^1P_1$ (SS, 1.1)

The $^1P_1$ shows the behaviour very clearly: it is not so clear-cut in the graphs of the other operators. For example, the $^3P_0$ operator shows less difference between the two regions:

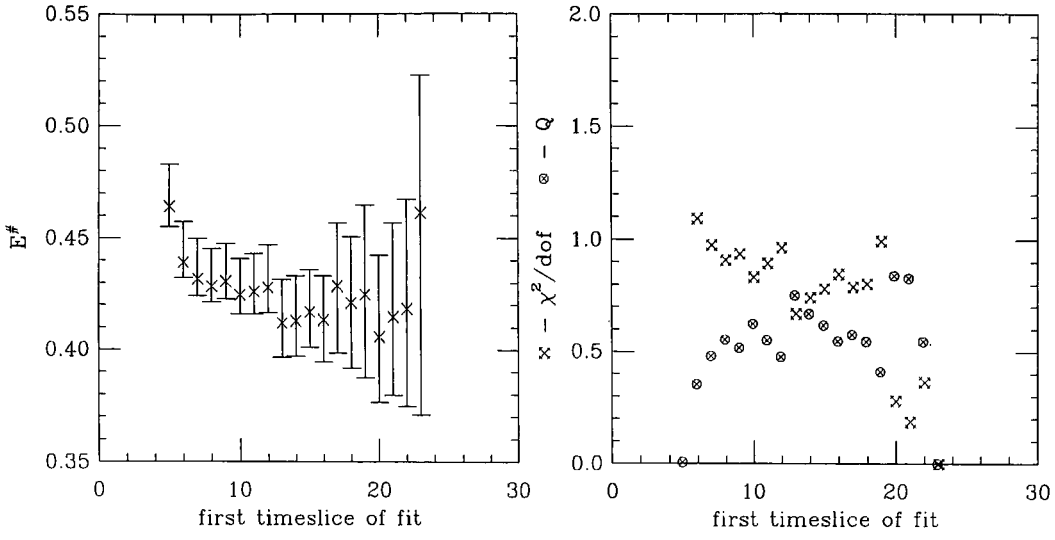

Figure 2.11 Concertina plots for $^3P_0$ (SS, 1.1)

The two $^3P_2$ operators are in very close agreement:

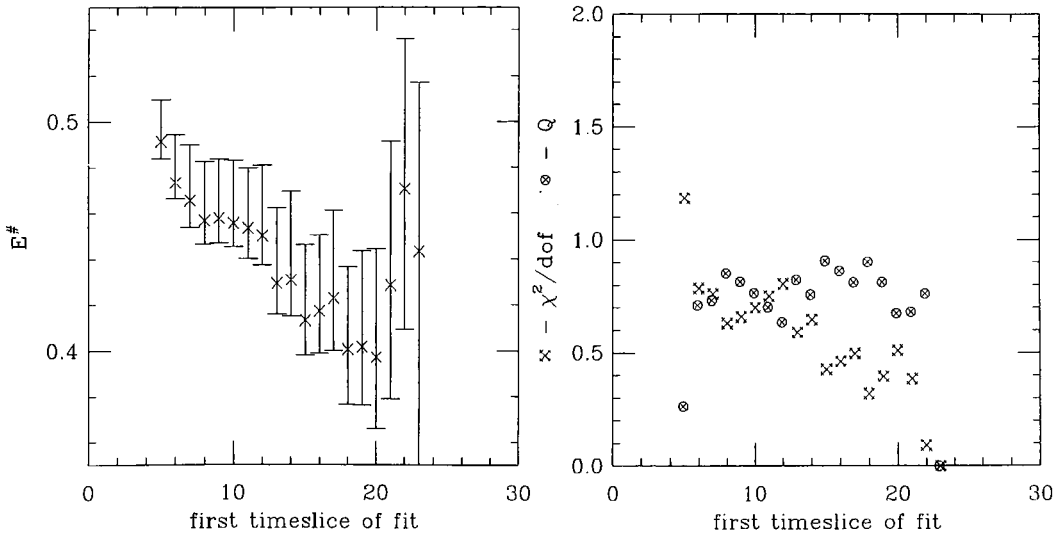

Figure 2.12 Concertina plots for $^3P_2$(T) (SS, 1.1)

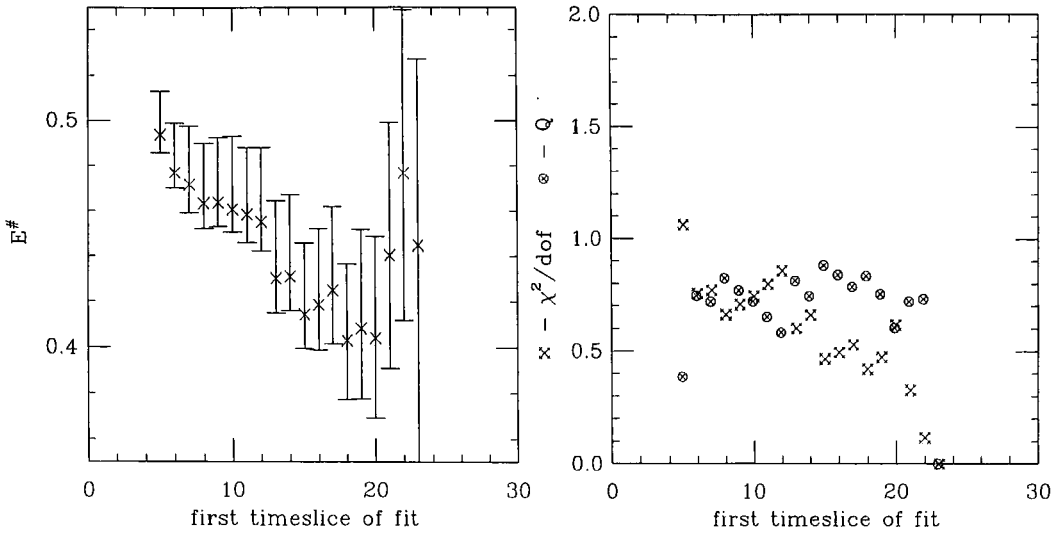

Figure 2.13 Concertina plots for $^3P_2$(E) (SS, 1.1)

The similarity between the fitted energy concertina graphs is remarkable, especially in the overall shape of the graphs. The first stability region is certainly not so well defined as those for the other operators. For example, if the value on timeslice 13 were moved up by half a standard deviation, the first region would hardly exist as a separate stable region.

It's not completely obvious what is happening here. The worry is that the first stable region is not a real plateau but just a statistical effect. In one sense the final flat region is a safer estimate, and I use this to estimate the scale of the system. I do not feel confident in estimating the fine structure of the P wave from the individual correlators. Ultimately, larger numbers of configurations would answer these questions, but to see if anything further can be gleaned from the data, I look at the ratio plots.

2.2.2 Splittings

I start with the $^3P_2$–$^3P_0$ splitting. This should be the largest splitting, and so be the easiest to isolate. As I have two operators for the $^3P_2$ state, any consistency will lend confidence to the conclusions I draw. Here is the SS data from the operator in the E representation:

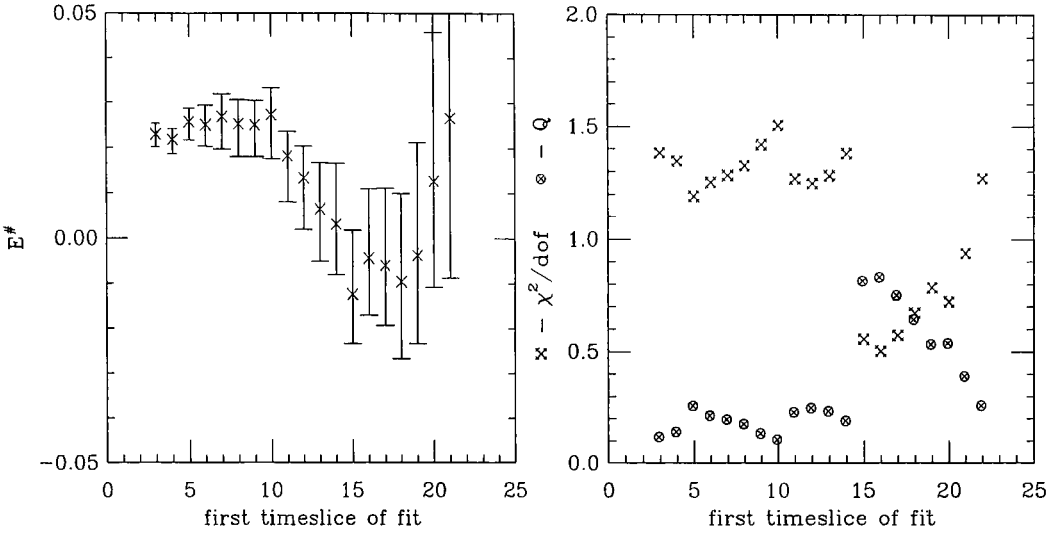

Figure 2.14 Concertina plots for $^3P_2$(E)– $^3P_0$ (SS, 1.1)

The figure shows three regions: a plateau beginning at timeslice 5 and lasting for 6 timeslices, a transitional region of two or three timeslices' length, and a final region of flatness. The final region is consistent with zero, and is a reflection of the collapse of the signals of the two operators to the same values. There is no stability in the intermediate region. The first plateau is more interesting. It begins on timeslice 5, where the component operators are outwith their initial plateau. I conclude that the ratio fit has eliminated the higher state contamination in the operator quotient. The values for the other smearing in the E representation and both smearings in the T representation are shown overleaf:

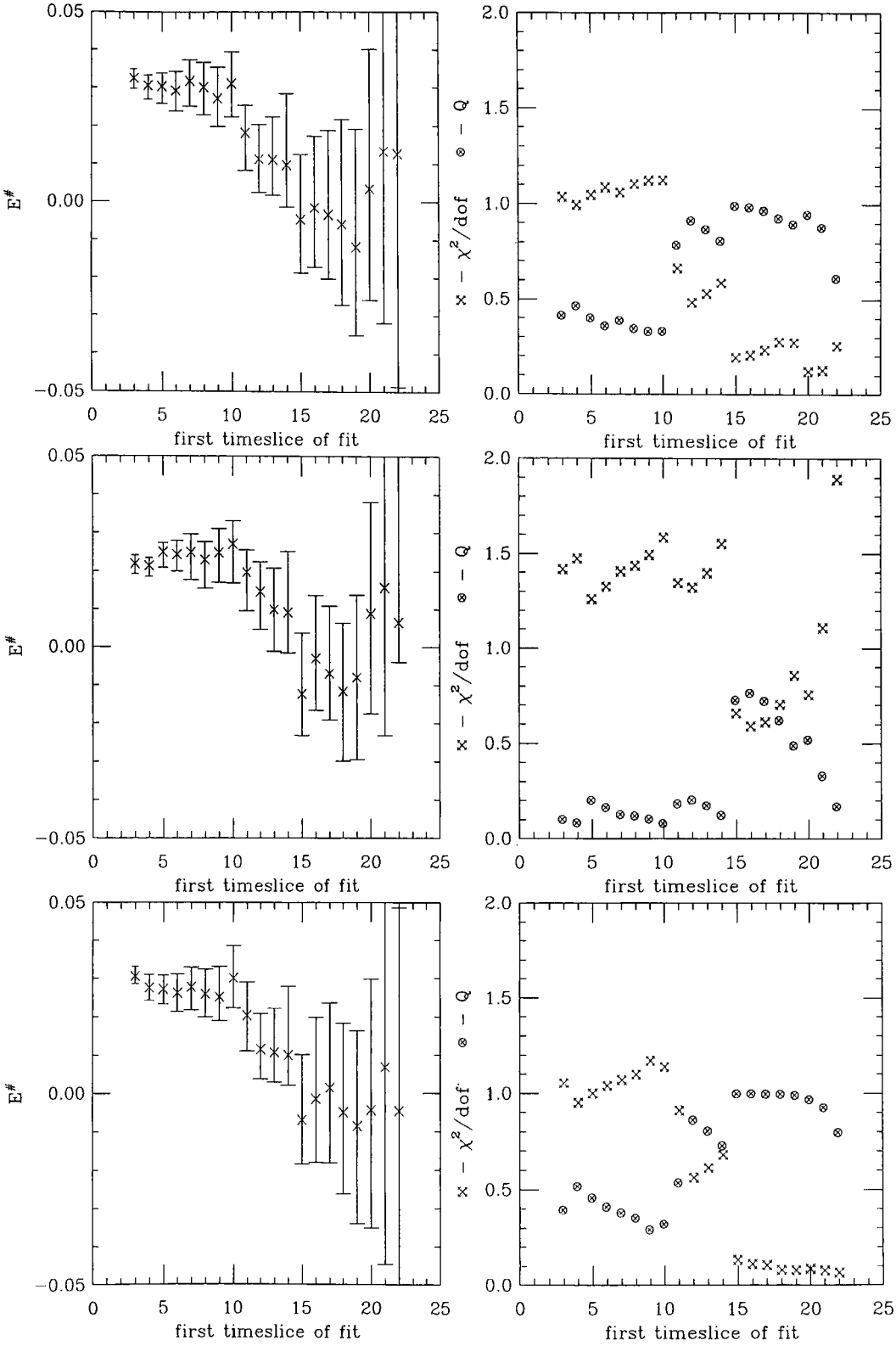

Figure 2.15 Concertina plots for $^3P_2 - ^3P_0$

These graphs further bolster my faith in the validity of the initial plateaux. The SS fitted energies are extraordinarily consistent. The SL energies agree within $\sigma/2$. Within the E representation, the numbers agree within σ, and the agreement is within $\sigma/2$ for the T representation.

The $^3P_2-^3P_0$ splitting can also be calculated by adding the $^3P_2-^3P_1$ splitting to the $^3P_1-^3P_0$ splitting.

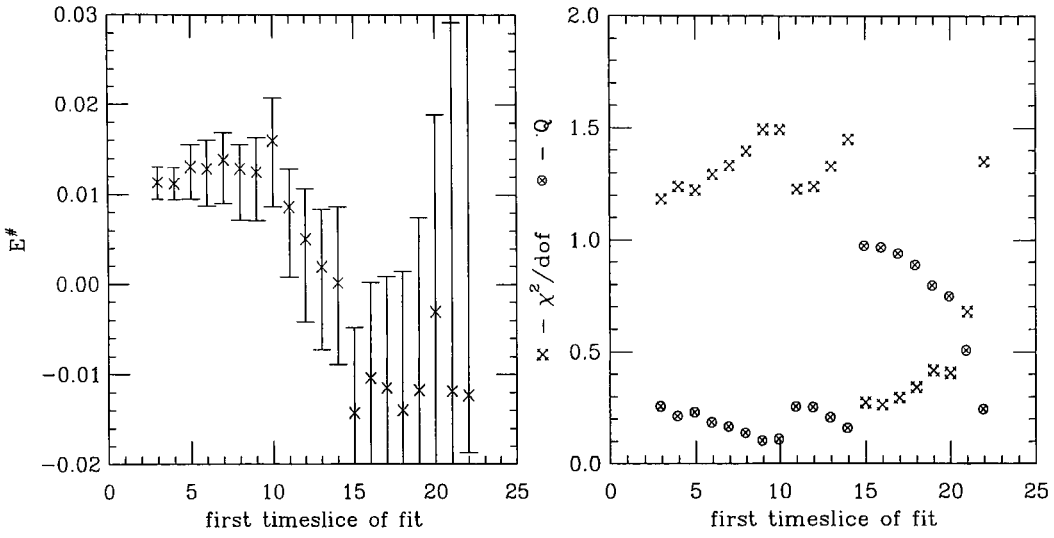

Figure 2.16 Concertina plots for $^3P_2(E)-^3P_1$ (SS, 1.1)

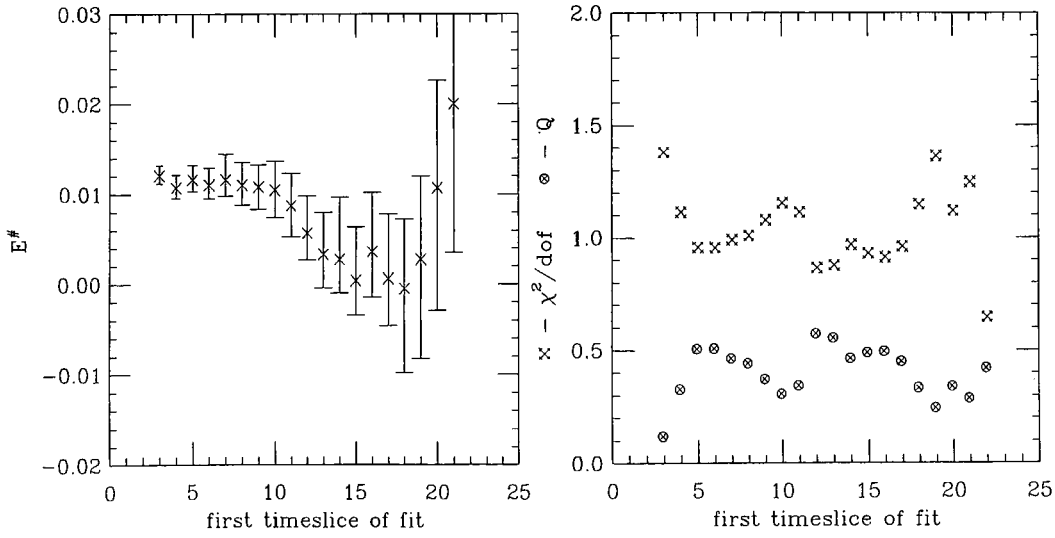

Figure 2.17 Concertina plots for $^3P_1-^3P_0$ (SS, 1.1)

The agreement between the sum of these two splittings and the previous estimate is good.

For completeness, I show some splittings with the $^1P_1$ operator. Here is the $^3P_0 - ^1P_1$ splitting:

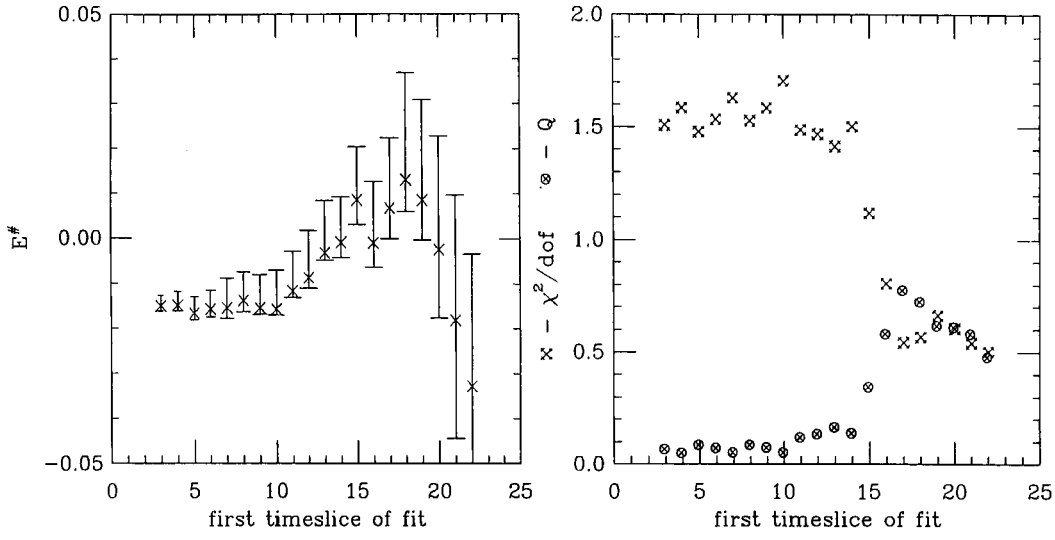

Figure 2.18 Concertina plots for $^3P_0 - ^1P_1$ (SS, 1.1)

and here is the $^3P_1 - ^1P_1$ splitting:

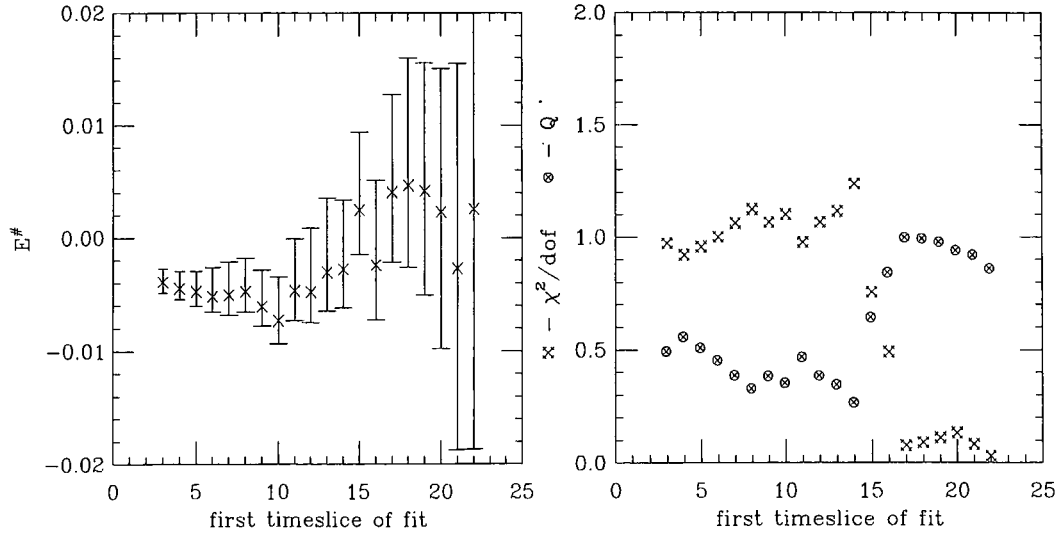

Figure 2.19 Concertina plots for $^3P_1 - ^1P_1$ (SS, 1.1)

I am convinced of the validity of the numbers obtained from the ratio fits. The splittings are consistent in terms of how they fit together, *e.g.* the splitting between $^3P_2$ and $^3P_0$ is equal to the sum of the splitting between $^3P_2$ and $^3P_1$ and the splitting between $^3P_1$ and $^3P_0$. The splittings from the ratio fits are consistent with those obtained from the differences in the simulation energies, if the simulation energies are taken in the initial plateau. Here are the final numbers:

Table 2.4 Inter P wave splittings (1.1)

		SL		SS	
		$E^{\#}$	$\chi^2/N_{\rm dof}$	$E^{\#}$	$\chi^2/N_{\rm dof}$
$^3P_2(E)$	$^3P_1$	0.0156^{+30}_{-41}	0.96	0.0148^{+99}_{-114}	0.98
	$^1P_1$	0.0090^{+18}_{-27}	1.45	0.0074^{+11}_{-12}	1.26
	$^3P_0$	0.0292^{+51}_{-55}	1.09	0.0250^{+44}_{-48}	1.25
$^3P_2(T)$	$^3P_1$	0.0122^{+30}_{-39}	0.95	0.0125^{+22}_{-37}	1.38
	$^1P_1$	0.0054^{+22}_{-25}	1.20	0.0063^{+13}_{-26}	1.38
	$^3P_0$	0.0263^{+50}_{-49}	1.04	0.0244^{+36}_{-45}	1.33
$^3P_1$	$^1P_1$	-0.0054^{+27}_{-14}	0.79	-0.0050^{+30}_{-18}	1.06
	$^3P_0$	0.0120^{+19}_{-17}	1.25	0.0110^{+19}_{-15}	0.96
$^3P_0$	$^1P_1$	-0.0188^{+32}_{-16}	1.09	-0.0167^{+37}_{-14}	1.48

Table 2.5 Inter P wave splittings (1.2)

		SL		SS	
		$E^{\#}$	$\chi^2/N_{\rm dof}$	$E^{\#}$	$\chi^2/N_{\rm dof}$
$^3P_2(E)$	$^3P_1$	0.0149^{+28}_{-39}	0.98	0.0119^{+27}_{-38}	1.30
	$^1P_1$	0.0087^{+17}_{-26}	1.46	0.0069^{+10}_{-12}	1.28
	$^3P_0$	0.0281^{+35}_{-42}	1.05	0.0229^{+40}_{-42}	1.26
$^3P_2(T)$	$^3P_1$	0.0115^{+28}_{-35}	1.01	0.0116^{+22}_{-35}	1.40
	$^1P_1$	0.0054^{+19}_{-24}	1.33	0.0059^{+13}_{-23}	1.45
	$^3P_0$	0.0246^{+44}_{-46}	1.09	0.0224^{+30}_{-46}	1.36
$^3P_1$	$^1P_1$	-0.0050^{+23}_{-13}	0.81	-0.0046^{+26}_{-16}	1.04
	$^3P_0$	0.0112^{+18}_{-16}	1.29	0.0100^{+18}_{-14}	1.00
$^3P_0$	$^1P_1$	-0.0170^{+37}_{-17}	1.17	-0.0142^{+36}_{-18}	1.43

Table 2.6 Inter P wave splittings (1.3)

		SL		SS	
		$E^{\#}$	$\chi^2/N_{\rm dof}$	$E^{\#}$	$\chi^2/N_{\rm dof}$
$^3P_2(E)$	$^3P_1$	0.0142^{+25}_{-37}	1.01	0.0111^{+26}_{-35}	1.34
	$^1P_1$	0.0084^{+16}_{-26}	1.46	0.0064^{+12}_{-22}	1.48
	$^3P_0$	0.0258^{+44}_{-54}	1.14	0.0212^{+39}_{-43}	1.31
$^3P_2(T)$	$^3P_1$	0.0108^{+25}_{-34}	1.04	0.0109^{+20}_{-34}	1.47
	$^1P_1$	0.0052^{+19}_{-22}	1.37	0.0056^{+12}_{-22}	1.56
	$^3P_0$	0.0229^{+41}_{-46}	1.13	0.0207^{+30}_{-45}	1.43
$^3P_1$	$^1P_1$	-0.0044^{+14}_{-10}	0.85	-0.0043^{+20}_{-12}	0.97
	$^3P_0$	0.0105^{+16}_{-16}	1.29	0.0091^{+17}_{-14}	1.02
$^3P_0$	$^1P_1$	-0.0157^{+35}_{-18}	1.22	-0.0129^{+34}_{-17}	1.40

2.3 Dispersion Relation

The data were fitted to the following forms:

$$E = m_0 + \frac{p^2}{2m_1} - \frac{p^4}{8m_2^3}$$

$$E = m_0 + \frac{p^2}{2m_1} - \frac{p^4}{8m_1^3}$$

$$E = m_0 + \frac{p^2}{2m_1}$$

The three lightest masses were fitted to the first two forms, and the three heaviest masses were fitted to the last two forms.

For the heavier masses, no difference was found between the fits to the two functional forms.

For the three lightest masses, slightly lower $\chi^2/N_{\rm dof}$'s were found using the first functional form than the second: the extra degree of freedom soaks up any noise in the data and makes a better fit.

To illustrate the quality of the data, here are the dispersion graphs for the (SS,1.2) data, with the fitted curves for the first and second functions, and also the fit using the last form to the (SS,6.0) data:

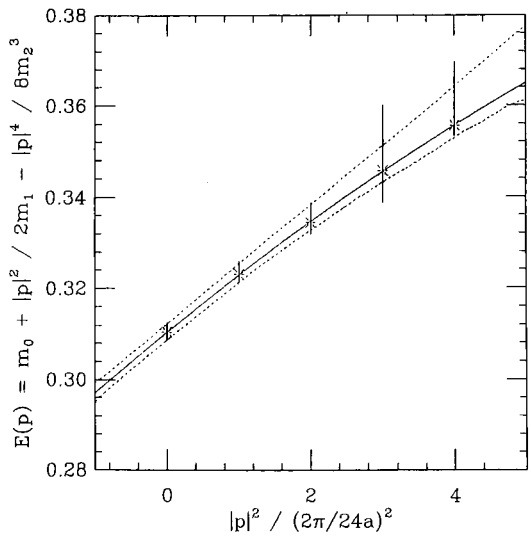

Figure 2.20 Dispersion of Vector (SS, 1.2)

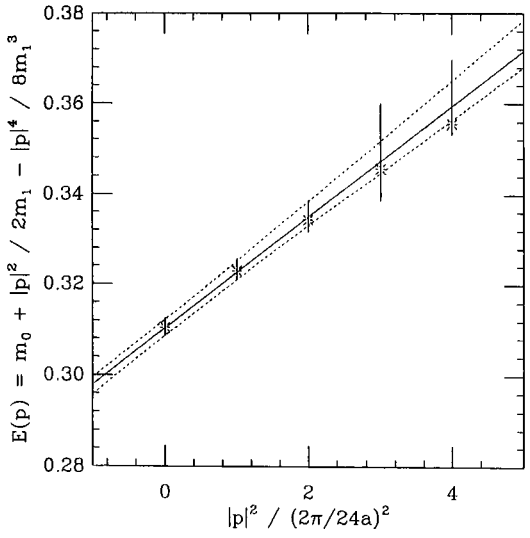

Figure 2.21 Dispersion of Vector (SS, 1.2)

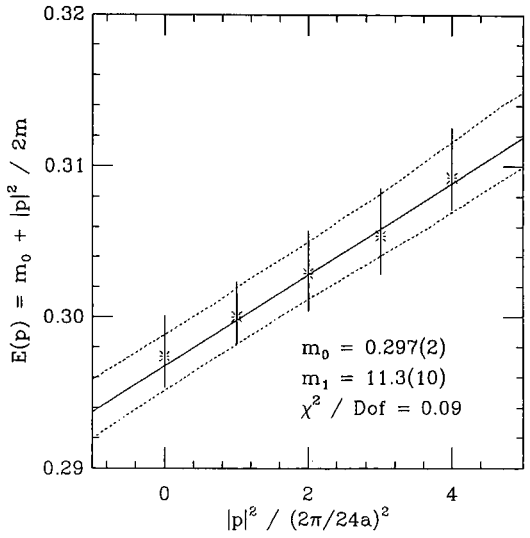

All fits for a given mass yielded similar parameters, consistent to within $\sigma/2$. In making the final choice, I selected the fits of lowest $\chi^2/N_{\rm dof}$ regardless of smearing or fit function. The final numbers are:

Table 2.7 Kinetic Masses

Mass	$m_1^{\#}$
1.1	$2.43\ ^{+0.28}_{-0.39}$
1.2	$2.66\ ^{+0.22}_{-0.24}$
1.3	$2.89\ ^{+0.14}_{-0.26}$
2.0	$4.88\ ^{+0.41}_{-0.52}$
4.0	$8.71\ ^{+0.43}_{-0.61}$
6.0	$11.32\ ^{+1.04}_{-1.23}$

Note that these figures are the kinetic masses for the heavy-heavy meson. The mass shifts

that will be used in heavy-light systems are half these.

2.4 Setting the Scale for Heavy-Heavy Systems

As discussed in §2.2, I am a little wary of the meanings of parts of the P wave data, specifically the initial plateaux in the concertina fits.

To estimate the scale for heavy-heavy systems I use the 1P−1S splitting. I take the final plateaux as my estimate of the position of 1P and choose the $^1P_1$ operator as I expect it to be the best behaved ‡

The numbers are:

Table 2.8 Simulation energies for the $^1P_1$

	SL		SS	
m_Q	$E^\#$	χ^2/N_{dof}	$E^\#$	χ^2/N_{dof}
1.1	0.438^{+24}_{-16}	0.65	0.430^{+32}_{-15}	0.61
1.2	0.451^{+20}_{-15}	0.67	0.448^{+30}_{-14}	0.57
1.3	0.466^{+24}_{-16}	0.77	0.458^{+28}_{-14}	0.55

Subtracting off the vector simulation energy:

Table 2.9 1P−1S splitting

	SL		SS	
m_Q	$E^\#$	χ^2/N_{dof}	$E^\#$	χ^2/N_{dof}
1.1	0.149(20)	–	0.141(23)	–
1.2	0.141(17)	–	0.138(22)	–
1.3	0.143(20)	–	0.135(21)	–

I shall use these in the next chapter to estimate the scale of for the heavy-heavy mesons.

‡ Why ? It is the least complicated of the P wave operators: there is no spin structure to it. I also expect it to lie close to the centre of the P wave

3

Comparison of Heavy Heavy Data

In this chapter I compare my results with those from other simulations and with the existing experimental data. First, I must convert the lattice results into dimensionful quantities. I discuss next the estimation of the scale:

3.1 Setting the Scale

The experimental values for the 1P – 1S splitting for the J/ψ and Υ systems are within 2% of each other. This mass independence makes this a good quantity from which to set the scale.

However, all lattice calculations so far made have shown mass dependence; both for relativistic (*e.g.* Boyle, 1997) and non-relativistic. Nevertheless, I shall use this splitting to set the scale. The initial problem is to calculate the splitting. As I mentioned in the previous chapter, I do not think my data allow identification of the absolute positions of the simulation energies. This of course is not a problem for the inter P wave splittings, which are calculated by ratio fits. However it does mean that a little care needs to be exercised for the 1P – 1S splitting.

The method I adopted is to take the best value of the final plateau for one of the P wave operators as the energy somewhere within the P wave. I then used the size of the physical splitting as an estimate of the systematic uncertainty on the scale. The physical value of the $^3P_{cm}-^3S_1$ splitting is 440 MeV.

Using the SS lattice values of the splitting tabulated in the previous chapter gives me the following values for the scale for the three masses: 3.1(4), 3.2(4), 3.3(4) GeV. The error is statistical. Although there is a definite trend in the scale with mass, there is nothing really to choose between them. I shall take the central value as my estimate of the scale. The statistical error on this is, of course, 400 MeV. The systematic error in picking one particular mass is of the order of 100 MeV, and the systematic error from the unknown position of the P state within the P wave used in this splitting is of the order of 100 MeV. I take my final value for the scale as 3.2(2) GeV. The uncertainty is the total systematic uncertainty above.

This is lower than McCallum's (1997) figure of 3.52(14) GeV from the 1P – 1S splitting, but similar to his value of 3.22(15) GeV from the 2S – 1S splitting. Catterall *et al.* (1994) find a value of 3.4 GeV from the 2S – 1S splitting.

3.2 Mass shifts

These are compared with values based on perturbative calculations of Morningstar, and quoted in Hein and Newton (1999)

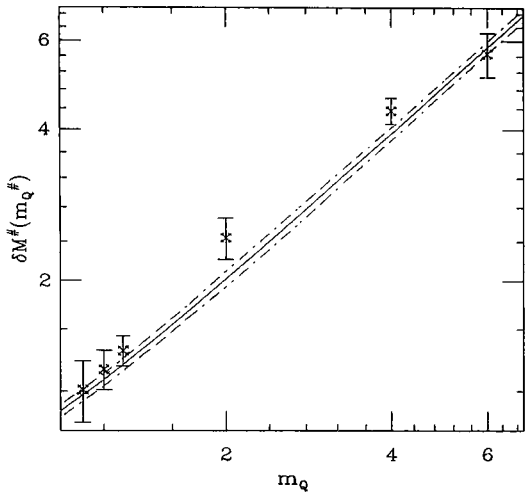

Figure 3.1 Heavy Quark Mass Shifts: Perturbative and Non-Perturbative

The agreement is very good. The behaviour of the shifts for lighter quarks lying above the perturbative estimates and those for heavier quarks lying below is seen is other calculations — see for example the $\beta 5.7$ data in Hein and Newton (1999). I don't use the perturbative values in my calculations, but quote them for the purposes of comparison.

Using the mass shift and vector simulation energy at $m_Q = 1.2$, together with the scale determined above, I calculate the vector meson mass to be 9.51(70) GeV. This is very close to the mass of the Υ, 9.46 GeV. I conclude that calculations using the $m_Q = 1.2$ Green's functions best represent the b quark. One could interpolate between the $m_Q = 1.2$ data and the $m_Q = 1.1$ to get the vector mass spot on, but at this level of accuracy there is little point.

3.3 Hyperfine Splitting

My estimation of the hyperfine splitting is

$$31\,^{+2}_{-1}\,(\text{statistical})\,^{+2}_{-2}\,(\text{systematic}) \quad \text{MeV}$$

There is no experimental number for this splitting, the pseudo-scalar belonging to the Υ system, η_b having not yet been observed.

Here are the results from other simulations:

Figure 3.2 Hyperfine splitting in the Υ system

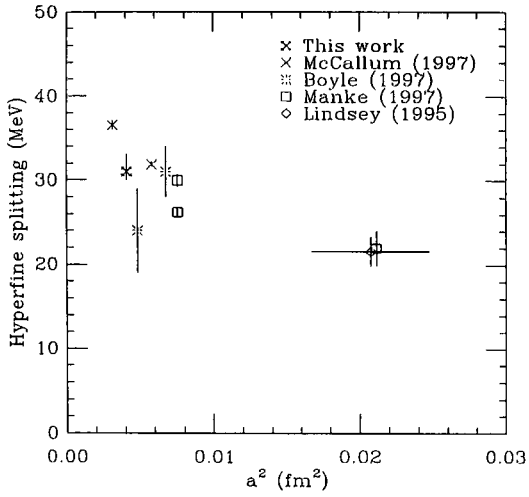

All data have been calculated using 1P − 1S to set the scale. The decorated cross is my result. The plain crosses come from McCallum (1997). The bursts are from Boyle (1997), using the Sheikholeslami Wohlert action, mean field improved. The squares are from Manke *et al.* (1997); the higher one is from a similar $\mathcal{O}(mv^4)$ action to ours, whilst the lower one is from a $\mathcal{O}(mv^6)$ action. The diamond is from a simulation of Lidsey (1995) at β5.7. All these data appear in Davies *et al.* (1998). McCallum found a far larger scale than I do: $a^{-1} = 3520$ MeV. If I use my value of the scale then his splitting falls to 32 MeV. Similarly, using my value of the scale instead of Boyle's value of 2840 MeV, his datum becomes 26 MeV.

The discretization errors are larger at larger lattice spacings, *i.e.* smaller values of β. If one then concentrates on the β6.2 and β6.0 data, as having smaller and similar discretization errors, then the values are similar, comparing like to like. The important matter is the value of the scale, and this can only be approached by larger statistics calculations. ¶

3.4 Inter P wave splittings

I calculate the following values of the splittings:

Table 3.1 P wave fine splittings in MeV

$^3P_2(E)-{}^3P_1$	38(10)
$-{}^1P_1$	22 (3)
$-{}^3P_0$	73(13)
$^3P_2(T)-{}^3P_1$	37(13)
$-{}^1P_1$	19 (6)
$-{}^3P_0$	71(12)
$^3P_1-{}^1P_1$	15 (7)
$-{}^3P_0$	32 (5)
$^3P_0-{}^1P_1$	45 (8)

¶ McCallum has far more configurations than I have — 216 compared with my 68.

Plotting these with reference to the Centre of Mass energy:

$$^3P_{CM} \stackrel{=}{\text{def}} \frac{1}{9}\left(5 \times ^3P_2 + 3 \times ^3P_1 + ^3P_0\right)$$

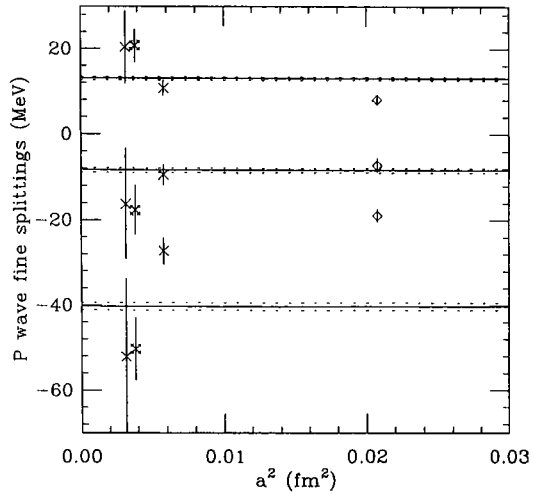

Figure 3.3 P wave fine splitting in the Υ system

The agreement with McCallum's results is very good. Interestingly, despite his larger set of configurations, I find smaller statistical errors. I think this is because the source in his evolution equation has only one spin component set.

The Peskin ratio is defined as:

$$\rho = \frac{^3P_2 - ^3P_0}{^3P_1 - ^3P_0}$$

and experimentally is 0.66. Looking at the numbers from Ali Khan, McCallum, and this work, for the values for the three lattices, the numbers are: $\rho_{5.7} = 1.4(3)$, $\rho_{6.0} = 1.1(2)$, and $\rho_{6.2} = 1.2(3)$.

It has been suggested, in the context of a charmonium spectrum calculation (Davies, 1995) that the disagreement with experiment for this ratio is due to discretization errors. The numbers of Manke using an action accurate to $\mathcal{O}(mv^6)$ give 0.56 and 0.7 for the ratio.

4

Heavy Light Spectrum

This chapter contains my results for heavy-light mesons. I had three light quark Green's functions, which were wedded to all six heavy quark NRQCD Green's functions for S-wave quantities and to the three lightest NRQCD propagators for P-wave quantities.

4.1 Additional Inputs

Before I can start, I need to know the values of some additional quantities:

4.1.1 The Lattice Spacing

It is believed that scales obtained from light hadron spectroscopy are more appropriate for heavy-light physics than those obtained from heavy-heavy spectroscopy (Ali Khan, 1996) Various quantities have been used to determine the lattice spacing for β6.2 lattices:

Table 4.1 Lattice Spacings for β6.2 lattices

Quantity	a^{-1} (GeV)	Reference
m_ρ	2.59^{+6}_{-10}	Rowland, 1997
m_N	2.34^{+7}_{-8}	Rowland, 1997
f_π	2.58^{+9}_{-9}	Lin, 1999
r_0	2.91^{+1}_{-1}	Guagnelli, 1998

In my calculations I shall use the value 2.59^{+32}_{-25} GeV where the central value comes from the ρ mass, and the errors cover the largest and smallest values in the table. These errors will be used to estimate the systematic uncertainty in setting the scale in quenched calculations. I am not concerned with the statistical errors in the individual scale calculations. Use of the ρ mass is also justified by the characteristic momentum of a gluon in a B meson being of similar size to the momentum in a light meson such as the ρ. Heavy quarkonium systems probe a higher physical scale, and so the scale determined in the previous chapter from the heavy-heavy 1P − 1S splitting isn't appropriate ¶.

4.1.2 Strange and critical κ values

I need also estimates of the κ corresponding to the strange quark, $\kappa_{\rm strange}$ and the value of $\kappa_{\rm critical}$. The following values come from Rowland, 1997:

¶ in a quenched calculation

Table 4.2 κ_{strange} and κ_{critical}

Quantity	Value	From
κ_{strange}	$0.13466\,^{+7}_{-7}$	m_K/m_ρ
	$0.13461\,^{+9}_{-21}$	m_{K^*}/m_ρ
	$0.13455\,^{+10}_{-21}$	m_ϕ/m_ρ
κ_{critical}	$0.135873\,^{+9}_{-40}$	Linear fit to three lightest pions

For consistency with other NRQCD studies, I use the value of κ_{strange} of 0.13466 calculated from m_K/m_ρ. The uncertainty in determining κ_{strange} should be treated as a source of systematic error. However, as this is much smaller than the other errors, both systematic and statistical, in the calculation, I ignore it.

4.2 Simulation Energies

4.2.1 S-wave

4.2.1.1 Bare Energies.

I shall describe the extraction of the simulation energy of a particular channel in some detail to exemplify my methodology, and to illustrate the nature of the data. I shall then discuss in less detail some other channels to show any significant differences or similarities.

I start with the Pseudo-scalar operator for the lightest heavy quark and heaviest light quark. This will be the best set of data for the heavy-light correlators because the disparity between the two masses is smallest and the operator is the best behaved. Below are graphs showing the fitted energy and χ^2/N_{dof} and Q for a concertina analysis of the channel.

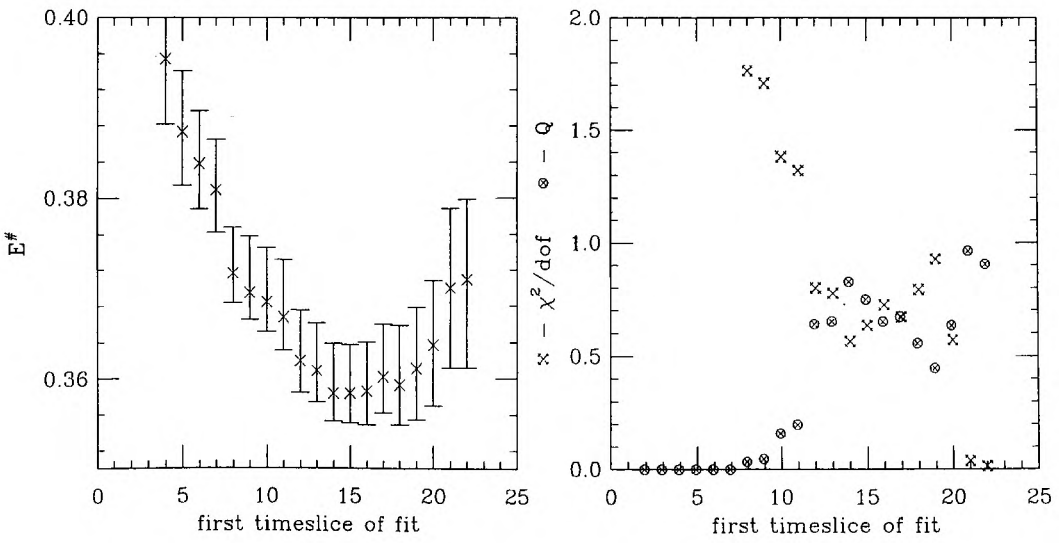

Figure 4.1 Concertina plots for PS from (0.13460, SS, 1.1)

The left hand graph shows fitted energy versus initial timeslice, the final timeslice of each fit always being 24. The right hand graph shows the corresponding $\chi^2/N_{\rm dof}$ and Q value. The data have been fitted to a single exponential. Note the mirroring of the $\chi^2/N_{\rm dof}$ and Q . The $\chi^2/N_{\rm dof}$ and Q suggest an initial timeslice of 12 or 13. However, the fitted energy is not yet stable for these initial timeslices, stability only being achieved at timeslice 14. I choose the fit beginning on timeslice 15 for the determination of the best energy as it shows stability for a variation of 1 in each direction in the initial timeslice. This value is consistent within $\sigma/2$ with fits beginning on timeslices upto 19. The energy rises for fits starting after timeslice 20, but this is just a reflection of the greater noise in the correlator data swamping the signal. To be sure of this, I performed fits over ranges ending on timeslice 20, and found excellent agreement with the fits terminating on timeslice 24. The Marquardt-Levenberg algorithm is seen to be giving little weight to these later timeslices.

Increasing the κ (and thereby decreasing the mass of the light quark) one sees a slight degradation in the behaviour of the fits.

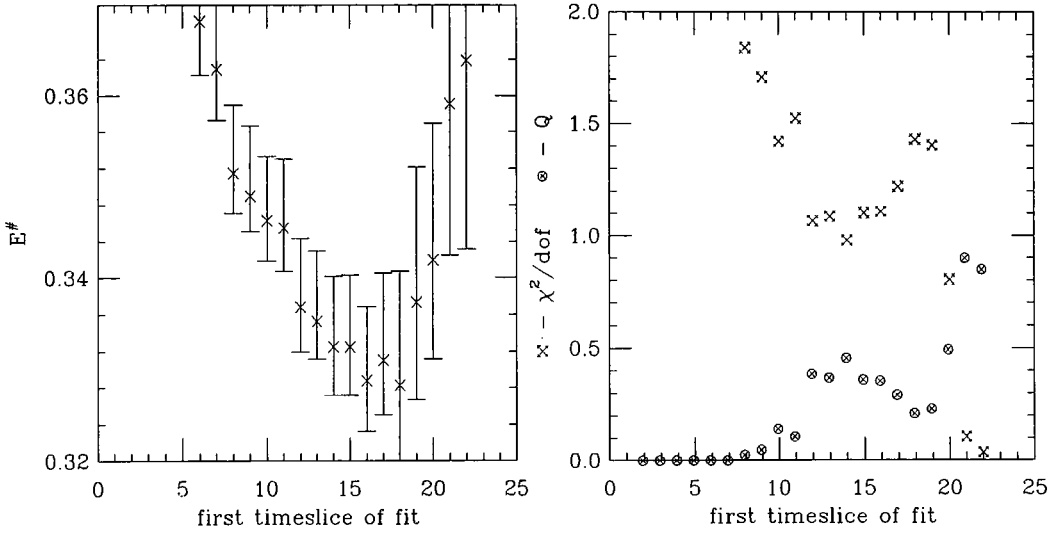

Figure 4.2 Concertina plots for PS from (0.13530, SS, 1.1)

As can be seen, the errors are larger and the length of the stable region slightly smaller. The $\chi^2/N_{\rm dof}$ values are also higher over this stable region. I choose for the best estimate the value obtained from a fit between timeslices 15 and 24. Again this is a compromise between an acceptable $\chi^2/N_{\rm dof}$ and stability. Similar behaviour is seen for the next two lightest heavy quark masses.

Turning to the other extreme, the (0.13530, SS, 6.0) PS data:

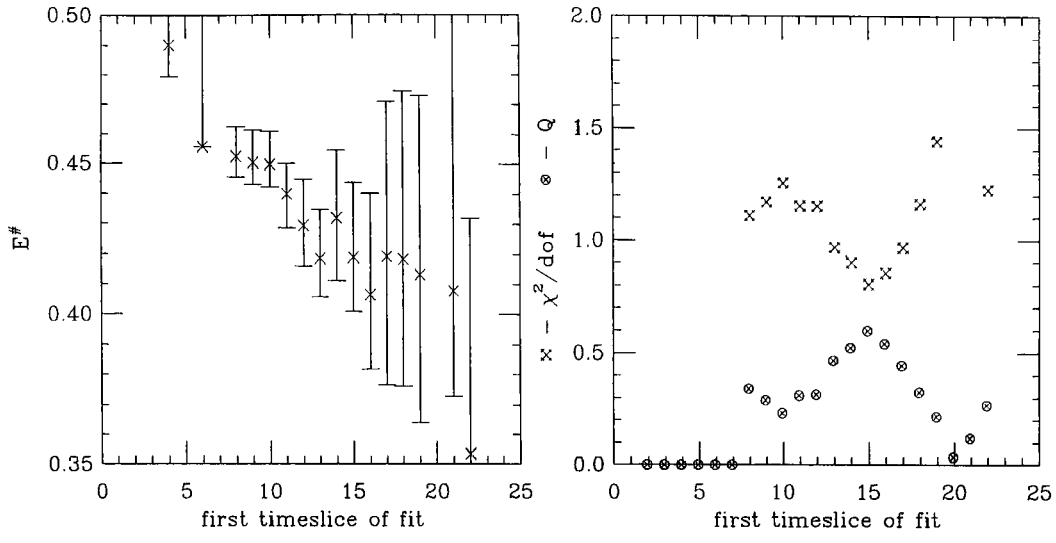

Figure 4.3 Concertina plots for PS operator from (0.13530, SS, 6.0) data

Again the same trends are noticed as before: more noise and less well defined region of stability. Note also the greater length of the stable region — the problem caused by the missing backwards propagating heavy quark is smaller with very heavy heavy quarks. The chosen fit range was 15 to 24.

The data for the vector channels are substantially the same, though slightly more noisy. The fitted results are shown overleaf.

I have also calculated the energy of the Spin Average state from:

$$E_{\overline{S}} = \frac{1}{4}\left(E_{\mathrm{PS}} + 3 \times E_{\mathrm{V}}\right)$$

As can be seen from the tables, there is good agreement between the SL data and SS data. The fitted energy decreases with increasing kappa, and increases with increasing heavy quark mass. The difference between the pseudo-scalar energy and vector energy decreases with increasing mass. This is the hyperfine splitting and will be discussed later in this chapter.

4.2.1.2 Extrapolated and Interpolated Results.

I now present results for the extrapolation to the chiral limit and interpolation to the strange quark mass. I did this by fitting the previously determined simulation energies at the three values of κ to the following form:

$$E(\kappa) = a + \frac{b}{\kappa}$$

and then using the parameters, a and b to find the energy at the two values, $\kappa_{\mathrm{strange}}$ and $\kappa_{\mathrm{critical}}$.

Table 4.3 S-wave unextrapolated fitted simulation energies: SL data

			$\kappa = 0.13460$		$\kappa = 0.13510$		$\kappa = 0.13530$	
Channel	Mass	n	$E^{\#}$	Q	$E^{\#}$	Q	$E^{\#}$	Q
Pseudo-Scalar	1.1	4	0.3585(42)	0.5	0.3428(58)	0.1	0.3360(67)	0.1
	1.2	3	0.3732(44)	0.5	0.3580(58)	0.2	0.3514(69)	0.1
	1.3	3	0.3833(45)	0.5	0.3686(61)	0.2	0.3619(75)	0.1
	2.0	2	0.4232(55)	0.5	0.4083(78)	0.4	0.398(10)	0.2
	4.0	1	0.4438(96)	0.8	0.427(13)	0.7	0.418(17)	0.5
	6.0	1	0.446(19)	0.7	0.426(29)	0.6	0.414(37)	0.5
Vector	1.1	4	0.3751(52)	0.8	0.3551(73)	0.2	0.3413(96)	0.1
	1.2	3	0.3883(50)	0.8	0.3723(73)	0.2	0.3651(95)	0.1
	1.3	3	0.3974(50)	0.8	0.3820(75)	0.3	0.3748(100)	0.1
	2.0	2	0.4307(60)	0.8	0.4128(97)	0.3	0.404(11)	0.1
	4.0	1	0.4466(94)	0.9	0.427(15)	0.7	0.417(18)	0.5
	6.0	1	0.444(19)	0.6	0.422(27)	0.5	0.413(22)	0.5
Spin Average	1.1	4	0.3709(49)	-	0.3520(64)	-	0.3400(82)	-
	1.2	3	0.3846(48)	-	0.3688(68)	-	0.3616(86)	-
	1.3	3	0.3939(47)	-	0.3786(69)	-	0.3716(88)	-
	2.0	2	0.4289(56)	-	0.4117(83)	-	0.403(11)	-
	4.0	1	0.4459(92)	-	0.427(14)	-	0.417(18)	-
	6.0	1	0.445(19)	-	0.423(27)	-	0.413(24)	-

Table 4.4 S-wave unextrapolated fitted simulation energies: SS data

			$\kappa = 0.13460$		$\kappa = 0.13510$		$\kappa = 0.13530$	
Channel	Mass	n	$E^{\#}$	Q	$E^{\#}$	Q	$E^{\#}$	Q
Pseudo-Scalar	1.1	4	0.3584(44)	0.7	0.3408(53)	0.4	0.3325(66)	0.4
	1.2	3	0.3728(46)	0.8	0.3553(54)	0.5	0.3471(67)	0.4
	1.3	3	0.3826(47)	0.8	0.3653(56)	0.5	0.3570(67)	0.4
	2.0	2	0.4204(56)	0.9	0.4048(75)	0.8	0.3976(95)	0.7
	4.0	1	0.4430(77)	0.8	0.425(10)	0.7	0.417(12)	0.6
	6.0	1	0.4492(99)	0.6	0.438(12)	0.4	0.419(21)	0.6
Vector	1.1	4	0.3740(50)	0.9	0.3531(83)	0.6	0.3423(96)	0.4
	1.2	3	0.3875(53)	0.9	0.3698(75)	0.7	0.3614(86)	0.5
	1.3	3	0.3968(59)	0.9	0.3793(78)	0.7	0.3711(91)	0.5
	2.0	2	0.4300(68)	0.9	0.4121(88)	0.8	0.404(12)	0.7
	4.0	1	0.447(11)	0.6	0.426(11)	0.6	0.417(14)	0.4
	6.0	1	0.460(13)	0.4	0.431(20)	0.5	0.415(24)	0.5
Spin Average	1.1	4	0.3701(45)	-	0.3500(72)	-	0.3399(84)	-
	1.2	3	0.3838(47)	-	0.3662(69)	-	0.3578(78)	-
	1.3	3	0.3932(55)	-	0.3758(72)	-	0.3675(80)	-
	2.0	2	0.4276(62)	-	0.4102(82)	-	0.402(10)	-
	4.0	1	0.4462(96)	-	0.426(11)	-	0.417(13)	-
	6.0	1	0.457(12)	-	0.433(16)	-	0.416(23)	-

Figure 4.4 Fits in $1/\kappa$ for pseudo-Scalar channel, SL and SS data, $m_Q = 1.1$

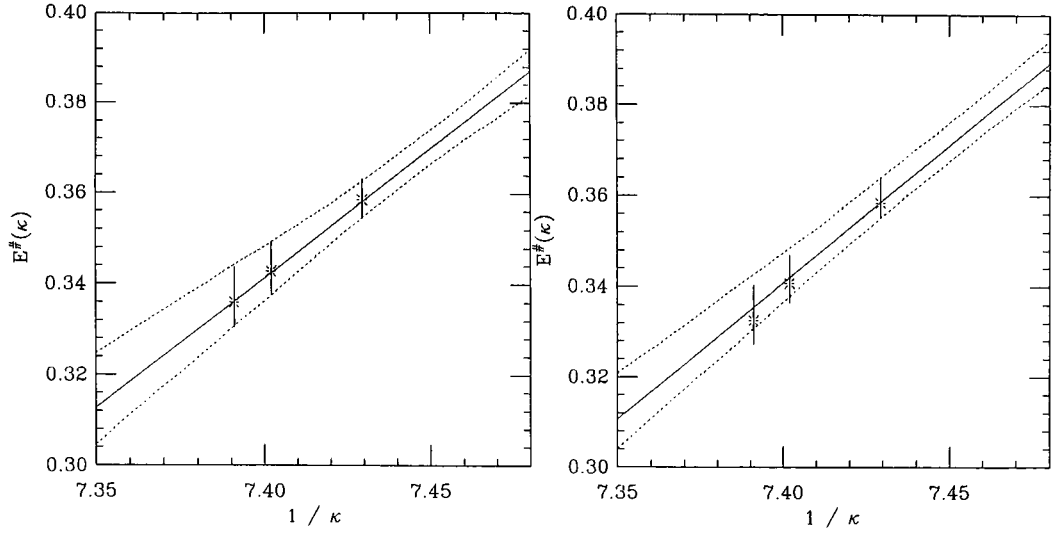

The above data are well described by a linear function. There is excellent agreement between the SL and the SS data in terms of the final numbers extracted, despite the difference in $\chi^2/N_{\rm dof}$

To contrast this, here are the data for the heaviest heavy quark mass, in the vector channel:

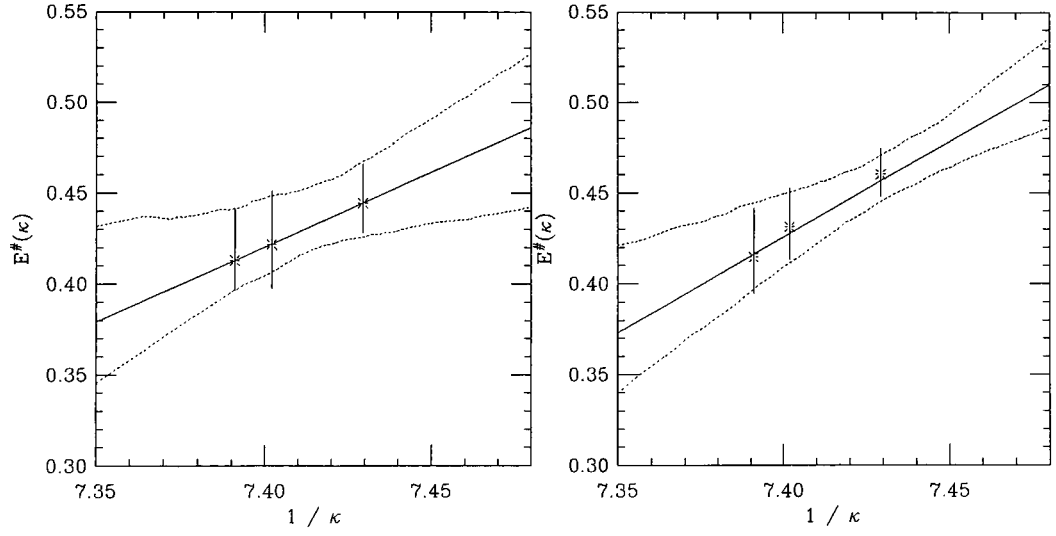

Figure 4.5 Fits in $1/\kappa$ for vector channel, SL and SS data, $m_Q = 6.0$

Again the same type of behaviour is observed. In contrast with the $m_Q = 1.1$ data, there are much larger errors, arising of course because of the larger errors in the original data. The discrepancy between the $\chi^2/N_{\rm dof}$ statistics is intriguing. However, the values of the fit parameters and the estimates at the physical κ 's are similar and consistent within errors. *N.B.* Both fits are correlated χ^2 fits.

All the extrapolated energies are shown overleaf:

Table 4.5 S wave extrapolated simulation energies: SL data

			$\kappa_{\text{chiral}} = 0.135873$			$\kappa_{\text{strange}} = 0.13466$		
Channel	Mass	n	$E^{\#}$	Q	χ^2/N_{dof}	$E^{\#}$	Q	χ^2/N_{dof}
Pseudo-Scalar	1.1	4	0.3183(92)	0.7	0.1	0.3562(41)	0.7	0.1
	1.2	3	0.3354(96)	0.7	0.2	0.3712(44)	0.7	0.2
	1.3	3	0.347(10)	0.7	0.2	0.3816(47)	0.7	0.2
	2.0	2	0.383(12)	0.6	0.3	0.4211(58)	0.6	0.3
	4.0	1	0.407(19)	0.6	0.3	0.4432(95)	0.6	0.3
	6.0	1	0.401(44)	0.6	0.3	0.444(20)	0.6	0.3
Vector	1.1	4	0.323(13)	0.2	1.4	0.3729(52)	0.2	1.4
	1.2	3	0.349(12)	0.7	0.1	0.3867(53)	0.7	0.1
	1.3	3	0.361(13)	0.6	0.2	0.3964(57)	0.6	0.2
	2.0	2	0.382(18)	0.5	0.4	0.4278(69)	0.5	0.4
	4.0	1	0.399(23)	0.4	0.6	0.443(10)	0.4	0.6
	6.0	1	0.387(39)	1.0	0.0	0.442(19)	1.0	0.0
Spin Average	1.1	4	0.323(11)	0.2	1.5	0.3691(50)	0.2	1.5
	1.2	3	0.346(11)	0.7	0.2	0.3829(49)	0.7	0.2
	1.3	3	0.358(12)	0.6	0.3	0.3927(52)	0.6	0.3
	2.0	2	0.389(14)	0.4	0.7	0.4272(59)	0.4	0.7
	4.0	1	0.405(20)	0.5	0.5	0.4449(93)	0.5	0.5
	6.0	1	0.389(38)	0.9	0.0	0.442(20)	0.9	0.0

Table 4.6 S wave extrapolated simulation energies: SS data

			$\kappa_{\text{chiral}} = 0.135873$			$\kappa_{\text{strange}} = 0.13466$		
Channel	Mass	n	$E^{\#}$	Q	χ^2/N_{dof}	$E^{\#}$	Q	χ^2/N_{dof}
Pseudo-Scalar	1.1	4	0.3166(77)	0.4	0.7	0.3566(45)	0.4	0.7
	1.2	3	0.3313(80)	0.4	0.7	0.3710(46)	0.4	0.7
	1.3	3	0.3414(79)	0.4	0.8	0.3807(48)	0.4	0.8
	2.0	2	0.383(12)	0.6	0.2	0.4189(61)	0.6	0.2
	4.0	1	0.396(16)	0.4	0.6	0.4387(82)	0.4	0.6
	6.0	1	0.417(19)	0.4	0.6	0.4481(98)	0.4	0.6
Vector	1.1	4	0.316(15)	0.3	1.0	0.3703(52)	0.3	1.0
	1.2	3	0.342(12)	0.4	0.7	0.3842(55)	0.4	0.7
	1.3	3	0.352(13)	0.5	0.4	0.3945(59)	0.5	0.4
	2.0	2	0.387(17)	0.8	0.1	0.4289(63)	0.8	0.1
	4.0	1	0.392(17)	0.9	0.0	0.4440(88)	0.9	0.0
	6.0	1	0.383(36)	0.3	1.0	0.453(13)	0.3	1.0
Spin Average	1.1	4	0.316(12)	0.3	1.1	0.3666(48)	0.3	1.1
	1.2	3	0.338(11)	0.4	0.8	0.3800(51)	0.4	0.8
	1.3	3	0.347(12)	0.5	0.6	0.3900(56)	0.5	0.6
	2.0	2	0.386(14)	0.7	0.2	0.4263(60)	0.7	0.2
	4.0	1	0.394(17)	1.0	0.0	0.4438(84)	1.0	0.0
	6.0	1	0.408(26)	0.3	1.0	0.457(12)	0.3	1.0

4.2.1.3 Meson masses.

The meson mass is calculated by adding in the heavy quark mass that was left out of the action.

$$M = \frac{1}{2}\delta + \widetilde{E}_{\text{simulation}}$$

in which δ is the mass shift measured from the dispersion of the heavy-heavy simulation data. For these heavy-light mesons we just need half of this. $\widetilde{E}_{\text{simulation}}$ is the extrapolated energy calculated previously. Adding in half of the shift gives the meson masses which are tabulated overleaf.

The very close agreement between the two sets of data is due to the mass shift being so much larger than the simulation energy. The errors in the meson masses are dominated by the errors in the mass shifts.

4.2.2 P wave

Results for operators in the P wave are of lower quality than those in the S wave because the operators used to create the P wave states all contain covariant derivatives. The fluctuations of the gauge links between configurations in these derivatives are an additional source of noise.

I have two operators with $J = 1$ which will both create a superposition of the physical $J = 1$ states: I label these, in analogy with the heavy-heavy operators, $^3P_1$ and $^1P_1$. The signal for P wave operators quickly dissolves into noise and so I was careful about choosing the end point for the fits. The part of the data that is just noise will have large errors, and so be of little importance in the χ^2 minimisation. This was demonstrated in the fits for the pseudo-scalar by moving the end point backwards and observing the lack of change in the fitted energy. But if there are more data that are noise than signal the minimisation routine will be inundated, and will produce a spurious result. The data that are noisy must be rejected. Rather than performing fits over all possible start and end points, which would take an inordinate amount of time and produce too much information, I looked at the effective mass for the channel in question to estimate the region where the signal occurs. I then made several concertina analyses with different end points to systematically scan a slightly larger region. To illustrate:

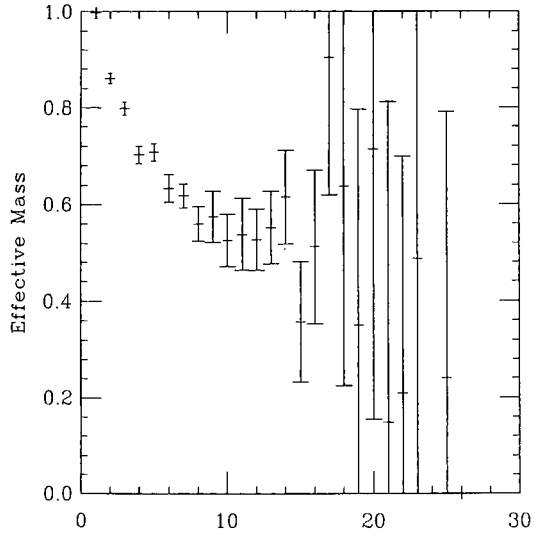

Figure 4.6 Effective Mass for $^3P_0$ from (0.13460, SS, 1.1)

Table 4.7 S wave meson masses: SL data

			$\kappa_{\text{chiral}} = 0.135873$	$\kappa_{\text{strange}} = 0.13466$
Channel	Mass	n	$E^{\#}$	$E^{\#}$
Pseudo-Scalar	1.1	4	1.53(17)	1.57(16)
	1.2	3	1.67(12)	1.70(12)
	1.3	3	1.79(10)	1.83(11)
	2.0	2	2.82(23)	2.86(23)
	4.0	1	4.76(26)	4.80(26)
	6.0	1	6.06(57)	6.10(57)
Vector	1.1	4	1.54(17)	1.59(16)
	1.2	3	1.68(12)	1.72(12)
	1.3	3	1.81(11)	1.84(11)
	2.0	2	2.82(23)	2.87(23)
	4.0	1	4.76(26)	4.80(26)
	6.0	1	6.04(56)	6.10(57)
Spin Average	1.1	4	1.54(17)	1.58(17)
	1.2	3	1.68(12)	1.71(12)
	1.3	3	1.80(11)	1.84(11)
	2.0	2	2.83(23)	2.87(23)
	4.0	1	4.76(26)	4.80(26)
	6.0	1	6.05(56)	6.10(57)

Table 4.8 S wave meson masses: SS data

			$\kappa_{\text{chiral}} = 0.135873$	$\kappa_{\text{strange}} = 0.13466$
Channel	Mass	n	$E^{\#}$	$E^{\#}$
Pseudo-Scalar	1.1	4	1.53(17)	1.57(16)
	1.2	3	1.66(12)	1.70(12)
	1.3	3	1.79(10)	1.83(10)
	2.0	2	2.82(23)	2.86(23)
	4.0	1	4.75(26)	4.80(26)
	6.0	1	6.07(57)	6.11(56)
Vector	1.1	4	1.53(17)	1.58(16)
	1.2	3	1.67(12)	1.72(12)
	1.3	3	1.80(11)	1.84(10)
	2.0	2	2.83(23)	2.87(24)
	4.0	1	4.75(27)	4.80(26)
	6.0	1	6.04(57)	6.11(57)
Spin Average	1.1	4	1.53(17)	1.58(16)
	1.2	3	1.67(12)	1.71(12)
	1.3	3	1.79(11)	1.84(10)
	2.0	2	2.83(23)	2.87(24)
	4.0	1	4.75(27)	4.80(26)
	6.0	1	6.07(57)	6.11(57)

From the effective mass a reasonable candidate for the plateau extends from timeslice 8 to timeslice 14. I therefore considered concertina fits between timeslices 6 and 15, 6 and 14, and 6 and 13. First consider the fits with maximum timeslice 13.

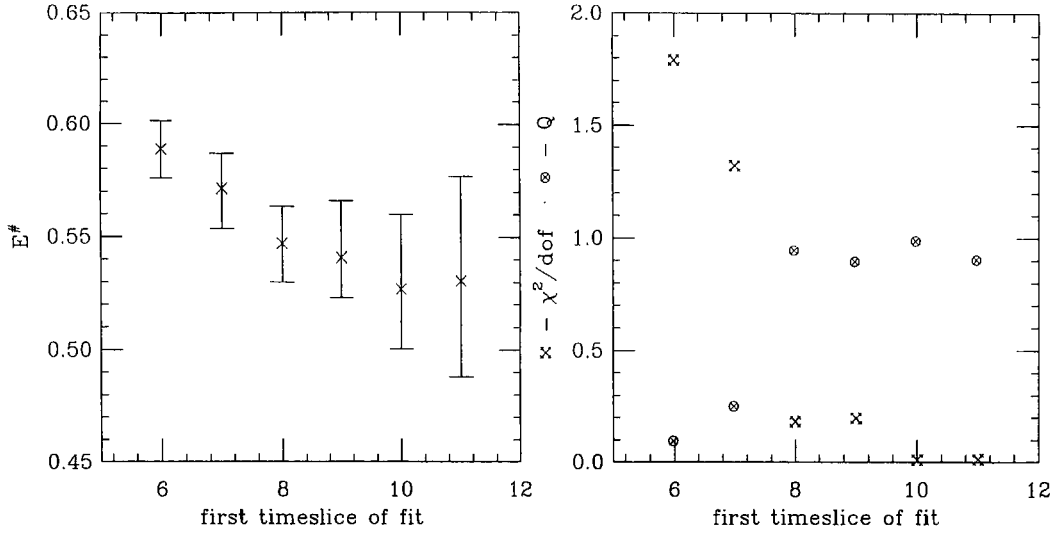

Figure 4.7 Concertina graphs with $t_{max} = 13$, (0.13460,SS,1.1) $^3P_1$

The beginnings of stability are seen at timeslice 8. The fit beginning at timeslice 9 is a candidate for the best fit, but doesn't satisfy the requirement of stability in the fitted energy for a variation of one either way in the initial timeslice. Energies for fits beginning timeslice 8 and timeslice 9 are very similar to each other, but not with that for a fit beginning on timeslice 10, which is nearly one sigma away. The fit starting on timeslice 10 is stable but is over a very small number of timeslices: this is reflected by the large error for this fit.

To see if the situation could be improved I moved the final timeslice out by 1 and looked at the concertina graphs again:

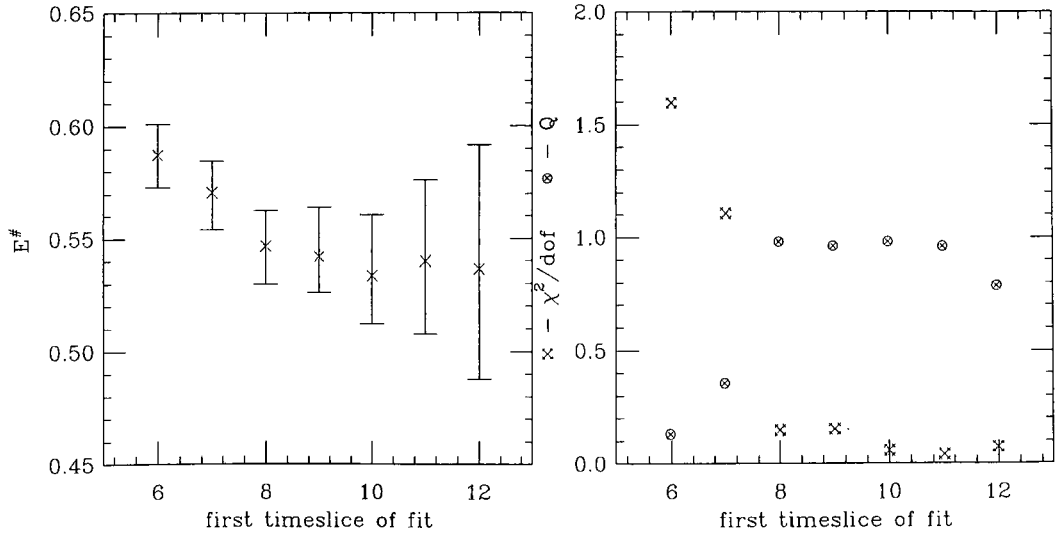

Figure 4.8 Concertina graphs with $t_{max} = 14$ (0.13460,SS,1.1) $^3P_1$

Here the situation is much better and the stability criterion can be satisfied. The variation in fitted energy when the first timeslice is 8, 9, or 10 is less than half-sigma. The fit over timeslice 9 to 14 is acceptable. Pushing the final timeslice to 15:

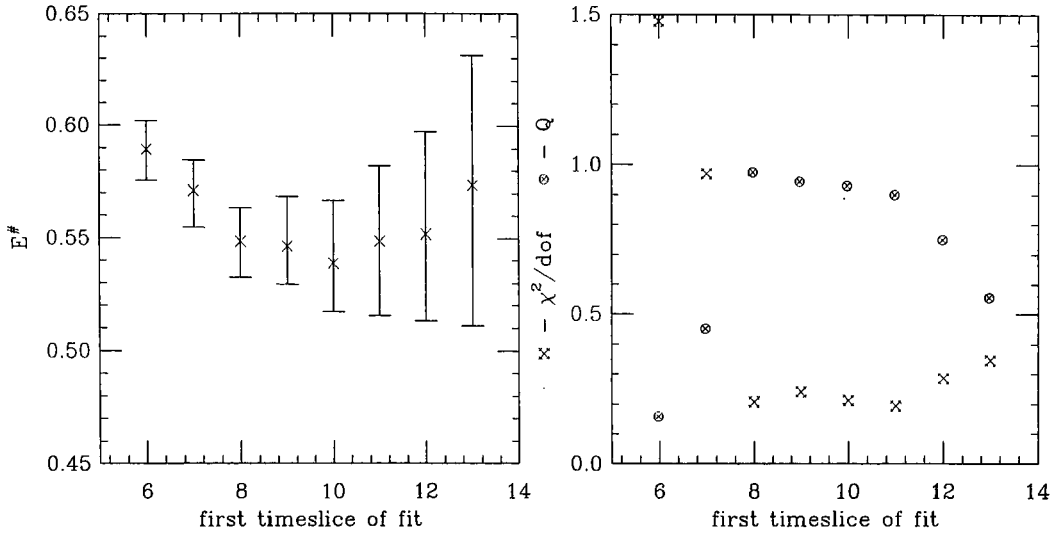

Figure 4.9 Concertina graphs with $t_{max} = 15$ (0.13460,SS,1.1) $^3P_1$

The fitted energies are almost identical to those of the fits with final timeslice 14. The rising χ^2/N_{dof} after timeslice 12 is a sign of the noise beginning to dominate the data. I choose the fits with final timeslice 14 as they have smaller values of χ^2/N_{dof} and use the fit between timeslices 9 and 14 as the best estimate.

4.2.2.1 $^3P_0$ *channel.*

Here are the final numbers for the $^3P_0$ states:

Table 4.9 $^3P_0$ simulation energies: SL data

		$\kappa = 0.13460$		$\kappa = 0.13510$		$\kappa = 0.13530$	
Mass	n	$E^\#$	χ^2/N_{dof}	$E^\#$	χ^2/N_{dof}	$E^\#$	χ^2/N_{dof}
1.1	4	0.545(17)	0.1	0.533(17)	0.2	0.529(20)	0.3
1.2	3	0.560(17)	0.1	0.548(18)	0.2	0.544(21)	0.3
1.3	3	0.571(18)	0.1	0.559(18)	0.2	0.556(21)	0.3

Table 4.10 $^3P_0$ simulation energies: SS data

		$\kappa = 0.13460$		$\kappa = 0.13510$		$\kappa = 0.13530$	
Mass	n	$E^\#$	χ^2/N_{dof}	$E^\#$	χ^2/N_{dof}	$E^\#$	χ^2/N_{dof}
1.1	4	0.542(19)	0.2	0.531(21)	0.3	0.527(26)	0.4
1.2	3	0.557(19)	0.1	0.546(21)	0.3	0.541(27)	0.4
1.3	3	0.568(18)	0.1	0.557(22)	0.3	0.552(26)	0.4

There is excellent agreement between the SL and SS data with differences between the two sets of data vastly smaller than the errors. There is distinct and definite variation with κ, even though within errors the energies agree. Similarly there is variation with heavy quark mass, m_Q, and again, although the energies agree within errors, the variation is a little more distinct. Despite the large errors the chiral extrapolations gave good results.

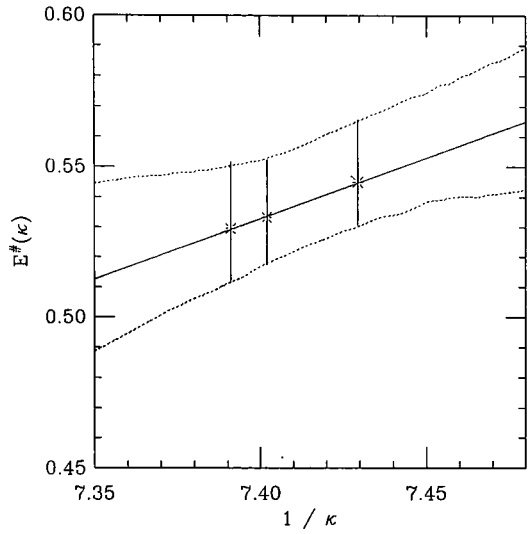

Figure 4.10 Fit in $1/\kappa$ for $^3P_0$ operator and 1.1, SL data

Table 4.11 $^3P_0$ extrapolated energies: SL data

		$\kappa_{chiral} = 0.135873$			$\kappa_{strange} = 0.13466$		
Mass	n	$E^{\#}$	Q	χ^2/N_{dof}	$E^{\#}$	Q	χ^2/N_{dof}
1.1	4	0.516(26)	1.0	6e-4	0.543(17)	1.0	6e-4
1.2	3	0.526(21)	0.7	0.10	0.556(19)	0.7	0.10
1.3	3	0.536(21)	0.7	0.11	0.567(19)	0.7	0.11

Table 4.12 $^3P_0$ extrapolated energies: SS data

		$\kappa_{chiral} = 0.135873$			$\kappa_{strange} = 0.13466$		
Mass	n	$E^{\#}$	Q	χ^2/N_{dof}	$E^{\#}$	Q	χ^2/N_{dof}
1.1	4	0.517(25)	0.9	0.02	0.542(20)	0.9	0.02
1.2	3	0.531(25)	0.9	0.01	0.557(21)	0.9	0.01
1.3	3	0.541(25)	0.9	0.01	0.567(20)	0.9	0.01

Again the differences between the two smearings are much smaller than the errors.

4.2.2.2 $^3P_2$ *channel.*

The fitted energies are:

Table 4.13 $^3P_2$ simulation energies: T representation operator: SL data

		$\kappa = 0.13460$		$\kappa = 0.13510$		$\kappa = 0.13530$	
Mass	n	$E^\#$	$\chi^2/N_{\rm dof}$	$E^\#$	$\chi^2/N_{\rm dof}$	$E^\#$	$\chi^2/N_{\rm dof}$
1.1	4	0.646(30)	0.6	0.644(36)	0.7	0.648(39)	0.7
1.2	3	0.659(30)	0.6	0.657(35)	0.7	0.661(40)	0.7
1.3	3	0.668(31)	0.7	0.666(35)	0.8	0.671(41)	0.8

Table 4.14 $^3P_2$ simulation energies: T representation operator: SS data

		$\kappa = 0.13460$		$\kappa = 0.13510$		$\kappa = 0.13530$	
Mass	n	$E^\#$	$\chi^2/N_{\rm dof}$	$E^\#$	$\chi^2/N_{\rm dof}$	$E^\#$	$\chi^2/N_{\rm dof}$
1.1	4	0.659(19)	0.6	0.657(23)	0.6	0.660(25)	0.6
1.2	3	0.673(19)	0.7	0.671(23)	0.7	0.674(26)	0.6
1.3	3	0.683(19)	0.7	0.680(23)	0.6	0.684(27)	0.6

Table 4.15 $^3P_2$ simulation energies: E representation operator: SL data

		$\kappa = 0.13460$		$\kappa = 0.13510$		$\kappa = 0.13530$	
Mass	n	$E^\#$	$\chi^2/N_{\rm dof}$	$E^\#$	$\chi^2/N_{\rm dof}$	$E^\#$	$\chi^2/N_{\rm dof}$
1.1	4	0.691(23)	1.0	0.693(25)	0.8	0.698(26)	0.7
1.2	3	0.706(23)	1.0	0.707(26)	0.8	0.713(26)	0.7
1.3	3	0.738(23)	1.5	0.718(26)	0.8	0.724(27)	0.7

Table 4.16 $^3P_2$ simulation energies: E representation operator: SS data

		$\kappa = 0.13460$		$\kappa = 0.13510$		$\kappa = 0.13530$	
Mass	n	$E^\#$	$\chi^2/N_{\rm dof}$	$E^\#$	$\chi^2/N_{\rm dof}$	$E^\#$	$\chi^2/N_{\rm dof}$
1.1	4	0.669(22)	0.7	0.668(24)	0.7	0.673(25)	0.7
1.2	3	0.682(23)	0.7	0.682(24)	0.7	0.687(27)	0.7
1.3	3	0.692(23)	0.7	0.692(25)	0.7	0.697(27)	0.6

There is absolutely no light κ dependence. The variation between the values of κ for given mass, representation, and smearing is no more than $\sigma/4$, and shows no consistent tendency. Agreement between the two representations is good, typically around $\sigma/2$ for the SS data, and just under 2σ for the SL data. Within each representation there is typically agreement between the SL data and the SS data of σ. There is variation with the heavy quark mass parameter. The difference between the lightest heavy quark mass and the heaviest is at the σ level.

4.2.2.3 $^3P_1$ *and* $^1P_1$.

I found good signals for the self-correlators but didn't see any reasonable signal from the cross-correlators. Attempts to diagonalise the matrix of correlators were unsuccessful. All that can be done is to assume that the lower energy of the two operators corresponds to the energy of the lighter physical state. The hope is that the higher state contamination has died out in the region from which the energy is extracted. Unfortunately, there is no way of

Table 4.17 $^1P_1$ and $^3P_1$ simulation energies - SL data

			$\kappa = 0.13460$		$\kappa = 0.13510$		$\kappa = 0.13530$	
Channel	Mass	n	$E^{\#}$	$\chi^2/N_{\rm dof}$	$E^{\#}$	$\chi^2/N_{\rm dof}$	$E^{\#}$	$\chi^2/N_{\rm dof}$
$^1P_1$	1.1	4	0.612(19)	0.5	0.601(21)	0.5	0.598(23)	0.6
	1.2	3	0.625(19)	0.5	0.615(21)	0.6	0.612(23)	0.6
	1.3	3	0.634(19)	0.5	0.624(22)	0.6	0.621(23)	0.6
$^3P_1$	1.1	4	0.595(16)	0.2	0.584(18)	0.1	0.581(20)	0.1
	1.2	3	0.607(16)	0.2	0.596(18)	0.1	0.593(20)	0.1
	1.3	3	0.616(16)	0.2	0.604(18)	0.1	0.601(20)	0.1

Table 4.18 $^1P_1$ and $^3P_1$ simulation energies - SS data

			$\kappa = 0.13460$		$\kappa = 0.13510$		$\kappa = 0.13530$	
Channel	Mass	n	$E^{\#}$	$\chi^2/N_{\rm dof}$	$E^{\#}$	$\chi^2/N_{\rm dof}$	$E^{\#}$	$\chi^2/N_{\rm dof}$
$^1P_1$	1.1	4	0.605(19)	0.7	0.595(22)	0.6	0.591(25)	0.6
	1.2	3	0.617(18)	0.6	0.607(22)	0.6	0.603(25)	0.6
	1.3	3	0.625(18)	0.6	0.615(22)	0.6	0.611(25)	0.6
$^3P_1$	1.1	4	0.584(18)	0.3	0.574(20)	0.2	0.571(23)	0.1
	1.2	3	0.597(17)	0.3	0.586(20)	0.2	0.583(23)	0.1
	1.3	3	0.605(17)	0.3	0.594(20)	0.2	0.591(23)	0.1

determining anything about the higher energy state. Looking at the raw data shown above, one sees consistency between the SL and SS data of better than $\sigma/2$. However the energies for the two operators are consistent within σ for both smearings.

These extrapolation fits, below, have reasonable $\chi^2/N_{\rm dof}$'s and very good agreement between the smearings, within $\sigma/2$. The values at $\kappa_{\rm strange}$ and $\kappa_{\rm critical}$ agree within σ and the values from the two operators agree within σ.

Table 4.19 $^1P_1$ and $^3P_1$ extrapolated energies — SL data

			$\kappa_{\rm chiral} = 0.135873$			$\kappa_{\rm strange} = 0.13466$		
Channel	Mass	n	$E^{\#}$	Q	$\chi^2/N_{\rm dof}$	$E^{\#}$	Q	$\chi^2/N_{\rm dof}$
$^1P_1$	1.1	4	0.593(34)	0.9	0.03	0.609(19)	0.9	0.03
	1.2	3	0.591(26)	0.5	0.49	0.624(19)	0.5	0.49
	1.3	3	0.606(27)	0.5	0.53	0.637(20)	0.5	0.53
$^3P_1$	1.1	4	0.563(21)	0.7	0.18	0.594(17)	0.7	0.18
	1.2	3	0.575(21)	0.6	0.21	0.607(17)	0.6	0.21
	1.3	3	0.585(21)	0.6	0.23	0.616(16)	0.6	0.23

Table 4.20 $^1P_1$ and $^3P_1$ extrapolated energies — SS data

			$\kappa_{\text{chiral}} = 0.135873$			$\kappa_{\text{strange}} = 0.13466$		
Channel	Mass	n	$E^{\#}$	Q	χ^2/N_{dof}	$E^{\#}$	Q	χ^2/N_{dof}
$^1P_1$	1.1	4	0.578(27)	0.9	0.01	0.604(19)	0.9	0.01
	1.2	3	0.590(26)	0.9	0.01	0.616(19)	0.9	0.01
	1.3	3	0.598(26)	0.9	0.02	0.624(19)	0.9	0.02
$^3P_1$	1.1	4	0.556(24)	0.9	0.03	0.583(18)	0.9	0.03
	1.2	3	0.568(24)	0.9	0.03	0.595(18)	0.9	0.03
	1.3	3	0.576(23)	0.9	0.03	0.604(17)	0.9	0.03

4.3 Fixing the b mass parameter

As a different scale is being used for the heavy-light systems from that used in the heavy-heavy systems, the estimate of the mass parameter corresponding to the b quark will be different. It is possible to repeat the tuning process for the heavy light case, but this would be complicated by the need to extrapolate in κ to the physical light quark. However as I was using the same NRQCD Green's functions as in the heavy-heavy calculation I was forced to extrapolate/interpolate to the right mass.

The B_s meson mass was used to to fix the b mass. This is advantageous for two reasons. It is a pseudo-scalar and so described by a well behaved operator, and has a strange light quark which won't introduce problems because of the extrapolation in κ. The meson masses were fitted to polynomials in $1/m_Q$ and the value of m_Q that corresponds to the physical value, at the chosen scale was determined. All subsequent data will then extrapolated in $1/m_Q$ to this value. It is believed that these extrapolated numbers are better estimates of the required quantities, and that they are close to the numbers that would be obtained had the simulation been carried out at the new of the mass parameter.

First of all I fit all of the data to a series of polynomials in $1/m_Q$. The idea is to that this will give me the most information about the m_Q dependence of the meson mass. Secondly, I take the data on each side of the physical mass and then extrapolate between them to determine the correct mass parameter. Here the idea is that these two data are the closest estimates to the correct value, and so should be the best basis for estimating where the actual values lie.

Here is the variation of the meson mass with the bare heavy quark mass parameter:

Figure 4.11 Pseudo-Scalar meson mass vs. $1/m_Q$ - SS data

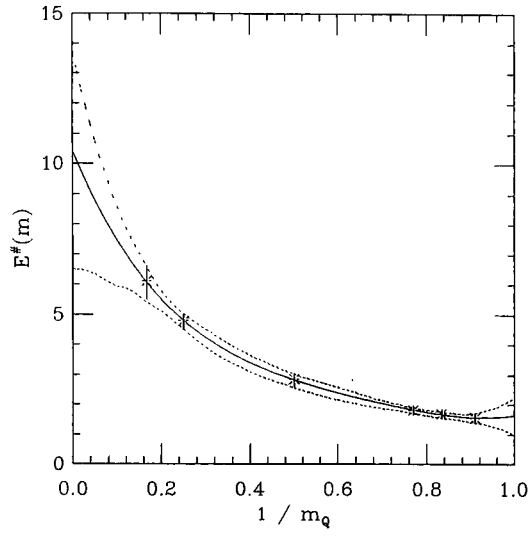

The solid line through the data is the best fit to a polynomial in $1/m_Q$ of order 5. Taking the inverse lattice spacing as 2.59 GeV, the mass of the B_s is 2.037 lattice units. The results for the various fits using the best estimate of the scale are:

Table 4.21 Best estimates for m_Q corresponding to the b quark, $a^{-1} = 2.59$ GeV

	SL		SS	
Order	m_b	χ^2/N_{dof}	m_b	χ^2/N_{dof}
2	$1.35\ ^{+4}_{-2}$	4	$1.35\ ^{+4}_{-2}$	4
3	$1.46\ ^{+9}_{-5}$	0.3	$1.46\ ^{+9}_{-5}$	0.3
4	$1.47\ ^{+13}_{-6}$	0.2	$1.47\ ^{+13}_{-6}$	0.2
5	$1.44\ ^{+15}_{-5}$	0.06	$1.44\ ^{+15}_{-5}$	0.07

The consistency between the SS and SL data is caused by the greater part of the meson energy being made up of the mass shift; only the simulation energy differs between the two sets of data, and this is small in comparison with the mass shifts. There is very good agreement between the fits from the different polynomials. Looking at the detail, shown overleaf, of the previous graph, the solid horizontal line is the value of B_s mass in lattice units. The curved solid line is the best fit from an order 5 polynomial, and the sloping diagonal dashed line is drawn between the two data closest to the physical value. Very similar numbers are obtained whatever method is chosen.

Figure 4.12 Pseudo-scalar meson mass vs. $1/m_Q$ - SS data

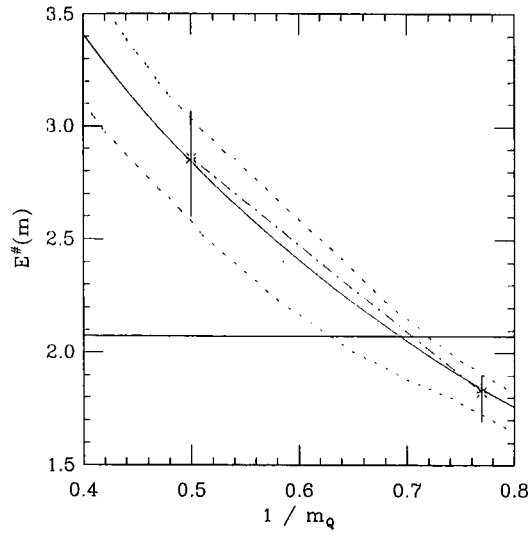

Here are the numbers using the larger and smaller values of the scale, using the polynomial fits to all six heavy masses:

Table 4.22 Best estimates for m_Q corresponding to the b quark, $a^{-1} = 2.91$ GeV

	SL		SS	
Order	m_b	χ^2/N_{dof}	m_b	χ^2/N_{dof}
2	$1.27\ ^{+4}_{-2}$	4	$1.27\ ^{+4}_{-2}$	4
3	$1.32\ ^{+9}_{-4}$	0.3	$1.32\ ^{+9}_{-4}$	0.3
4	$1.30\ ^{+10}_{-5}$	0.2	$1.30\ ^{+10}_{-5}$	0.2
5	$1.30\ ^{+9}_{-4}$	0.06	$1.30\ ^{+9}_{-4}$	0.07

Table 4.23 Best estimates for m_Q corresponding to the b quark, $a^{-1} = 2.34$ GeV

	SL		SS	
Order	m_b	χ^2/N_{dof}	m_b	χ^2/N_{dof}
2	$1.44\ ^{+5}_{-3}$	4	$1.44\ ^{+5}_{-3}$	4
3	$1.59\ ^{+10}_{-6}$	0.3	$1.59\ ^{+10}_{-6}$	0.3
4	$1.62\ ^{+15}_{-7}$	0.2	$1.63\ ^{+15}_{-7}$	0.2
5	$1.58\ ^{+18}_{-8}$	0.06	$1.59\ ^{+18}_{-8}$	0.07

As my final estimate of the heavy quark mass parameter that corresponds to the b quark I take the numbers from the SS data fitted to a polynomial of order 5, thus:

$$m_b^{\#} = 1.44\ ^{+15}_{-5}(\text{statistical})\ ^{+15}_{-14}\begin{pmatrix}\text{systematic}\\ \text{from scale}\end{pmatrix}$$

In physical units (GeV) this becomes:

$$m_b = 3.73\ ^{+39}_{-13}(\text{statistical})\ ^{+39}_{-36}\begin{pmatrix}\text{systematic}\\ \text{from scale}\end{pmatrix}\ \text{GeV}$$

4.4 Mass Splittings

In this section I concentrate on the mass splittings. Because of the removal of the mass term from the action, these are the real predictions of the theory.

4.4.1 B_s – B splitting

I calculate this splitting by subtracting the strange interpolated simulation energy from the chirally extrapolated one, and using the bootstrap distribution to estimate the error. Here are the results for the splitting between the B_s and B systems, for the Pseudo-scalar, Vector, and Spin Average states.

Table 4.24 Mass splittings for B_s and B systems: SL data

		Pseudo–Scalar	Vector	Spin Average
Mass	n	$E^{\#}$	$E^{\#}$	$E^{\#}$
1.1	4	0.0379(60)	0.050(11)	0.0462(86)
1.2	3	0.0358(64)	0.0372(75)	0.0367(67)
1.3	3	0.0344(67)	0.0349(86)	0.0347(76)
2.0	2	0.0379(87)	0.046(15)	0.0385(97)
4.0	1	0.037(12)	0.044(14)	0.039(13)
6.0	1	0.043(28)	0.054(39)	0.053(41)

Table 4.25 Mass splittings for B_s and B systems: SS data

		Pseudo-Scalar	Vector	Spin Average
Mass	n	$E^{\#}$	$E^{\#}$	$E^{\#}$
1.1	4	0.0401(48)	0.055(12)	0.051(10)
1.2	3	0.0397(50)	0.0418(79)	0.0425(71)
1.3	3	0.0392(51)	0.0422(95)	0.0429(85)
2.0	2	0.0356(78)	0.042(12)	0.041(10)
4.0	1	0.043(11)	0.052(18)	0.050(15)
6.0	1	0.031(17)	0.070(29)	0.049(22)

The numbers obtained from the two smearings are consistent within errors, typical agreement being $\sigma/2$. I found no consistent dependence on the heavy quark mass. To this end, for each group of data I fit the numbers to a constant to obtain a better estimate of the value of this splitting.

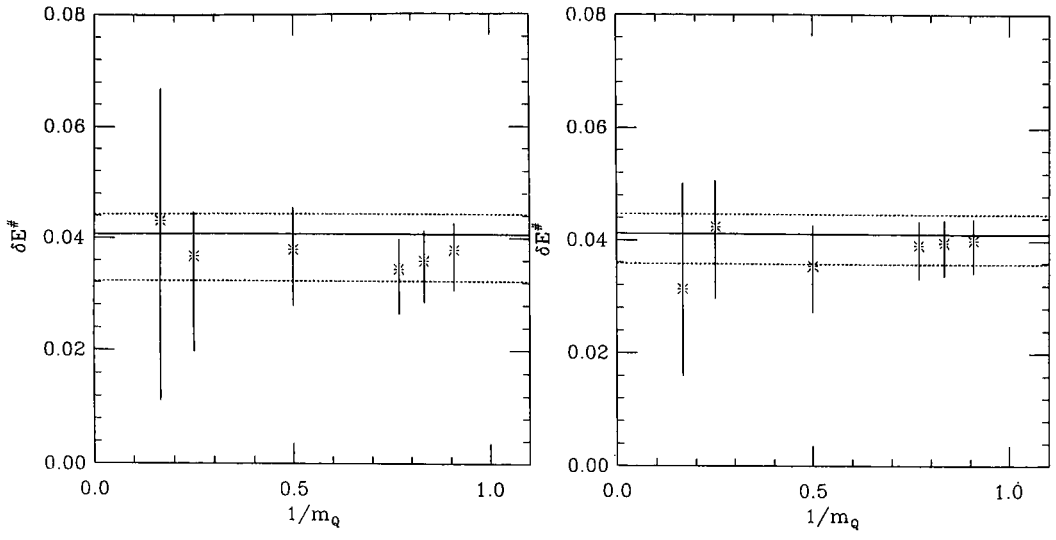

Figure 4.13 B_s- B splitting — pseudo-scalar

Here are the results for the best fits to the data:

Table 4.26 Best fits to B_s- B splitting

	SL		SS	
Channel	$E^{\#}$	$\chi^2/N_{\rm dof}$	$E^{\#}$	$\chi^2/N_{\rm dof}$
Pseudo-Scalar	$0.041\ ^{+4}_{-8}$	0.57	$0.041\ ^{+3}_{-5}$	0.40
Vector	$0.042\ ^{+6}_{-8}$	0.44	$0.045\ ^{+7}_{-8}$	0.58
Spin Average	$0.041\ ^{+4}_{-8}$	0.49	$0.045\ ^{+6}_{-7}$	0.38

There is good agreement between the two smearings and the $\chi^2/N_{\rm dof}$ values show that the data are well described by a constant.

And finally, converting these into physical units, using the lowest $\chi^2/N_{\rm dof}$ fits for each channel:

Table 4.27 Final Numbers for B_s-B splitting

Channel	Result (MeV)
Pseudo-scalar	$106\ ^{+8}_{-13}$(stat) $^{+13}_{-10}$(syst)
Vector	$109\ ^{+16}_{-20}$(stat) $^{+13}_{-11}$(syst)
Spin Average	$117\ ^{+16}_{-18}$(stat) $^{+14}_{-11}$(syst)

The value for the spin average is oddly high compared with the vector number. A lower estimate of 108 MeV is obtained by using the pseudo-scalar and vector numbers in the spin average formula.

4.4.2 Hyperfine Splitting

There are two ways of extracting this splitting: either directly from the difference between the fitted vector simulation energy and the pseudo-scalar energy, or by means of a ratio fit. The two methods must give compatible numbers, but ratio fits tend to yield smaller errors. I shall present numbers for both methods, but only use the numbers from the ratio fits in further analysis. The numbers from the direct method (with bootstrap errors) and the ratio method are shown below:

Table 4.28 Hyperfine splitting, direct method: SL data

		$\kappa = 0.13460$	$\kappa = 0.13510$	$\kappa = 0.13530$
Mass	n	$E^{\#}$	$E^{\#}$	$E^{\#}$
1.1	4	0.0166(30)	0.0123(67)	0.0054(94)
1.2	3	0.0152(32)	0.0143(47)	0.0137(62)
1.3	3	0.0142(33)	0.0134(47)	0.0128(61)
2.0	2	0.0076(44)	0.0045(82)	0.0059(83)
4.0	1	0.0028(43)	0.0007(67)	-0.0009(79)
6.0	1	-0.0021(67)	-0.0047(80)	-0.001(29)

Table 4.29 Hyperfine splitting, direct method: SS data

		$\kappa = 0.13460$	$\kappa = 0.13510$	$\kappa = 0.13530$
Mass	n	$E^{\#}$	$E^{\#}$	$E^{\#}$
1.1	4	0.0156(31)	0.0123(67)	0.0099(83)
1.2	3	0.0147(31)	0.0145(49)	0.0143(61)
1.3	3	0.0142(33)	0.0140(50)	0.0140(63)
2.0	2	0.0096(35)	0.0073(61)	0.0065(74)
4.0	1	0.0043(72)	0.0002(52)	0.0006(64)
6.0	1	0.0110(86)	-0.007(15)	-0.0043(93)

Table 4.30 Hyperfine splitting, ratio method: SL data

		$\kappa = 0.13460$		$\kappa = 0.13510$		$\kappa = 0.13530$	
Mass	n	$E^{\#}$	χ^2/dof	$E^{\#}$	χ^2/dof	$E^{\#}$	χ^2/dof
1.1	4	0.0153(18)	1.0	0.0157(23)	1.2	0.0159(26)	1.3
1.2	3	0.0141(18)	1.0	0.0145(23)	1.2	0.0147(26)	1.4
1.3	3	0.0131(18)	1.1	0.0134(23)	1.3	0.0136(27)	1.4
2.0	2	0.0079(17)	1.4	0.0079(22)	1.3	0.0080(27)	1.3
4.0	1	0.0020(15)	1.2	0.0008(20)	0.9	-0.0001(24)	0.9
6.0	1	-0.0005(17)	0.6	-0.0022(24)	0.4	-0.0034(26)	0.4

Table 4.31 Hyperfine splitting, ratio method: SS data

		$\kappa = 0.13460$		$\kappa = 0.13510$		$\kappa = 0.13530$	
Mass	n	$E^{\#}$	χ^2/dof	$E^{\#}$	χ^2/dof	$E^{\#}$	χ^2/dof
1.1	4	0.0154(24)	1.2	0.0146(36)	1.4	0.0140(40)	1.5
1.2	3	0.0141(24)	1.3	0.0132(36)	1.5	0.0127(41)	1.6
1.3	3	0.0130(24)	1.4	0.0121(36)	1.6	0.0116(42)	1.7
2.0	2	0.0077(25)	1.9	0.0072(32)	1.9	0.0072(39)	2.0
4.0	1	0.0026(23)	1.3	0.0024(30)	1.0	0.0024(33)	0.9
6.0	1	-0.0016(22)	0.7	-0.0026(30)	0.4	-0.0041(38)	0.4

The numbers obtained from the two methods are consistent within errors, and as expected, the errors on the ratio fit numbers are smaller. I shall concentrate from now on solely on the ratio fit results. The two smearings show different variation with κ: the SL data splitting increases with increasing κ whilst the SS data decreases with κ. There is excellent agreement between the two smearings for $\kappa = 0.13460$, and agreement to at least $\sigma/2$ for the other two values of κ. If I fit each set of mass and smearing data to a constant to average the two slopes, I get far better agreement between the two smearings. If I fitted to a linear form in $1/\kappa$ I got lower $\chi^2/N_{\rm dof}$ values, but the two smearings gave slopes of opposite sign.

Table 4.32 Hyperfine splitting — SL and SS data

		SL		SS	
Mass	n	$E^{\#}$	$\chi^2/N_{\rm dof}$	$E^{\#}$	$\chi^2/N_{\rm dof}$
1.1	4	$0.0151\ ^{+16}_{-16}$	0.06	$0.0157\ ^{+22}_{-20}$	0.12
1.2	3	$0.0140\ ^{+17}_{-16}$	0.05	$0.0145\ ^{+22}_{-20}$	0.12
1.3	3	$0.0129\ ^{+17}_{-16}$	0.04	$0.0134\ ^{+22}_{-19}$	0.13
2.0	2	$0.0079\ ^{+15}_{-15}$	0.02	$0.0082\ ^{+22}_{-17}$	0.09
4.0	1	$0.0022\ ^{+15}_{-14}$	0.79	$0.0027\ ^{+20}_{-18}$	0.01
6.0	1	$-0.0002\ ^{+17}_{-13}$	1.49	$-0.0020\ ^{+22}_{-19}$	0.60

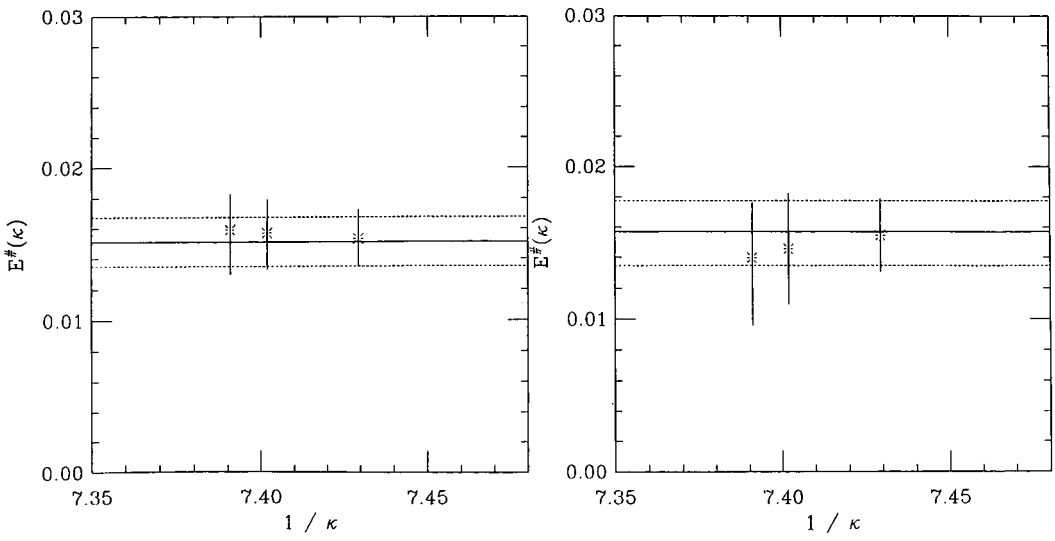

Figure 4.14 Hyperfine splitting SL and SS data, $m_{\rm Q}$=1.1

I then fitted these data to a linear form in $1/m_Q$ and found that they were well described by this. I also investigated the effect of progressively removing the heavier data from the fits as I was less confident in their veracity. Here is a typical plot:

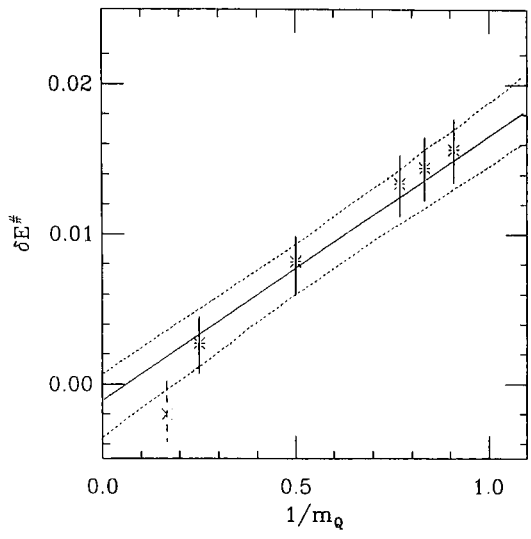

Figure 4.15 Hyperfine vs. $1/m_Q$ — SS data with fit to five lightest masses

Performing the consistency fits, striking data, gives the following numbers for the intercept (a) and slope (b):

Table 4.33 Hyperfine splitting — fits to $1/m_Q$

	SL			SS		
Nº of Masses	a	b	χ^2/N_{dof}	a	b	χ^2/N_{dof}
6	-0.0020 $^{+15}_{-15}$	0.0174 $^{+26}_{-20}$	1.13	-0.0028 $^{+23}_{-16}$	0.0188 $^{+30}_{-22}$	1.32
5	-0.0013 $^{+16}_{-15}$	0.0170 $^{+26}_{-18}$	0.90	-0.0011 $^{+25}_{-18}$	0.0176 $^{+31}_{-22}$	0.36
4	-0.0001 $^{+23}_{-19}$	0.0157 $^{+30}_{-20}$	0.83	-0.0003 $^{+33}_{-25}$	0.0172 $^{+35}_{-23}$	0.44
3	0.0017 $^{+33}_{-21}$	0.0146 $^{+35}_{-17}$	0.98	0.0009 $^{+39}_{-25}$	0.0160 $^{+38}_{-21}$	0.05

and these fits give the following values for the splitting at $m_Q = 1.44$:

Table 4.34 Hyperfine splitting at b quark

Nº of Masses	SL	SS
6	0.0101 $^{+14}_{-9}$	0.0102 $^{+16}_{-16}$
5	0.0105 $^{+13}_{-10}$	0.0112 $^{+18}_{-17}$
4	0.0108 $^{+14}_{-11}$	0.0116 $^{+21}_{-19}$
3	0.0119 $^{+18}_{-15}$	0.0120 $^{+23}_{-20}$

As the final value I take the value from the fit of the 5 lightest masses SS data. This fit has the lowest χ^2/N_{dof} excepting the fit to the three lightest masses for SS, which I do not use because it would be extrapolating to the b quark rather than interpolating to it.

$$29\,{}^{+5}_{-4}\begin{pmatrix}\text{statistics in}\\ \text{interpolation}\end{pmatrix}\,{}^{+7}_{-6}\begin{pmatrix}\text{systematics}\\ \text{from scale}\end{pmatrix}\,{}^{+1}_{-3}\begin{pmatrix}\text{statistics in}\\ \text{fixing } m_b\end{pmatrix}\,\text{MeV}$$

The central value was obtained by interpolating to $m_Q = 1.44$ and converting to physical units with the scale $a^{-1} = 2.59$ GeV. The statistical uncertainty for the interpolation procedure was obtained from the bootstrap distribution. The systematic uncertainty was obtained by repeating the procedure using the masses obtained from fixing the B_s meson mass by the two other values of the scale, and converting the central value of the interpolation into physical units with the relevant scale. The final statistical error was obtained by interpolating to the statistical bounds for m_b obtained from the scale $a^{-1} = 2.59$ GeV and converting to physical units with this scale.

4.4.3 Inter P wave splittings

I was unable to perform successful ratio fits for these splittings. This is because the range of timeslices over which a signal can be seen for the P wave operators is very small and different for different operators. The range of timeslices over which a valid signal for the ratio is thus even smaller, and in this calculation, too small to extract anything from.

To illustrate, consider the ${}^3P_2(T)-{}^3P_0$ splitting. Here is the effective mass for the ${}^3P_2(T)$ operator, (0.13460, SS, 1.1) data:

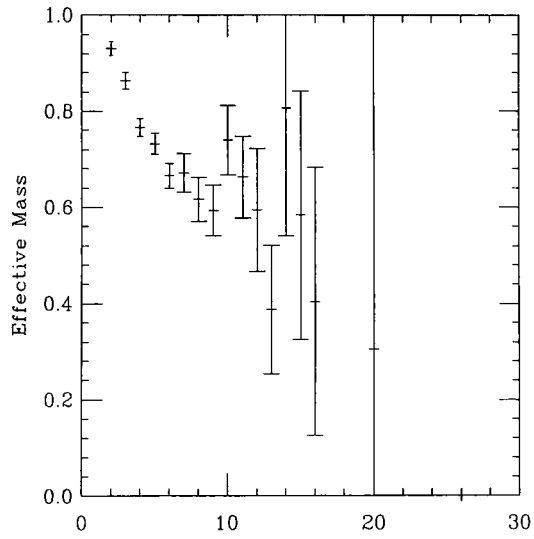

Figure 4.16 Effective mass, ${}^3P_2(T)$ from (0.13460,SS,1.1)

(The corresponding effective mass for the ${}^3P_0$ channel has already been shown). Considering just the effective masses for the moment, the ${}^3P_2(T)$ data have dissolved into noise by timeslice 13, whereas for the ${}^3P_0$ this doesn't happen until timeslice 15. The plateau for ${}^3P_0$ starts at timeslice 8, whereas for the the ${}^3P_2(T)$ it is starting at timeslice 6. The concertina analyses support this conclusion.

It is reasonable then, to expect the plateau in the ratio to be between timeslices 8 and 12. The effective mass for the ratio supports this conclusion:

Figure 4.17 Effective mass, $^3P_2(T)-^3P_0$ ratio - (0.13460,SS,1.1) data

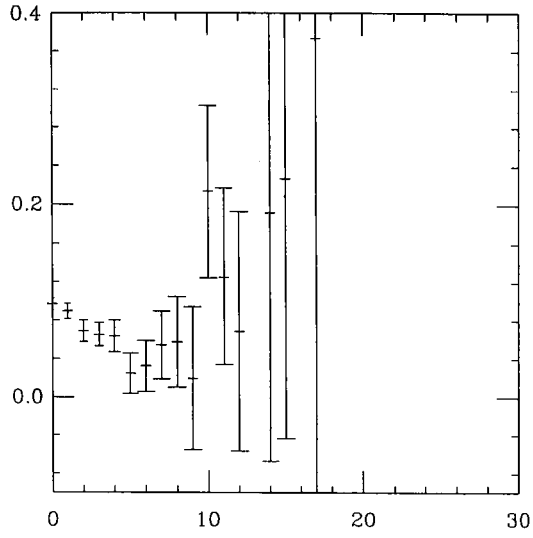

So the region over which one can expect a signal for the ratio is just noise, though it just about consistent with the direct splitting, and so no ratio fit it possible. The concertina plots for the ratio data show no region of stability:

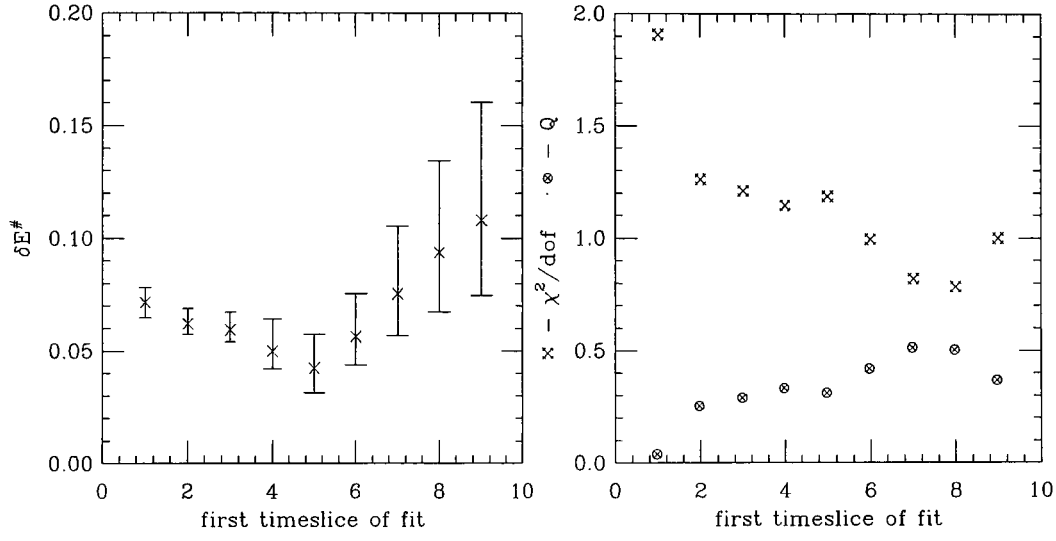

Figure 4.18 Concertina analysis, $^3P_2(T)-^3P_0$ ratio - (0.13460,SS,1.1)

This is true for the other P wave splittings and masses.

I therefore extract estimates of the splittings using differences in fitted energies. The errors for such fits will be larger than would be obtained if ratio fits were performed.

4.4.3.1 $^3P_2-\ ^3P_0$ *splittings.*

Because there is no variation with κ for the $^3P_2$ states, I calculated the splittings at the three simulation κ 's and then extrapolated the splittings to the physical κ 's. As a check, I fitted the $^3P_2$ data to a constant and then found the difference between the value of this constant

and the chirally extrapolated and strange interpolated numbers for $^3P_0$. The numbers were consistent within errors. I present numbers for the extrapolated differences however, because I believe them to be more reliable because there is one extrapolation in their calculation. Here are the unextrapolated data:

Table 4.35 $^3P_2(T) - {}^3P_0$ splitting — SL data

		$\kappa = 0.13460$		$\kappa = 0.13510$		$\kappa = 0.13530$	
Mass	n	$E^{\#}$	$\chi^2/N_{\rm dof}$	$E^{\#}$	$\chi^2/N_{\rm dof}$	$E^{\#}$	$\chi^2/N_{\rm dof}$
1.1	4	$0.101\ ^{+32}_{-32}$	-	$0.110\ ^{+39}_{-41}$	-	$0.119\ ^{+46}_{-50}$	-
1.2	3	$0.099\ ^{+32}_{-31}$	-	$0.108\ ^{+40}_{-42}$	-	$0.117\ ^{+46}_{-52}$	-
1.3	3	$0.097\ ^{+32}_{-32}$	-	$0.107\ ^{+42}_{-44}$	-	$0.115\ ^{+47}_{-54}$	-

Table 4.36 $^3P_2(T) - {}^3P_0$ splitting — SS data

		$\kappa = 0.13460$		$\kappa = 0.13510$		$\kappa = 0.13530$	
Mass	n	$E^{\#}$	$\chi^2/N_{\rm dof}$	$E^{\#}$	$\chi^2/N_{\rm dof}$	$E^{\#}$	$\chi^2/N_{\rm dof}$
1.1	4	$0.117\ ^{+23}_{-26}$	-	$0.125\ ^{+27}_{-29}$	-	$0.134\ ^{+32}_{-32}$	-
1.2	3	$0.116\ ^{+23}_{-24}$	-	$0.124\ ^{+29}_{-30}$	-	$0.133\ ^{+33}_{-33}$	-
1.3	3	$0.115\ ^{+24}_{-25}$	-	$0.123\ ^{+29}_{-31}$	-	$0.132\ ^{+32}_{-34}$	-

Table 4.37 $^3P_2(E) - {}^3P_0$ splitting — SL data

		$\kappa = 0.13460$		$\kappa = 0.13510$		$\kappa = 0.13530$	
Mass	n	$E^{\#}$	$\chi^2/N_{\rm dof}$	$E^{\#}$	$\chi^2/N_{\rm dof}$	$E^{\#}$	$\chi^2/N_{\rm dof}$
1.1	4	$0.146\ ^{+23}_{-29}$	-	$0.159\ ^{+25}_{-33}$	-	$0.168\ ^{+25}_{-36}$	-
1.2	3	$0.146\ ^{+23}_{-29}$	-	$0.159\ ^{+24}_{-33}$	-	$0.168\ ^{+26}_{-35}$	-
1.3	3	$0.167\ ^{+2}_{-52}$	-	$0.159\ ^{+26}_{-33}$	-	$0.168\ ^{+28}_{-35}$	-

Table 4.38 $^3P_2(E) - {}^3P_0$ splitting — SS data

		$\kappa = 0.13460$		$\kappa = 0.13510$		$\kappa = 0.13530$	
Mass	n	$E^{\#}$	$\chi^2/N_{\rm dof}$	$E^{\#}$	$\chi^2/N_{\rm dof}$	$E^{\#}$	$\chi^2/N_{\rm dof}$
1.1	4	$0.127\ ^{+24}_{-27}$	-	$0.137\ ^{+26}_{-32}$	-	$0.146\ ^{+26}_{-35}$	-
1.2	3	$0.125\ ^{+25}_{-28}$	-	$0.136\ ^{+26}_{-31}$	-	$0.145\ ^{+28}_{-35}$	-
1.3	3	$0.124\ ^{+25}_{-28}$	-	$0.135\ ^{+27}_{-32}$	-	$0.145\ ^{+27}_{-35}$	-

As expected from the behaviour of the $^3P_2$ data, there is good agreement (at least $\sigma/2$) between the two representations for the SS data. The representations for the SL data agree within $3\sigma/2$.

Looking now at the extrapolated data, tabulated overleaf. As expected, the SL data are unsatisfactory. Although there is agreement between the numbers from the two representations sometimes to within σ, it is frequently within 2σ.

Table 4.39 Extrapolated $^3P_2(T)$–$^3P_0$ splitting — SL data

		$\kappa_{chiral} = 0.135873$		$\kappa_{strange} = 0.13466$	
Mass	n	$E^{\#}$	χ^2/N_{dof}	$E^{\#}$	χ^2/N_{dof}
1.1	4	$0.133\ ^{+58}_{-70}$	0.0	$0.103\ ^{+33}_{-33}$	0.0
1.2	3	$0.096\ ^{+40}_{-44}$	0.6	$0.091\ ^{+30}_{-31}$	0.6
1.3	3	$0.095\ ^{+41}_{-46}$	0.6	$0.089\ ^{+31}_{-33}$	0.6

Table 4.40 Extrapolated $^3P_2(T)$–$^3P_0$ splitting — SS data

		$\kappa_{chiral} = 0.135873$		$\kappa_{strange} = 0.13466$	
Mass	n	$E^{\#}$	χ^2/N_{dof}	$E^{\#}$	χ^2/N_{dof}
1.1	4	$0.119\ ^{+31}_{-29}$	0.8	$0.114\ ^{+24}_{-25}$	0.8
1.2	3	$0.119\ ^{+30}_{-30}$	0.8	$0.113\ ^{+24}_{-25}$	0.8
1.3	3	$0.119\ ^{+31}_{-31}$	0.7	$0.112\ ^{+24}_{-25}$	0.7

Table 4.41 Extrapolated $^3P_2(E)$ – $^3P_0$ splitting — SL data

		$\kappa_{chiral} = 0.135873$		$\kappa_{strange} = 0.13466$	
Mass	n	$E^{\#}$	χ^2/N_{dof}	$E^{\#}$	χ^2/N_{dof}
1.1	4	$0.186\ ^{+29}_{-47}$	0.0	$0.148\ ^{+23}_{-29}$	0.0
1.2	3	$0.171\ ^{+34}_{-35}$	0.7	$0.149\ ^{+22}_{-30}$	0.7
1.3	3	$0.194\ ^{+34}_{-50}$	0.0	$0.139\ ^{+28}_{-32}$	0.0

Table 4.42 Extrapolated $^3P_2(E)$ – $^3P_0$ splitting — SS data

		$\kappa_{chiral} = 0.135873$		$\kappa_{strange} = 0.13466$	
Mass	n	$E^{\#}$	χ^2/N_{dof}	$E^{\#}$	χ^2/N_{dof}
1.1	4	$0.139\ ^{+31}_{-34}$	0.9	$0.128\ ^{+24}_{-28}$	0.9
1.2	3	$0.138\ ^{+31}_{-33}$	0.9	$0.126\ ^{+25}_{-28}$	0.9
1.3	3	$0.137\ ^{+32}_{-33}$	0.8	$0.125\ ^{+25}_{-28}$	0.8

I decided that the SL data were not trustworthy, and so didn't consider them further. Looking now at the SS data, there is more satisfactory agreement, to within $2/3\sigma$ for the data extrapolated to $\kappa_{critical}$ and to within $\sigma/2$ for the data interpolated to $\kappa_{strange}$. Interestingly, there is no dependence on m_Q for the $^3P_2(T)$–$^3P_0$ numbers at κ_{chiral}.

I then performed extrapolations in $1/m_Q$ to the previous data. I calculated values for the splittings at the best estimate of the mass parameter corresponding to the b quark, and at the static point ($m_Q = \infty$). The numbers obtained are:

Table 4.43 $^3P_2(T)$–$^3P_0$ splitting — SS data

	$m_Q = 1.44$	$m_Q = \infty$	χ^2/N_{dof}
$\kappa_{critical}$	$0.124\ ^{+35}_{-34}$	$0.123\ ^{+43}_{-41}$	0.08
$\kappa_{strange}$	$0.107\ ^{+30}_{-29}$	$0.094\ ^{+35}_{-33}$	0.04

Table 4.44 $^3P_2(E)-^3P_0$ splitting — SS data

	$m_Q = 1.44$	$m_Q = \infty$	χ^2/N_{dof}
$\kappa_{critical}$	$0.132\ ^{+35}_{-35}$	$0.122\ ^{+47}_{-39}$	0.04
$\kappa_{strange}$	$0.117\ ^{+32}_{-29}$	$0.097\ ^{+37}_{-36}$	0.1

As can be seen, there is good agreement between the two representations for $m_Q = 1.44$, typically of the order $\sigma/3$, and superb agreement for the static limit. Because the slope is so small, I did not calculate the errors due to the systematic uncertainty in fixing the b quark: the errors shown in the tables are just statistical. Converting into physical units gives:

Table 4.45 Physical numbers for $^3P_2-^3P_0$ splitting

	T (MeV)	E (MeV)
B	321^{+91}_{-88} (stat) $^{+40}_{-31}$ (syst)	342^{+91}_{-91} (stat) $^{+42}_{-33}$ (syst)
B_s	277^{+77}_{-75} (stat) $^{+34}_{-27}$ (syst)	303^{+78}_{-75} (stat) $^{+37}_{-29}$ (syst)

4.4.3.2 $^3P_1-^3P_0$ *splitting.*

This is the only other inter P-wave splitting that can be calculated. Looking at the raw data below:

Table 4.46 $^3P_1-^3P_0$ splitting — SL data

		$\kappa = 0.13460$		$\kappa = 0.13510$		$\kappa = 0.13530$	
Mass	n	$E^\#$	χ^2/N_{dof}	$E^\#$	χ^2/N_{dof}	$E^\#$	χ^2/N_{dof}
1.1	4	$0.050\ ^{+15}_{-19}$	-	$0.050\ ^{+17}_{-19}$	-	$0.051\ ^{+20}_{-21}$	-
1.2	3	$0.047\ ^{+16}_{-18}$	-	$0.048\ ^{+17}_{-19}$	-	$0.048\ ^{+20}_{-20}$	-
1.3	3	$0.045\ ^{+16}_{-17}$	-	$0.046\ ^{+17}_{-19}$	-	$0.046\ ^{+20}_{-20}$	-

Table 4.47 $^3P_1-^3P_0$ splitting — SS data

		$\kappa = 0.13460$		$\kappa = 0.13510$		$\kappa = 0.13530$	
Mass	n	$E^\#$	χ^2/N_{dof}	$E^\#$	χ^2/N_{dof}	$E^\#$	χ^2/N_{dof}
1.1	4	$0.042\ ^{+17}_{-18}$	-	$0.043\ ^{+21}_{-21}$	-	$0.044\ ^{+25}_{-24}$	-
1.2	3	$0.039\ ^{+16}_{-17}$	-	$0.040\ ^{+20}_{-21}$	-	$0.041\ ^{+24}_{-24}$	-
1.3	3	$0.037\ ^{+16}_{-17}$	-	$0.037\ ^{+19}_{-21}$	-	$0.039\ ^{+23}_{-24}$	-

There is good ($\sigma/2$) agreement between the two smearings. The κ dependence is very small. Nevertheless I performed the extrapolation and interpolation to $\kappa_{critical}$ and $\kappa_{strange}$ and found the following numbers: ¶

¶ I could have performed a constant fit. However I judged that the data were sloping consistently with κ. Of course, at this level of statistics, such choices amount to niceties. The slope obtained from the linear fit was extremely small.

Table 4.48 Extrapolated $^3P_1-^3P_0$ splitting — SL data

		$\kappa_{\rm chiral} = 0.135873$		$\kappa_{\rm strange} = 0.13466$	
Mass	n	$E^\#$	$\chi^2/N_{\rm dof}$	$E^\#$	$\chi^2/N_{\rm dof}$
1.1	4	$0.051\ ^{+26}_{-29}$	0.0	$0.050\ ^{+15}_{-18}$	0.0
1.2	3	$0.048\ ^{+23}_{-22}$	0.0	$0.047\ ^{+16}_{-18}$	0.0
1.3	3	$0.046\ ^{+23}_{-22}$	0.0	$0.045\ ^{+16}_{-17}$	0.0

Table 4.49 Extrapolated $^3P_1-^3P_0$ splitting — SS data

		$\kappa_{\rm chiral} = 0.135873$		$\kappa_{\rm strange} = 0.13466$	
Mass	n	$E^\#$	$\chi^2/N_{\rm dof}$	$E^\#$	$\chi^2/N_{\rm dof}$
1.1	4	$0.039\ ^{+27}_{-22}$	0.1	$0.041\ ^{+17}_{-17}$	0.1
1.2	3	$0.036\ ^{+26}_{-22}$	0.1	$0.038\ ^{+17}_{-17}$	0.1
1.3	3	$0.034\ ^{+26}_{-22}$	0.1	$0.036\ ^{+17}_{-17}$	0.1

Performing a linear fit in $1/m_{\rm Q}$ to these data, I obtained the following results:

Table 4.50 $^3P_1-^3P_0$ splitting — SL data

	$m_{\rm Q} = 1.44$	$m_{\rm Q} = \infty$	$\chi^2/N_{\rm dof}$
$\kappa_{\rm critical}$	$0.044\ ^{+24}_{-22}$	$0.024\ ^{+33}_{-26}$	0.009
$\kappa_{\rm strange}$	$0.041\ ^{+19}_{-15}$	$0.015\ ^{+22}_{-18}$	0.02

Table 4.51 $^3P_1-^3P_0$ splitting — SS data

	$m_{\rm Q} = 1.44$	$m_{\rm Q} = \infty$	$\chi^2/N_{\rm dof}$
$\kappa_{\rm critical}$	$0.031\ ^{+24}_{-23}$	$0.009\ ^{+34}_{-26}$	0.04
$\kappa_{\rm strange}$	$0.034\ ^{+18}_{-17}$	$0.009\ ^{+20}_{-19}$	0.01

There is $\sigma/2$ agreement between the sets of data. The values at the static limit are compatible with zero. There is no consistent variation with the light quark mass. I use the SS numbers as the final estimate of the splitting. In physical units the results for the $^3P_1-^3P_0$ splitting are

$$\kappa_{\rm critical} \qquad 80\ ^{+62}_{-60}\ \text{(statistical)}\ ^{+10}_{-8}\ \text{(systematic)}\quad \text{MeV}$$

$$\kappa_{\rm strange} \qquad 88\ ^{+47}_{-44}\ \text{(statistical)}\ ^{+11}_{-9}\ \text{(systematic)}\quad \text{MeV}$$

4.4.4 Intra $P - S$ wave splitting

4.4.4.1 $^3P_0 - \overline{S}$.

Here are the unextrapolated data for this splitting:

Table 4.52 $^3P_0 - \overline{S}$ — SL data

Mass	n	$\kappa = 0.13460$	$\kappa = 0.13510$	$\kappa = 0.13530$
1.1	4	$0.174\ ^{+19}_{-15}$	$0.181\ ^{+22}_{-16}$	$0.189\ ^{+25}_{-19}$
1.2	3	$0.175\ ^{+18}_{-15}$	$0.179\ ^{+19}_{-16}$	$0.183\ ^{+24}_{-18}$
1.3	3	$0.177\ ^{+18}_{-15}$	$0.180\ ^{+19}_{-16}$	$0.184\ ^{+23}_{-18}$

Table 4.53 $^3P_0 - \overline{S}$ — SS data

Mass	n	$\kappa = 0.13460$	$\kappa = 0.13510$	$\kappa = 0.13530$
1.1	4	$0.172\ ^{+21}_{-18}$	$0.181\ ^{+25}_{-20}$	$0.187\ ^{+30}_{-25}$
1.2	3	$0.173\ ^{+21}_{-18}$	$0.180\ ^{+24}_{-19}$	$0.184\ ^{+30}_{-23}$
1.3	3	$0.175\ ^{+22}_{-19}$	$0.181\ ^{+24}_{-19}$	$0.185\ ^{+29}_{-23}$

There is excellent agreement between the two smearings. I could perform successful extrapolations in $1/\kappa$:

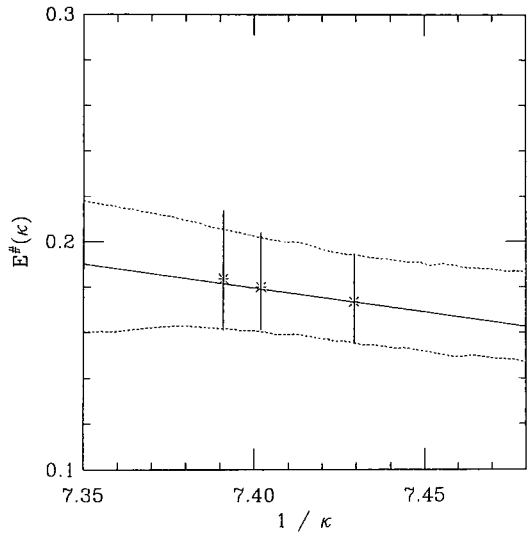

Figure 4.19 Linear Extrapolation in $1/\kappa$ for $^3P_0 - \overline{S}$, $m_Q = 1.2$, SS data

The data also support fits to a constant, but these have larger values of $\chi^2/N_{\rm dof}$. The final numbers obtained from such fits agree at the σ level with those from fits to a linear form. I therefore used the linear fits to provide the estimates at the physical values of κ:

Table 4.54 Extrapolated $^3P_0$–$\overline{S}$ — SL data

		$\kappa_{chiral} = 0.135873$		$\kappa_{strange} = 0.13466$	
Mass	n	$E^{\#}$	χ^2/N_{dof}	$E^{\#}$	χ^2/N_{dof}
1.1	4	$0.202\ ^{+31}_{-25}$	0.0	$0.175\ ^{+18}_{-15}$	0.0
1.2	3	$0.181\ ^{+22}_{-21}$	0.3	$0.175\ ^{+18}_{-16}$	0.3
1.3	3	$0.180\ ^{+23}_{-22}$	0.4	$0.176\ ^{+19}_{-15}$	0.4

Table 4.55 Extrapolated $^3P_0$–$\overline{S}$ — SS data

		$\kappa_{chiral} = 0.135873$		$\kappa_{strange} = 0.13466$	
Mass	n	$E^{\#}$	χ^2/N_{dof}	$E^{\#}$	χ^2/N_{dof}
1.1	4	$0.193\ ^{+32}_{-29}$	0.1	$0.173\ ^{+22}_{-18}$	0.1
1.2	3	$0.188\ ^{+28}_{-27}$	0.0	$0.174\ ^{+21}_{-18}$	0.0
1.3	3	$0.189\ ^{+28}_{-28}$	0.0	$0.175\ ^{+22}_{-18}$	0.0

When I performed fits of this data to linear functions in $1/m_Q$, I got reasonable χ^2/N_{dof} values. However the slopes from the two smearings were of opposite sign and consistent with zero. The constant terms were within σ of each other. Therefore I decided to fit the data to a constant. When I did this, I achieved very good consistency between the smearings. Here are the numbers:

Table 4.56 Final $^3P_0$–$\overline{S}$ splittings

	SL		SS	
	$E^{\#}$	χ^2/N_{dof}	$E^{\#}$	χ^2/N_{dof}
$\kappa_{critical}$	$0.182\ ^{+23}_{-21}$	0.7	$0.184\ ^{+28}_{-27}$	0.2
$\kappa_{strange}$	$0.172\ ^{+19}_{-15}$	0.8	$0.167\ ^{+23}_{-21}$	0.4

4.4.4.2 $^3P_1$–$\overline{S}$.

Here are the unextrapolated data:

Table 4.57 $^3P_1$–$\overline{S}$ — SL data

Mass	n	$\kappa = 0.13460$	$\kappa = 0.13510$	$\kappa = 0.13530$
1.1	4	$0.224\ ^{+19}_{-14}$	$0.232\ ^{+20}_{-17}$	$0.241\ ^{+25}_{-20}$
1.2	3	$0.223\ ^{+17}_{-15}$	$0.227\ ^{+20}_{-18}$	$0.231\ ^{+22}_{-21}$
1.3	3	$0.222\ ^{+18}_{-14}$	$0.226\ ^{+20}_{-18}$	$0.230\ ^{+21}_{-21}$

Table 4.58 $^3P_1$–$\overline{S}$ — SS data

Mass	n	$\kappa = 0.13460$	$\kappa = 0.13510$	$\kappa = 0.13530$
1.1	4	$0.214\ ^{+20}_{-17}$	$0.224\ ^{+24}_{-20}$	$0.231\ ^{+28}_{-22}$
1.2	3	$0.213\ ^{+19}_{-17}$	$0.220\ ^{+22}_{-20}$	$0.225\ ^{+25}_{-23}$
1.3	3	$0.212\ ^{+19}_{-18}$	$0.219\ ^{+21}_{-19}$	$0.223\ ^{+25}_{-23}$

Again there is good agreement between the two smearings — not quite as good as the $^3P_0$ case, but within $\sigma/2$. As the variation with κ is so small, I tested whether it was significant or not by fitting the data to a constant as well as a linear form. For the SL data I got a lower χ^2/N_{dof} with the constant form, but the numbers obtained at $\kappa_{critical}$ and $\kappa_{strange}$ were nearly identical to those obtained from the linear fit. For the SS data I obtained a lower χ^2/N_{dof} with the linear form, and the estimates from this were again near identical to those from the SL data. The numbers obtained for the constant fit were within $\sigma/2$ of the other numbers. For the final numbers I use the results from the linear fits:

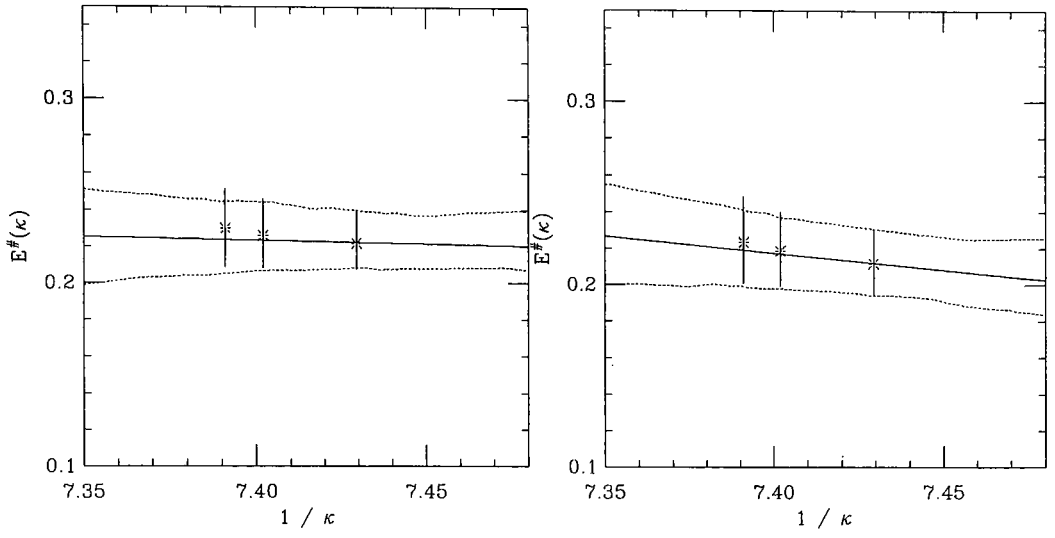

Figure 4.20 Chiral Extrapolation $^3P_1$–$\overline{S}$, $m_Q = 1.3$ SL and SS data

Table 4.59 Linearly Extrapolated $^3P_1$–$\overline{S}$ — SL data

		$\kappa_{chiral} = 0.135873$		$\kappa_{strange} = 0.13466$	
Mass	n	$E^\#$	χ^2/N_{dof}	$E^\#$	χ^2/N_{dof}
1.1	4	$0.234\ ^{+31}_{-30}$	0.4	$0.217\ ^{+20}_{-17}$	0.4
1.2	3	$0.226\ ^{+27}_{-26}$	0.2	$0.214\ ^{+20}_{-17}$	0.2
1.3	3	$0.225\ ^{+27}_{-24}$	0.2	$0.213\ ^{+19}_{-18}$	0.2

Table 4.60 Linearly Extrapolated $^3P_1$–$\overline{S}$ — SS data

		$\kappa_{chiral} = 0.135873$		$\kappa_{strange} = 0.13466$	
Mass	n	$E^\#$	χ^2/N_{dof}	$E^\#$	χ^2/N_{dof}
1.1	4	$0.234\ ^{+31}_{-30}$	0.4	$0.217\ ^{+20}_{-17}$	0.4
1.2	3	$0.226\ ^{+27}_{-26}$	0.2	$0.214\ ^{+20}_{-17}$	0.2
1.3	3	$0.225\ ^{+27}_{-24}$	0.2	$0.213\ ^{+19}_{-18}$	0.2

For the $1/m_Q$ behaviour of the data I found lower χ^2/N_{dof} for the linear fits compared with the constant fits, and slopes consistent with zero. All fit parameters were consistent, regardless of smearing or fit function. I used linear fits to determine the final numbers tabulated below.

Table 4.61 Final $^3P_1-\overline{S}$ splittings

	SL		SS	
	$E^{\#}$	χ^2/N_{dof}	$E^{\#}$	χ^2/N_{dof}
$\kappa_{critical}$	$0.221\ ^{+27}_{-26}$	0.01	$0.224\ ^{+26}_{-25}$	0.4
$\kappa_{strange}$	$0.222\ ^{+17}_{-14}$	0.3	$0.212\ ^{+19}_{-18}$	0.5

Of course, as the extrapolating is to a point so close to the data and the slope of the data is so small, whatever form is chosen to fit to will make insignificant difference to the final numbers.

4.4.4.3 $^3P_2-\overline{S}$.

The SL data disagreed by as much as 2σ between the two representations, so are not considered any further. The raw SS data agreed typically within $\sigma/2$:

Table 4.62 $^3P_2(T)-\overline{S}$ — SS data

Mass	n	$\kappa = 0.13460$	$\kappa = 0.13510$	$\kappa = 0.13530$
1.1	4	$0.289\ ^{+22}_{-18}$	$0.307\ ^{+27}_{-23}$	$0.320\ ^{+30}_{-27}$
1.2	3	$0.289\ ^{+22}_{-18}$	$0.304\ ^{+26}_{-22}$	$0.317\ ^{+29}_{-26}$
1.3	3	$0.289\ ^{+22}_{-19}$	$0.305\ ^{+25}_{-22}$	$0.317\ ^{+29}_{-26}$

Table 4.63 $^3P_2(E)-\overline{S}$ — SS data

Mass	n	$\kappa = 0.13460$	$\kappa = 0.13510$	$\kappa = 0.13530$
1.1	4	$0.299\ ^{+23}_{-22}$	$0.318\ ^{+26}_{-25}$	$0.333\ ^{+29}_{-26}$
1.2	3	$0.299\ ^{+24}_{-22}$	$0.316\ ^{+25}_{-25}$	$0.329\ ^{+28}_{-26}$
1.3	3	$0.299\ ^{+24}_{-23}$	$0.316\ ^{+27}_{-26}$	$0.329\ ^{+29}_{-28}$

When I performed the chiral extrapolations, I got numbers that agreed within σ between the two representations, but with very large χ^2/N_{dof} .

Table 4.64 Extrapolated $^3P_2(T)-\overline{S}$ — SS data

		$\kappa_{chiral} = 0.135873$		$\kappa_{strange} = 0.13466$	
Mass	n	$E^{\#}$	χ^2/N_{dof}	$E^{\#}$	χ^2/N_{dof}
1.1	4	$0.307\ ^{+31}_{-29}$	3.7	$0.283\ ^{+21}_{-18}$	3.7
1.2	3	$0.296\ ^{+26}_{-26}$	3.4	$0.281\ ^{+21}_{-19}$	3.4
1.3	3	$0.298\ ^{+28}_{-27}$	3.2	$0.280\ ^{+21}_{-20}$	3.2

Table 4.65 Extrapolated $^3P_2(E)-\overline{S}$ — SS data

		$\kappa_{chiral} = 0.135873$		$\kappa_{strange} = 0.13466$	
Mass	n	$E^{\#}$	χ^2/N_{dof}	$E^{\#}$	χ^2/N_{dof}
1.1	4	$0.334\ ^{+34}_{-32}$	4.1	$0.302\ ^{+23}_{-22}$	4.1
1.2	3	$0.321\ ^{+32}_{-30}$	3.8	$0.298\ ^{+24}_{-23}$	3.8
1.3	3	$0.322\ ^{+33}_{-31}$	3.5	$0.297\ ^{+24}_{-24}$	3.5

I actually found slightly lower values of $\chi^2/N_{\rm dof}$ with fits to a constant. The final numbers from such fits agreed with those from the linear fits to within σ (at $\kappa_{\rm critical}$) and $\sigma/2$ (at $\kappa_{\rm strange}$). However, the unextrapolated data suggest linear dependence and so I use the linear fits. The problem is that these splittings are at the limit of what the simulation's capability.

Fitting these numbers to a linear form in $1/m_{\rm Q}$ and extrapolating to $m_{\rm Q} = 1.44$:

Table 4.66 Final numbers for $^3{\rm P}_2-\overline{\rm S}$ splitting

	T		E	
	$E^{\#}$	$\chi^2/N_{\rm dof}$	$E^{\#}$	$\chi^2/N_{\rm dof}$
$\kappa_{\rm critical}$	$0.296\ ^{+28}_{-28}$	0.9	$0.321\ ^{+33}_{-31}$	1
$\kappa_{\rm strange}$	$0.276\ ^{+21}_{-20}$	0.4	$0.291\ ^{+24}_{-23}$	2

The slopes in these fits were very shallow, and there is little difference in the final numbers if fits to a constant are used instead.

4.5 End

I have detailed the calculation of various spectroscopic quantities pertaining to the B and $\rm B_s$ systems. I have exhibited a representative selection of the data used in the calculations. For some of the quantities I have investigated what functional forms best describe the data. In the next chapter I shall compare the results with those from other calculations and with the experimental data, where they exist.

5

Comparison of Heavy Light Data

I now compare my data with those from other simulations, non-relativistic and relativistic, and with experiment. I also compare them with the predictions of HQET.

5.1 B_s – B splitting

This splitting should be dominated by the difference between the current strange and light quark masses. One expects the heavy quark mass dependence to be caused by the difference of the kinetic and hyperfine energies of the heavy quark between the two mesons, *i.e.* the splitting to be independent of the heavy quark mass up to terms $\mathcal{O}(m_s/m_Q)$. Only the part due to the kinetic energies remains in the spin averaged splitting.

The experimental numbers are:

Table 5.1 Experimental B_s–B splittings — Caso *et al.* (1998)

Channel	(MeV)
Pseudo-Scalar	90.1 ± 2.7
Vector	91.4 ± 3.8
Spin Average	91.1 ± 2.9

The corresponding numbers for D mesons show an increase of approximately 10%.

I found no meaningful dependence on m_Q. The Pseudo-scalar, vector, and spin average states give very similar numbers:

Table 5.2 Calculated B_s–B splittings

Channel	Result (MeV)
Pseudo-scalar	$106\ ^{+8}_{-13}$(stat) $^{+13}_{-10}$(syst)
Vector	$109\ ^{+16}_{-20}$(stat) $^{+13}_{-11}$(syst)
Spin Average	$117\ ^{+16}_{-18}$(stat) $^{+14}_{-11}$(syst)

The spin average value was calculated from the difference between the spin average energies. If it is calculated from the pseudo-scalar and vector splittings, a value of 108 MeV is obtained.

Here are the results from other calculations:

Figure 5.1 $B_s - B$ splitting

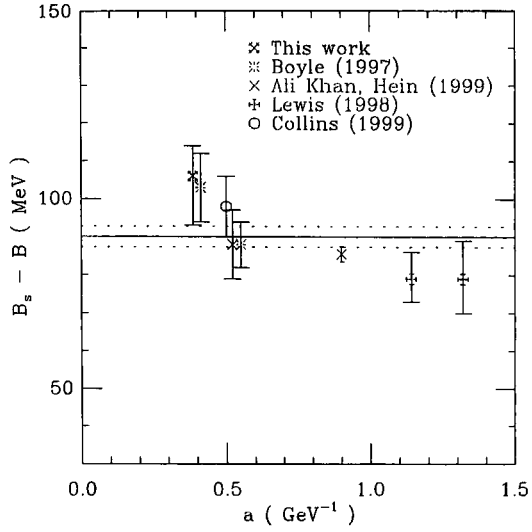

All errors shown are purely statistical. All the points are for the pseudo-scalar splitting, and were converted to physical units using a scale fixed from m_ρ. The crossed cross is this work. The two bursts are from Boyle (1997). This is a fully relativistic calculation using mean-field improved Sheikholeslami-Wohlert Green's functions for both quarks: the configurations in this $\beta 6.2$ simulation were the same as those in the present work, but a larger number were used. The two crosses are from NRQCD calculations using mean-field improved Sheikholeslami-Wohlert Green's functions for the light quarks. The coarser lattice calculation is at $\beta 5.7$ on a $12^3 \times 24$ lattice, Hein (1999). The finer lattice (Ali Khan 1999) is at $\beta 6.0$ and is $16^3 \times 48$. The two fancy pluses are from calculations by Lewis and Woloshyn (1998) at $\beta 6.8$ and $\beta 7.0$, also using mean field improved Sheikholeslami Wohlert light quarks. The circle is from a partly unquenched calculation of Collins *et al.* (1999), at $\beta 5.6$ with $n_{\text{flavours}} = 2$. Boyle used fuzzing, Collins *et al.* , Hein, and Ali Khan *et al.* used Coulomb gauge fixed hydrogen wavefunctions, whilst Lewis and Woloshyn used no smearing at all. All the NRQCD calculations used evolution equations up to $\mathcal{O}(1/m^2)$.

The agreement is in general good and within errors. The agreement between calculations on similar lattices (Boyle and this work, Boyle and Ali Khan *et al.*) is very striking. The statistical errors on the partly unquenched calculation are too large to determine whether there is a systematic effect caused by the unquenching.

Lewis and Woloshyn also calculated this splitting using an NRQCD Hamiltonian containing terms up to $\mathcal{O}(1/m)$ and $\mathcal{O}(1/m^3)$ and found no difference in this splitting.

The differences are due not to NRQCD but the light degrees of freedom. The systematic increase of the splitting with finer lattices is down to this. Their lattice spacing was 1.16GeV^{-1}. Ewing *et al.* (1996) found a value of 87(13) MeV on a similar lattice to mine, using the static approximation and Sheikholeslami Wohlert light quarks, without mean field improvement, but with rotation of these fields.

5.2 Hyperfine splitting

In the HQET picture, this splitting arises because of the interaction of the heavy quark spin with the colour field. The first term through which this can happen is the $\boldsymbol{\sigma} \cdot \boldsymbol{B}$ term, which occurs at $\mathcal{O}(1/2m)$. The splitting should vanish in the limit of infinite heavy quark mass as the vector and pseudo-scalar states become degenerate.

The experimental values are 45.78 ± 0.35 MeV for the B system, and 47.0 ± 2.6 MeV for the B_s system (Caso, *op.cit.*).

I found no consistent variation of the raw data with κ, and so fitted it to a constant. Thus I do not have separate predictions for the B and B_s systems. I did, however, find strong dependence on m_Q, with a infinite mass intercept consistent with zero. The value of 29 MeV is clearly too low. However, by comparing with other calculations:

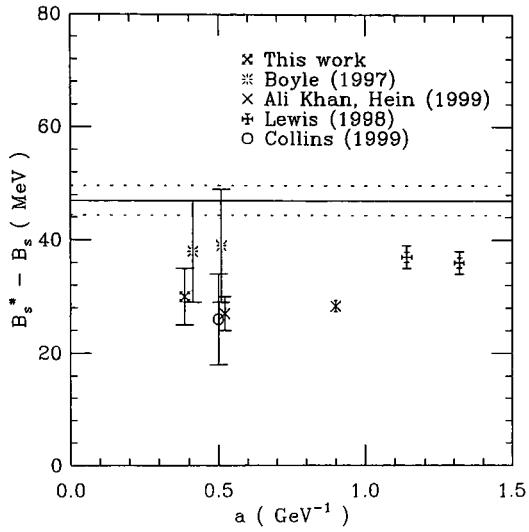

Figure 5.2 B_s Hyperfine splitting

one can see that underestimation of this splitting is characteristic of all calculations. The symbols in the graph are the same as for the previous section. Even the partly unquenched calculation is too low. However the four NRQCD calculations on lattices with spacings finer than 1.0 Gev^{-1} show very flat scaling. A calculation of the $D^* - D$ splitting (Boyle, 1997), finds 106(8) MeV, lower than the experimental value of 142 MeV. Lewis and Woloshyn *op.cit.* found small increases when they moved to a $\mathcal{O}(1/m^3)$ formulation from the $\mathcal{O}(1/m^2)$ formulation These increases, of roughly 2 MeV, are at the level of σ though.

5.3 P wave fine structure

There are few experimental data here. There is a broad resonance at 5698(12) MeV, (Caso *et al.* 1998), the spin of which has not been determined but is believed to be a superposition of the P states. There is a preliminary number from the DELPHI collaboration (1996) for a narrow P state 81 MeV heavier than this resonance. The spin is not resolved, but is believed to be either $J = 1$ or $J = 2$.

5.3.1 $^3P_2 - ^3P_0$

I found no discernible variation of the $^3P_2$ mass with κ, and so all variation for this splitting comes from the $^3P_0$. The numbers are:

Table 5.3 Physical $^3P_2 - ^3P_0$ splitting

	T (MeV)	E (MeV)
B	$321\,^{+91}_{-88}\,(\text{stat})\,^{+40}_{-31}\,(\text{syst})$	$342\,^{+91}_{-91}\,(\text{stat})\,^{+42}_{-33}\,(\text{syst})$
B_s	$277\,^{+77}_{-75}\,(\text{stat})\,^{+34}_{-27}\,(\text{syst})$	$303\,^{+78}_{-75}\,(\text{stat})\,^{+37}_{-29}\,(\text{syst})$

As can be seen there is agreement between the two representations, but with huge statistical errors. I also found finite static values of 316 MeV for the light, and 251 MeV for the strange. A recent NRQCD calculation at $\beta 6.0$ (Ali Khan, 1999) has found this splitting to be 155(32) MeV at the light, and 136(23) MeV for the strange. Calculations at $\beta 5.7$ (Hein, 1999) have failed to resolve any P wave structure: presumably the lattice used in this calculation was too coarse to see the detail of the states in the P wave. The discrepancy between the calculations on the three lattices is large but consistent. It also seems to be a feature of NRQCD: this spreading of the size of the P wave was seen in the Υ spectrum calculations.

5.3.2 $^3P_1 - ^3P_0$ *splitting*

I assume this is the splitting between the lighter physical state, 1^+ and the $^3P_0$. I found a static limit consistent with zero (23 ± 56 MeV) as one would believe from HQET. My predictions are (in MeV):

Table 5.4 Predictions for the $^3P_1 - ^3P_0$ splitting

System	Result MeV
B	$80\,^{+62}_{-60}\,^{+10}_{-8}$
B_s	$88\,^{+47}_{-44}\,^{+11}_{-9}$

Ali Khan *op.cit.* found 54 ± 38 MeV for this splitting in the B system, and 61 ± 26 MeV in the B_s system, with a static point intercept of 12 ± 40 MeV . Boyle *op.cit.* found 50(20) MeV and 42(10) MeV for these splittings at $\beta 6.0$.

5.4 Intra P−S wave splittings

These splittings are expected to be controlled by the light degrees of freedom. The two main contributions to the spin averaged 1P − 1S should come from the energy required to excite

the light quark to one unit of angular momentum and the difference in the kinetic energy of the heavy quark in a S wave and a P wave light quark background. These are $\mathcal{O}(\Lambda_{\rm QCD})$ and $\mathcal{O}(\Lambda^2_{\rm QCD}/m)$.

5.4.1 Individual splittings

My estimates for the individual splittings are:

5.4.1.1 $^3P_0 - \bar{S}$ splitting.

I was unable to determine any dependence on $m_{\rm Q}$, but did find evidence for weak dependence on κ.

Table 5.5 Estimates of $^3{\rm P}_0 - \overline{\rm S}$ splitting

System	Result MeV
B	$476\ ^{+73}_{-70}\ ^{+60}_{-46}$
$\rm B_s$	$433\ ^{+60}_{-54}\ ^{+53}_{-42}$

5.4.1.2 $^3P_1 - \bar{S}$ splitting.

I found evidence for weak dependence on $m_{\rm Q}$ and κ.

Table 5.6 Estimates of $^3{\rm P}_1 - \overline{\rm S}$ splitting

System	Result MeV
B	$580\ ^{+67}_{-75}\ ^{+72}_{-56}$
$\rm B_s$	$549\ ^{+49}_{-47}\ ^{+68}_{-53}$

5.4.1.3 $^3P_2 - \bar{S}$ splitting.

The data here were not satisfactory. I didn't really have enough evidence to decide between very weak dependence on $m_{\rm Q}$ and κ and no dependence.

Table 5.7 Estimates of $^3{\rm P}_2 - \overline{\rm S}$ splitting

System	Result MeV
B	$831\ ^{+85}_{-80}\ ^{+103}_{-80}$
$\rm B_s$	$754\ ^{+62}_{-60}\ ^{+93}_{-73}$

Here is a graph of my splittings with those of Ali Khan and those of Hein:

Figure 5.3 Splittings between individual P states and $\overline{S}$

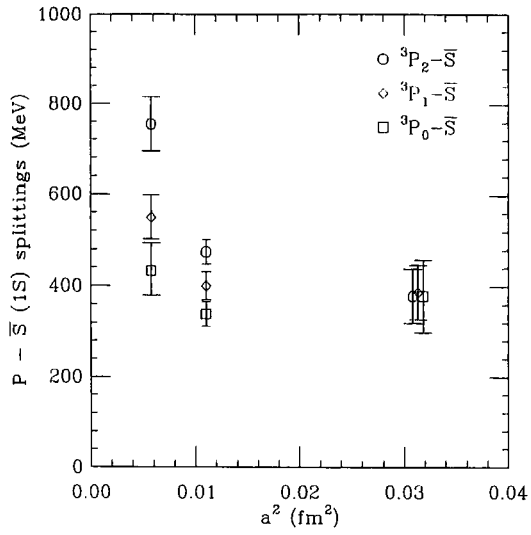

The circles are $^3P_2(E)$ values, the diamonds $^3P_1$ values, and the square are the $^3P_0$ values.

The lattice of Hein is too coarse to be able to resolve the structure of the P states. The increase of the splittings with smaller lattice spacing is due to two effects. The first is down to NRQCD, and is the spreading of the P wave with decreasing lattice spacing. This was seen in the inter P wave Υ spectrum. The second effect is caused by problems arising out of the light quark sector and gluon sector of the lattice theory. We can illustrate this better by looking at the P wave spin average to S wave spin average splitting:

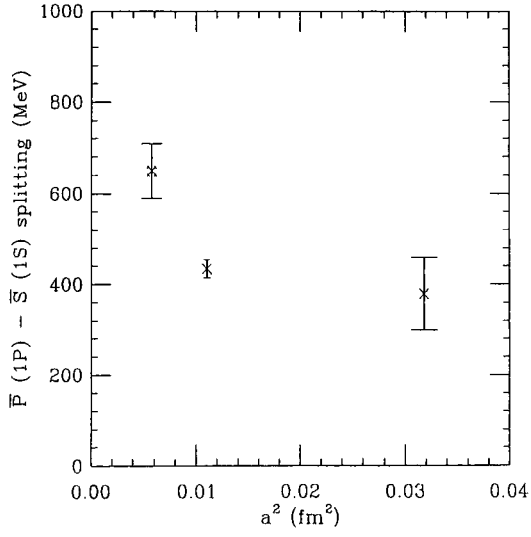

Figure 5.4 Splittings between $\overline{P}$ and $\overline{S}$

The centre of mass of the P wave is heavily influenced by the $^3P_2$ state, and so any problems with this operator will alter the value of the splitting. I am predisposed to be more sceptical of this operator than the others, because it has the most complicated structure. In addition, the non-dependence of the mass of the state with κ is unsettling. This may be just because it is hidden in the statistical noise of the calculation.

6

Conclusion

6.1 Summary of this work

I have calculated the Υ spectrum, and the spectra of the B systems, simulating the beauty quark directly on the lattice, without the need for extrapolation.

I have demonstrated that the heavy quark mass that was taken out of the NRQCD action can be successfully put back at the end of the calculation I have also shown that the procedure of looking at maximally correlated polarization combinations is not as good as the straightforward method of correlating polarization averages.

The results of the $B_s - B$ splitting indicates that the chiral extrapolations are working well. The value of this splitting scales very well. The underestimation of the hyperfine splitting is characteristic of all quenched calculations. However, this splitting also scales very well with other NRQCD calculations from coarser lattices. At the present moment, partially unquenched calculations have not changed the value of the splitting substantially. The $1P - 1S$ splittings for the heavy-light mesons show considerable scaling violations. This indicates problems with the gluon and light quark sectors of the theory. This may also be hampered by problems with the $^3P_2$ operators, which because of the complexity of their structure, require more statistics for reliable evaluation.

The new smearing method tried out in this calculation works well for the ground state but seems to cause difficulties in the extraction of the excited states. I believe this to be caused by the smearing functions increasing, rather than decreasing, the overlap with the excited states. Successful extraction of the excited states requires large differences in the relative overlaps of the ground and first excited states for the correlators used in the row or matrix fit routines. I am not sure whether this would be cured by greater statistics and more careful tuning of the smearing radius.

6.2 Future work

More configurations are the desiderata of all lattice calculations, and the main conclusion from this work. Apart from the general decrease in statistical noise, this would produce signals for the cross correlators and so allow the higher energy spin 1 P wave state to be resolved. Higher order NRQCD calculations also are indicated, especially for spin splittings.

A

Particle Masses

A.1 Υ System

Name	J^{PC}	$^{2S+1}L_J$	Mass (MeV)
$\eta_b(1S)$	0^{-+}	$1\ ^1S_0$	Not yet observed
$\eta_b(2S)$	0^{-+}	$2\ ^1S_0$	Not yet observed
$\Upsilon(1S)$	1^{--}	$1\ ^3S_1$	9460.37 ± 0.21
$\Upsilon(2S)$	1^{--}	$2\ ^3S_1$	10023.30 ± 0.31
$h_b(1P)$	1^{+-}	$1\ ^1P_1$	Not yet observed
$\chi_{b0}(1P)$	0^{++}	$1\ ^3P_0$	9859.8 ± 1.3
$\chi_{b1}(1P)$	1^{++}	$1\ ^3P_1$	9891.9 ± 0.7
$\chi_{b2}(1P)$	2^{++}	$1\ ^3P_2$	9913.2 ± 0.6

A.2 B System

Name	J^P	$^{2S+1}L_J$	Mass (MeV)
B	0^-	$1\ ^1S_0$	5279.05 ± 1.8
B^*	1^-	$1\ ^3S_1$	5324.9 ± 1.8
B_{1L}	1^+	$1\ ^1P_1$	Not yet observed
B_0^*	0^+	$1\ ^3P_0$	Not yet observed
B_{1H}	1^+	$1\ ^3P_1$	Not yet observed
B_2^*	2^+	$1\ ^3P_2$	Not yet observed

A.3 B_s system

Name	J^P	$^{2S+1}L_J$	Mass (MeV)
B_s	0^-	$1\ ^1S_0$	5369.3 ± 2.0
B_s^*	1^-	$1\ ^3S_1$	5416.3 ± 3.3
B_{s1L}	1^+	$1\ ^1P_1$	Not yet observed
B_{s0}^*	0^+	$1\ ^3P_0$	Not yet observed
B_{s1H}	1^+	$1\ ^3P_1$	Not yet observed
B_{s2}^*	2^+	$1\ ^3P_2$	Not yet observed

All values come from Caso *et al.* (1998)

B

Details of Code

B.1 Code

B.1.1 Form of code

B.1.1.1 General.

The code was originally designed to run on a Thinking Machines CM-200. Coding was begun for this in Connection Machine Fortran (CMF). The original conception was to generate the NRQCD Green's functions using stand-alone code and to store these on the CM-200's high speed mass-store, the Data Vault. The light quark propagators were to be transferred to this off-line. A second piece of code was then to correlate the NRQCD Green's functions with themselves and with the light propagators.

Unfortunately the Data Vault failed whilst the codes were being written. The alternatives possessed neither the storage capacity nor the speed of the Data Vault. The two codes were therefore merged and changed so that only the time-sliced meson correlators were saved. This cut down on I/O and storage requirements.

Unfortunately, whilst the new code was being tested, the Connection Machine itself failed. The decision was taken to port the existing code to High Performance Fortran (HPF) and run it on the Cray T3D. HPF and CMF are very similar languages. An additional problem then became apparent. The HPF that existed on the machine at the time was a converting compiler of the Portland Group which produces Fortran 77 with propriety message passing. Although the converted code worked it didn't utilise the full capabilities of the machine. The disk transfer rates were appallingly slow. This problem was partially solved by writing tailor made I/O routines in the underlying Fortran 77 and explicitly controlling the transfer of the loaded data to the nodes of the machine. Once the loading was completed control was passed back to the HPF code.

The final code amounts to some ten thousand lines.

B.1.1.2 Detailed.

The code was designed to be as robust as possible. Initially it was written so as to minimise the number of potential sources of trouble, and later optimisation was carried out, and the new code checked against the old. In particular, as much reuse of functions as possible was made. Initially these were coded in as simple a manner as possible.

For example, the second correction term can either be written as the difference of two derivatives or as a total derivative on the $\boldsymbol{E}$ field. The derivative in the second form is different from those in the first, because of the different transformation properties of the objects acted on. The first form was therefore chosen to reuse the existing code.

B.1.2 Verification of code

The form of the code made verification very difficult because it incorporated so many different functions.

The principle requirement is of gauge invariance. Correlators generated from two configurations that are gauge transformations of each other must be identical up to machine precision. This will only check colour index operation, and can say nothing about faults in the spin structure or space co-ordinate operations.

The co-ordinate operations of the leading order evolution operator by timeslicing the Green's function itself. The off-diagonal elements in spin and colour space will be zero and the leading ones will be 1 for each timeslice, by Green's theorem.

In the unit gauge the $\boldsymbol{E}$ and $\boldsymbol{B}$ fields are both zero. This can be checked directly by looking at these fields. Colourless combinations of the fields can be made, and these will be identically zero for the unit gauge and random gauge transfers thereof. The kinetic term can be switched off and correction terms involving just the fields can be used.

The pseudo-scalar correlator can be calculated directly from the formula

$$\sum_{\alpha\beta ij\boldsymbol{x}} \left| G^{ij}_{\alpha\beta}(\boldsymbol{x},t) \right|^2$$

and this compared with the value from the correlator function in the code.

To check the loading of the gauges was carried out successfully, the plaquette average can was calculated, and checked against the tabulated values for the configurations.

The loading of the light quark propagators was checked by calculating the pion correlator and comparing it with the known values which are tabulated for each configuration.

B.1.3 Optimisation

Loops residing on a single processor (usually involving spin, colour, and direction) were unwound. This was achieved by a series of perl scripts that produced the fortran code on output.

The NRQCD Green's functions were encoded as:

$$N_{\text{colour}} \times N_{\text{colour}} \times 2 \cdot N_{\text{Pauli}}$$

matrices. N_{Pauli} is 2, the number of spins for a non-relativistic quark field. The point of doing this was to make the Green's function conformable with the gauge field arrays. This was originally a Connection Machine optimisation, but was retained in the Cray code.

The number of inter-processor communications was reduced as much as possible. For example, in the derivative function ¶, which implements:

$$U_\mu(x)G(x+a\widehat{\mu}) - U^\dagger_\mu(x-a\widehat{\mu})G(x-a\widehat{\mu})$$

the second term was calculated in the order: multiply, shift rather than shift, shift, multiply.

The phases used during the making of the finite momentum correlators were pre-calculated at the beginning of the code.

¶ *i.e.* subprogram

B.2 Calculation Details

The calculations were carried out at $\beta 6.2$ on a $24^3 \times 48$ lattice. The gauge configurations were generated from Wilson's action by a combination of the Over Relaxed algorithm and the Cabibbo-Marinari algorithm in proportion 5:1. The number of updates separating the configurations was 2400. Periodic boundary conditions were used. The calculation used 68 configurations.

The NRQCD Green's functions were calculated for the following values of the mass and stability parameters: (1.1,4), (1.2,3), (1.3,3), (2.0,2), (4.0,1), (6.0,1) using the symmetrised $\mathcal{O}(mv^4)$ accurate evolution equation. The boundary conditions were periodic in all directions Mean field improvement was used with the value $u_0 = 0.88506$.

The light quark propagators were calculated from the non-perturbatively improved action with coefficient $c_{SW} = 1.6138$ using these algorithms: Over Relaxed Minimal Residual, Bi-Conjugate Gradient, Quasi-Minimal Residual, and Stabilised Bi-Conjugate Gradient. The Bi-Conjugate Gradient and Quasi-Minimal Residual algorithms exploited the γ_5 symmetry of the fermion matrix. All the algorithms incorporated red-black preconditioning. The boundary conditions were periodic in the space directions and anti-periodic in the time direction. The propagators were generated at three values of the hopping parameter: 0.13460, 0.13510, 0.13530.

The heavy-heavy correlators were produced at all of the masses and were calculated for 48 timeslices. The channels in the S wave were also calculated at the finite momenta:

(1,0,0), (0,1,0), (0,0,1)
(1,1,0), (1,0,1), (0,1,1)
(1,1,1)
(2,0,0), (0,2,0), (0,0,2)

The heavy-light correlators were calculated for all three values of κ, and were only evaluated for 28 timeslices. For the S wave channels all the heavy quark masses were used, whilst for the P wave operators, only the three lightest were used.

The smearing was applied to the heavy quark only. All four combinations of smearing at the source and sink were produced.

REFERENCES

Ali Khan, A., *et al.* (1996) *Phys.Rev.*D, **53**, 6433

Ali Khan, A., *et al.* (1999) *Heavy-light Mesons and Baryons with b quarks — In Preparation*, Ohio State University Preprint OHSTPY-HEP-T-98-018

Baxter, R., (1993) Ph.D. Thesis, Edinburgh University

Boyle, P., (1997) Ph.D. Thesis, Edinburgh University

Caso, C., *et al.* (1998), The Review of Particle Physics, *European Physical Journal* C **3** 1

Catterall, S. M., *et al.* (1994) *Phys.Lett.* **B321** 246

Collins, S., *et al.* (1999) 'Sea Quark Effects in B Spectroscopy and Decay Constant' hep-lat/9901001 OHSTPY-HEP-T-98-019

Creutz, M., (1998) *Grassmann Integrals by Machine Presented at 16th Internation Symposium on Lattice Field Theory, Boulder* hep-lat/9804021

The Delphi Collaboration (1996) *Contribution to ICHEP '96* DELPHI 96-93 and DELPHI 97-102 CONF 84

Davies, C.T.H., *et al.* (1995) *Phys.Rev.*D **52** 6519

Davies, C.T.H., (1998) 'Scaling of the Υ spectrum in Lattice NRQCD' hep-lat/9802024v2

DeGrand, T. A. and Loft, R. D., (1991) *Computer Phys. Comm.* **65** 84

El-Khadra, A. X. *et al.* (1997) *Phys Rev.*D **55** 3933

Ewing, A. *et al.* (1996) *Phys.Rev.*D **54** 3526

Guagnelli, M. *et al.* (1998) DESY and Oxford University Preprint, hep-lat/9806005 v2

Güsken, S., *et al.* (1990) *Nucl.Phys. B (Proc.Suppl.)* **17** 36

Hein, J., (1999) Private Communication

Hein, J., and Newton, H., (1999) *Scaling of the B and D meson spectrum in lattice QCD* In Preparation

Hamber, H. W. and Wu, C. M., (1984) *Phys.Lett.* **B136** 255

Lacock, P., and Michael, C., (1995) *Phys.Rev.*D 51 6403

Lehmann, H., and Symanzik, K. & Zimmermann, W. (1955), *Nuovo cim. Ser 10* **1**, 205

Lepage, G. P. *et al.* (1992) *Phys.Rev.*D **46** 4052

Lepage, G. P., and Mackenzie, P. (1993) *Phys.Rev.*D, **48**, 2250

Lepage, G. P., and Trottier, H., (1997) *Nucl.Phys.B.(Proc.Suppl.)* **63** 865

Lewis, R., and Woloshyn. R. M. (1998) *Phys.Rev.*D **58** hep-lat/9803004v2

Lidsey, A. J., (1995) Ph.D. Thesis, Glasgow University

Lin, D., (1999) Ph.D. Thesis, Edinburgh University

Lüscher, M. and Wolff, U., (1990) *Nucl.Phys.*B **339** 222

Manke, T., *et al.* (1997a) *Phys.Lett.* **B408** 308

Manke, T., *et al.* (1997b) *Nucl.Phys.B.(Proc.Suppl.)* **63** 332

McCallum, P., (1997) Ph.D. Thesis, Glasgow University

Morningstar, C., (1994) *Phys.Rev.*D **50** 5902

Neubert, M. (1994) *Phys.Rep.* **245** 259

Nielsen, H.B. and Ninomiya, M. (1981) *Nucl.Phys.*B **183** 103

Osterwalder, K., and Schrader, R., (1975), *Comm.Math.Phys.* **42** 281

Richtmyer, R.D., (1967) 'Difference Methods for Initial Value Problems', 2nd Edition, Wiley (Interscience) New York

Rowland, P., (1997) Ph.D. Thesis, Edinburgh University

Sheikholeslami, B., and Wohlert, R., (1985) *Nucl.Phys.*B **259**, 572

Symanzik, K., (1983) *Nucl.Phys.*B **226**, 187

Thacker, B.A. and Lepage G.P. (1991) *Phys.Rev.*D **43**, 196

Wilson, K., (1974) *Phys.Rev.*D **10**, 2445

So have I heard, and do in part believe.

Horatio, in *Hamlet*,*c*.1601